Addis Ababa University

Addis Ababa Institute of Technology

School of Mechanical and Industrial Engineering

Modelling the Heat Transfer during the Solidification of a Sand-Casting Process by Using Finite Element Method: The Case of “Akaki Basic Metal Industry”

By

Biniyam Mulugeta Digafie

September -2021

Addis Ababa, Ethiopia

Addis Ababa University

Addis Ababa Institute of Technology

School of Mechanical and Industrial Engineering

Modelling the Heat Transfer during the Solidification of a Sand-Casting Process by Using Finite Element Method: The Case of "Akaki Basic Metal Industry"

By

Biniyam Mulugeta Digafie

A Thesis Submitted for the Partial Fulfillment of Degree of Masters of Science (M.Sc.) in Mechanical Engineering (Thermal Engineering), in Addis Ababa University (AAU), Addis Ababa Institute of Technology (AAiT).

Advisor

Dr.-Ing. Demiss Alemu Ambie

September -2021

Addis Ababa, Ethiopia

Letter of Certification

Addis Ababa University

Addis Ababa Institute of Technology

School of Graduate Studies

This is to certify that the thesis prepared by Biniyam Mulugeta Digafie entitled "*Modelling the Heat Transfer during Solidification of a Sand-Casting Process by Using FEM: The Case of Akaki Basic Metal Industry*" in partial fulfillment of the requirements for the degree of Masters of Science in Mechanical Engineering (Thermal Engineering) compiles with the regulation of Addis Ababa University and meets the accepted standards concerning originality and quality.

Board of Examining Committee:

Dr.-Ing: Demiss Alemu Signature: _____ Date: 29/10/2021
Advisors:

Dr. Yilma Tadesse Signature: _____ Date: 01/10/2021
External examiner:

Dr. Muaz Bedru Signature: _____ Date: 01/10/2021
Internal examiner:

Dr. Yilma Tadesse Signature: _____ Date: 01/10/2021
Chair of Department

Declaration

I, the under signed, declare that this thesis is the result of my work and that all sources or materials used for this thesis have been dually acknowledged. This work is submitted in partial fulfillment of the requirements for a Master's Degree in Mechanical engineering (Thermal Engineering) at Addis Ababa University, Addis Ababa Institute of Technology, School of Mechanical and Industrial Engineering. I certainly declare that this thesis has not been submitted to any other institution anywhere for the award of any academic degree, diploma, and/or certificate.

29/10/2021

Biniyam Mulugeta Digafie — Date

This is to certify that the above declaration made by the candidate is correct to the best of my knowledge.

29/10/2021

Dr.-Ing: Demiss Alemu Ambie — Date

Acknowledgment

Glory be to the Father, and to the Son, and to the Holy Spirit, one God; for his immeasurable love and guidance in what had seemed like an insurmountable journey, Amen! My veneration and gratitude to the Holy Virgin Saint Merry, for lifting me up in every bit of this journey and for making the path brighter.

I wish to express my sincere appreciation to my Advisor Dr.-Ing. Demiss Alemu for the useful comments, remarks and encouragement throughout this thesis work.

My wife, Akliseya Habtamu (□□□), thank you for your Love, encouragement, constant support and, understanding all the time, and for keeping me sane during this thesis. But most of all, thank you for being my best friend. I owe you everything.

To my mother, Fitfit Alabachew Tadesse, for your incessant assistantship in every aspect of my life, for believing in me, and for inheriting the discipline and meticulousness, no words would be enough to describe how thankful I'm. May God bless you with long life and health, I love you dearly! To my father, Mulugeta Digafie Zewdie, thank you for your support, advice and for giving me strength. My brothers and sisters deserve my wholehearted thanks as well.

Furthermore, I wish to express my thanks to Dr. Yilmaz Tadesse, Dr. Abdulkadir Aman, Mr. Facade, Mr. Natnael for the support along the way. Also, I like to thank my peers in the class and at the campus such as Haile Mikael Solomon, Kassa Abera, Ashenafi Abebe, who have shared their support and precious time during many lively technical discussions about the thesis.

I would like to thank my friends who have supported me throughout this journey in many different ways.

Abstract

Even though sand-casting process is one of the oldest techniques to produce different products, the method is known as process of uncertainty since it is difficult to control process parameter and identify the real cause for defects associated to the process. Most defects encountered during casting identifies after the process is completed and then it leads to remelting and wastage of material, time and manpower. Currently modern casting foundries utilizes a significant effort to understand the underlying physics involved in solidification casting process to and to model casting process. However, local foundries used floor trial method to eliminate casting defects that leads to less productivity and decrease competitiveness in the market.

The main purpose of this study is to numerically model the solidification heat transfer during sand-casting process in case of Akaki Basic Metal Industry (ABMI). The model employs finite element method (FEM) utilizing fixed mesh technique. Computational simulation of the problem modeled using ANSYS software. Three cases selected from the foundry, casting of ash cleaner door and manhole cover by grey cast iron and casting of aluminum flywheel. The actual density of sand mold measured experimentally using analytical balance as 2506 kg/m^3.

The simulation of a two-dimensional transient thermal analysis result shows the temperature distribution, heat flux distribution and nodal values. The result of the simulation depicts the total solidification times are 2249, 177, and 133 seconds for case 1, case, 2 and case 3 simulation. Besides parametric study analysis was performed to investigate the effect of mold size, pouring temperature and mold property on the cooling of solidification. Validation of results with experimental literature shows a good agreement with experimental literature data.

The study result can be an input to the foundry for controlling process parameters without performing actual casting in the floor. The study recommends that local foundries could give attention in using numerical models to predict the casting process in order to increase their productivity and competitiveness.

Key words: Heat Transfer, Numerical Modeling, Finite Element Method, Solidification, Sand-Casting, Solidification, Phase Change, Cooling Curve

List of Abbreviations

ABMI	Akaki Basic Metal Industry
ANOVA	Analysis of variance
FDRE	Federal Democratic Republic of Ethiopia
FE	Finite Element
FEA	Finite Element Analysis
FEM	Finite Element Method
GTP	Gross Total Product
JICA	Japan International Corporation Agency
MIDI	Metal Industry Development Institute

Nomenclatures

C_{avg} : Average specific heat

C_S : Specific heat at solidus temperature

C_L : Specific heat at liquidus temperature

C^* : Specific heat at transition

L: Latent heat of the material

H_- : Enthalpy below the solidus temperature

C: Specific heat at a given temperature t

H_s : Enthalpy at solidus temperature

C_s : Specific heat at solidus temperature

T_s : Solidus temperature

T_l : Liquidus temperature

T_i : Nodal Temperature

T_f : Film temperature

T_∞ : Ambient temperature

T_w : Wall temperature of the mold

T^e : elemental temperature

H_l : Enthalpy at liquidus temperature

H_+ : Enthalpy above the liquidus temperature and

ρ : Density

ρ_l : Density at liquidus temperature

ρ_s : Density at solidus temperature

ρ_{sand} : Density of the sand

ρ_{air} : Density of the air at given temperature

ρ_{water} : Density of water at given temperature

m_{sand} : mass of the sand

V_{sand} : Volume of the sand

C: Specific heat capacity,

k: Thermal conductivity of liquid

Γ : Boundary of the domain Ω

Ω : Domain of region

n_x : Directional cosine in x direction

n_y : Directional cosine in y direction

L: latent heat of freezing and

f_s : Fraction solid.

M: Number of nodes assigned to element e and the

T_i : Nodal temperatures.

N_i : Interpolation or shape functions.

N_i: weighting function and

$d\Omega$: Differential domain

d_x : Change in the x direction

d_y : Change in the y direction

x_i and y_i : coordinate values at i^{th} node and

β : Temperature coefficient of thermal conductivity

υ : Kinematic viscosity of air at film temperature

h : Convective heat transfer coefficient between the mold and the surrounding

Nu : Nusselt number

k : Thermal conductivity

L : Characteristic length

As : Surface area

Table of Contents

List of Figures

List of Tables

Chapter 1: Introduction

1.1 Background of the Study

Solidification and melting are a process in which a phase change between liquid and solid or vice versa is occurred. Both processes are considered as the major topics in the study of fluid flow, heat transfer and mass transfer science since materials processing, metallurgy, solidification of casting and ingots, purification of metals, welding, electro slag melting, thermal energy storage using phase change materials involve melting and solidification [1].

Casting is as glamorous as it is ancient, beginning with the dawn of human civilization and interwoven with legends of fantastic weapons and exquisite artworks made of precious metals. It is estimated that castings are used in 90% or more of all manufactured goods and in all capitals, goods machinery used in manufacturing. Traditional techniques include lost-wax casting (which may be further divided into centrifugal casting, and vacuum assist direct pour casting), plaster mold casting and sand casting. The modern casting process is subdivided into two main categories: expendable and non-expendable casting. It is further broken down by the mold material, such as sand or metal, and pouring method, such as gravity, vacuum, or low pressure. The various processes differ primarily in the mold material (whether sand, metal, or other material). Among the processes sand-casting is the most widely used and ancient technique [2]–[5]

Despite of the popularity of sand-casting in the industries, the process suffers from poor quality and productivity due to involvement of number of uncontrolled process parameters namely shrinkage, porosity, hot spot, crack and the like in casting process. Even in a completely controlled process, defects in casting are observed and hence casting process is also known as process of uncertainty which challenges explanation about the cause of casting defects [6].

Final product of a sand-casting process can be influenced by different parameters involved in the process. Solidification, pouring temperature, heat transfer, composition of cast metal, property of mold, geometry of mold, and mold pre-heat strongly influences the final quality and the process productivity. This leads to the presence of defects on the final products of the casting. The cause of the defects cannot be clearly determined due to its uncontrolled parameters and complexity of the process [7], [8]

Solidification related defects mostly occurs during the initial and final stage of solidification. Common solidification related defects are; macroscopic cavity formation due to concentration of material called shrinkage cavity [9], [10], formation of hot tears or hot spots due to faster solidification and alloys with wider freezing ranges are more [11], warpage defects during sand due to non-uniform cooling rates throughout the casting [12], and micro porosity due to shrinkage of metal [13].

Controlling the solidification process during sand-casting of a metal processing is a vital to improve the quality of cast and reduce the number of rejects [14]. A complete understanding of the solidification phenomena during casting process, involves an analysis of the various processes that accompany it. The most important of these processes, from a macroscopic point of view, is the heat transfer process. This is accompanied by the release, or absorption, of the latent heat of fusion at the solid – liquid interface [1],[15].

Solidification process is a heat transfer process governed by the basic energy equation[16]–[18]. Analytical solution by solving the partial differential equation for phase change process is difficult task. Performing an experimental investigation during sand-casting process is expensive and difficult [19]. Alternative method of solving the energy equation during the solidification of sand-casting process is numerical method. Numerical models can simulate the solidification of sand-casting process utilizing less time, manpower and cost [7], [20]

Compared to other numerical approaches, the finite element method (FEM) offers the potential to realistically investigate the nonlinear material property and complex geometry by discretizing the given domain. In the FEM the continuous body is replaced by a system of finite elements (FE). An approximate solution within each element for the variable field is developed at a discrete number of points within the FE system. The FEM has been applied for solving the sand-casting problems by using piecewise continuous functions as approximations for continuous quantities in the solution domain. FEM result show the heat transfer pattern that is the desired parameter to control the casting quality [21]–[26].

Solving the transient nature of heat transfer by using the FEM for the solidification phase change problem during sand-casting process is becoming a solution to: predict the pattern of solidification, evaluate the solidification time, show the palace where the solidification starts and finishes, obtain the temperature history at all nodes inside the casting, and plot cooling curve and heat transfer coefficient and thermal gradient plot at elements and nodes. Thus the result of the simulation is used to further analysis to make the casting process sound [5], [23], [26], [27]

Numerical modelling of the transient and non-linear heat transfer analysis of the sand-casting process by using FEM will be a powerful option for local foundries including Akaki Basic Metal Industry (ABMI). Besides numerical simulation could be a powerful modeling tool for metal processing and manufacturing sectors in order to increase the quality and yield of casting process, and reduce the waste of production, reduce the use of energy, and reduce the time and man power.

With an accurate predictive numerical model, the foundry will be able to dramatically reduce defects, determine the optimum placement and size of risers, minimize trial runs and scrap metal, and even control the mechanical properties of the final products by using modulation of thermal analysis and cooling rates analysis [27] [28]. However, in the case of Akaki Basic Metal Industry (ABMI), such problem-solving method is not introduced.

To increase the competitiveness of basic metal industries like ABMI alternative methods to produce good final product is necessary. Computer modelling of the metal processing including solidification process during sand-casting process is promising technique to control metal processes including sand-casting process rather than using the old trial and error method in the industries [3]. Therefore, this study addresses the modelling of solidification process during the sand-casting process by using FEM.

1.2 Statement of the problem

Even though basic metal industries were considered as the primary industry to contribute the import-substitution based industrial development, the Global competitiveness and the gross total product (GTP) contribution for the economy of Ethiopia is still infant [29], [30]. According to report from the Federal Democratic Republic of Ethiopia (FDRE) plan and development commission ten-year plan, the current status of manufacturing industry has low domestic market share (30%), ineffective utilization of average capacity (50%), producing less quality product, and less competent [31]. As of the ten years plan the major focus of manufacturing sector including basic metal industries includes: raising production and productivity, satisfying domestic demand, and supplying global market by producing competitive products.

As largest and oldest industry, ABMI has a capacity of 450, 000 ton of casting, 1.6 million piece of spare parts, and 600,000 industrial hand tool products annually. The interview data from industrial survey and previous literatures [32]–[38] done on ABMI depicted that low productivity, improper process improvement, less product quality, poor innovation, improper research and design center, and low yield of casting are major problems the company faced. Owing to this the company production

rate is diminishing consequently this intern declines the competitiveness in domestic and global market.

Despite the fact there is no recorded data on frequency and percentage of defect and rejection rate of cast product in the foundry shop. The foundry personnel have witnessed the rejection of casting product due to different defects leads to wastage of products. The most common defects encountered in ABMI foundry is porosity, blow holes, sand inclusion, sand burning, cracks, hot tears, surface cracks, rough surface finish, pin holes and shrinkage. Those defects directly affect company's productivity, quality and competitiveness. Photographs from foundry that show different defects of cast products are given below in Figure 1.1.

(a) Void on the surface

(b) Porosity

(c) Blow holes

(d) Rapid shrinkage cavity

(e) Shrinkage cavity and Sand sintering

(f) Surface crack

Figure 1.1: Photograph of defects encountered in ABMI
Courtesy: Netsanet and Asmamaw [38], and foundry personnel's

Identifying the cause of casting defects is a complex problem since the casting process incorporates a complex science, fluid flow during filling of mold cavity and heat transfer during solidification and under cooling stage. However, the foundry designers identify the cause of the defect and try to optimize the process using the design of experiment, cause and effect, and trial and error method; some of the defects are still present after the casting is completed. This leads to the company in wastage of material, energy, time and even workforce. Thus, the foundry engineers could look at another alternative method to design the casting process, modelling the casting solidification process numerically.

The modelling casting process using the numerical method offers a basis for predicting the solidification pattern of the molten metal. The solidification patterns then show the place where the solidification starts and finishes; thermal history at nodes in the system; heat transfer pattern on the cast and mold. The result of the simulation can be used to redesign the process; increase the efficiency of casting; predict the performance of the feeding system; and control process parameters to make the casting [22], [26], [39].

Therefore, this study attempts to address the modelling of the heat transfer during the solidification process of the sand-casting process by using FEM utilizing fixed mesh technique to model the solidification pattern in the case of ABMI. The lack of attention to numerical modelling of metal processes to increase the productivity and competitiveness of local foundries is the motivation to undertake this study.

1.3 Objective of the Study

1.3.1 General Objectives

The general objective of this study is to numerically model the transient heat transfer during the solidification of the sand-casting process by using FEM.

1.3.2 Specific objectives

To achieve the general objective stated above, different specific tasks are to be implemented throughout the study. The specific objectives are:

(1) Process selection and data collection.
(2) Determinations of the thermo-physical properties of the mold and the cast material.
(3) Computational modelling and simulation of the sand-casting process using software "ANSYS 19.2" FEM software by varying different process parameters and scenarios.
(4) Validation of the computational models with available experimental data.

1.4 Scope of the Research

This study intends to probe the transient heat transfer analysis of casting process with the main objectives of modelling the solidification process, predicting the locations casting where metal solidifies last where the defect associated with the process arises by using FEM applying fixed mesh technique. The simulation data validated with the experimental result. The study does not include the experimental investigation of the solidification problem.

1.5 Significance of the Study

The output of the sand-casting process simulation can be used for further analysis for the foundry engineer to enhance the productivity and competitiveness of the company. The technique used in modelling the sand-casting process gives an insight to a company to conduct large numbers of simulations within a short time and with significantly less cost than physical trials. Also, this study's result improves the industries' capacity in developing fundamental models to describe the physics and selected manufacturing process.

Result of sand-casting model used as a tool for process optimization in the foundry shop for both existing castings and those under development for the first time, by eliminating shop-floor trials as shown in Figure 1.2. During modelling, several iterations carried out until the desired quality and

yield achieved. Even minor improvements in existing castings produced in large numbers can lead to significant improvements in the utilization of material, energy, equipment and labor resources.

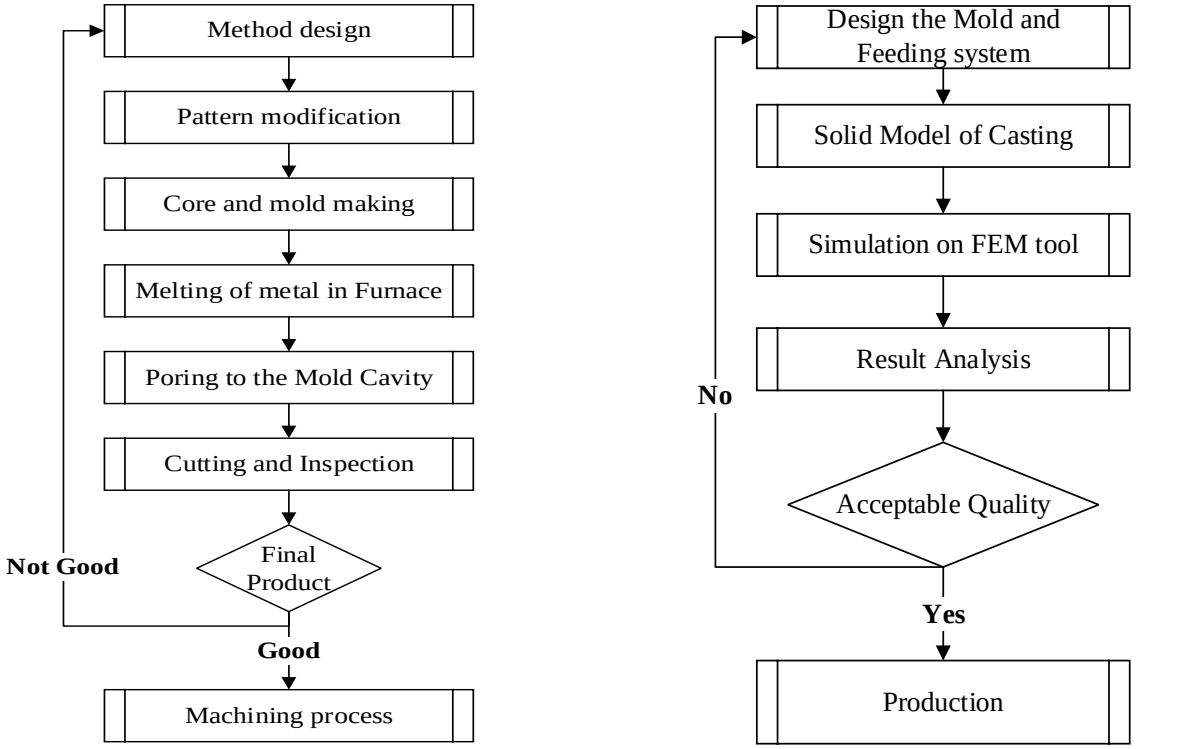

a. Conventional foundry Floor-Trial b. Numerical Simulation

Figure 1.2: Method optimization in (a) conventional and (b) numerical simulation
Source: Adopted from B. Ravi [3], with some modification

Generally, computational methods and numerical simulations in metal casting allow local foundries, including ABMI, to shift from conventional ‘‘trial-and-error’’ to ‘‘proof-of-concept’’ approach in the product development process. Furthermore, the result of modelling of the sand-casting process can have the following significances:

- Enhance academia and industry linkage.
- Tool used in industrial problem-solving.
- Reduce the financial risk associated with new materials and processes.
- Establish foundry process parameters.
- Save
  - Time
  - Manpower
  - Energy for the company
- Increase the competitiveness of the company.

- Increase customer satisfaction.

1.6 Limitation of the Research

The casting process is a complex problem. Almost all the factors involved during the process will take effect on the quality of a final product. As modelling of solidification complex as of the process, this focuses on simulating the sand-casting process's solidification. This study considers issues relevant to this topic and has limitations to the generalization of these results listed hereafter.

1. Thermophysical data for the cast and mold material used for the simulation is not recorded and documented in detail in the company. So, in this study, relevant data from the literature is used.
2. The magnitude of defects encountered in the company not recorded well.
3. The experimental simulation of the sand-casting process not conducted due to financial and laboratory access limitations.

1.7 Organization of the Thesis

The study organized as of five chapters:

Chapter One: Presented the background of the topic about the phase change process, history of casting, description of the sand-casting process, solidification process and its modelling, problems encountered in the foundry, and the importance of process modelling in sand-casting foundry. Then, the statement of the problem; general objective and five specific objectives to be achieved; five methodologies to be implemented; scope of the study; the significance of the study; and limitation of the study are discussed.

Chapter Two: It discusses the theoretical and conceptual literature related to; casting process; solidification processing; solidification of casting, modelling of the solidification process, numerical modelling of casting process; heat transfer in solidification of pure and alloy metals; finite element modelling technique; the advantages of using numerical modelling for solidification process; casting defects; and solidification related parameters affect the microstructure and mechanical property of cast discussed. The empirical review section discusses the previous works on modelling the sand-casting process and empirical study on ABMI. Finally, the research potential is discussed.

Chapter Three: In this section, process selection and data collection; thermophysical property determination; finite element formulation; and computational modelling of the sand-casting process using ANSYS software presented.

Chapter Four: In this chapter, the simulation results presented and discussed concerning different models under different parameters. The parametric study to analyze the effects of mold size, mold material property, and pouring temperature on the cooling of the cast metal for all models were discussed.

Chapter Five: Finally, conclusions are presented based on the result of the study and possible courses of action for the foundry and research areas point out for future recommendations.

Chapter 2: Literature Review

2.1 Introduction

There have been critical advances in modelling the solidification process, especially the casting process depicting the heat transfer, fluid flow, and mass transfer. Theoretical and conceptual review part gives an overview about the existing knowledge about casting process, solidification process, solidification of casting, modeling of solidification processing, defects in casting and parameters affecting casting process. Besides, published literature on computational modelling of the casting process, particularly the sand-casting solidification process also reviewed.

2.2 Theoretical and Conceptual Review

This part aims to concretely review the corpus of theory that has accumulated regarding the solidification process. The theoretical and conceptual literature review help establish what solidification and sand-casting already exist, the relationships between them, and the degree to which the existing theories have investigated.

2.2.1 Casting Process

The casting process is an ancient metal forming process that begins before 6000 years' ago. In the early stage of the process, people used casting to make idols worship. Nowadays, casting products are spread in most industrial applications due to their versatility and advantage to produce the required shape using different metals as a raw material [40].

Casting industries can be classified by the mold material used, method of mold production, and filling mechanism. The primary classification of the casting process are sand-casting, investment casting, centrifugal casting, die casting and gravity casting [41].

2.2.1.1 Sand-casting

In the Sand-casting process, sand mixes with the binders and water are compacted around wood or metal pattern halves to produce a mold. The mold removed from the pattern, assembled with cores, if necessary, and metal poured in to the resultant cavities. After cooling, mold broken to remove the casting. This process is suitable for casting in any metal (both ferrous and nonferrous), size and shape complexity. This process is the most widely used and accounts for 90% of the casting produced.[40]

2.2.1.2 Centrifugal Casting

In the centrifugal casting process, molten metal is poured into a revolving mold and allowed to solidify molten metal by the pressure of centrifugal force. It is employed for the mass production of circular casting as the castings produced by this process are free from impurities. Due to centrifugal force, the castings produced will be of high density and good strength [42].

The products possess high strength, good mechanical properties and produced at comparatively high rates. However, the variety of shapes that this process can produce are limited to symmetrical, circular-shaped products. There are also limitations on the type of metal cast, as the centrifugal process can cause the separation of alloys. Typical products manufactured by this process include cast-iron pipes and tubes, propeller shafts, and mill rolls [43].

2.2.1.3 Investment Casting

The investment casting, also known as 'lost wax', in the initial step requires the production of an expendable pattern in wax or plastic; this is then coated (invested) in a suitable refractory coating, dried and then fired. During the firing process the refractory becomes strongly bonded and the wax investment is melted out. Plastic investments, usually polystyrene, are burned out without leaving a residue. The metal is then cast into the resulting hollow mold.

The investment casting process allows the casting engineer to use enormous capability and flexibility inherent in the process. Parts produced by this process are indeed functional, cost-effective, and aesthetically pleasing. A wide range of parts from a few grams to more than 1000 kg can competitively be produced with this process [44].

2.2.1.4 Die Casting

In the die casting process, nonferrous parts of complex geometry are mass-produced to near net shape aluminum, magnesium, zinc, and copper alloys commonly used in this process. Products range from small valve fittings and housings to large transmission casings. Die castings generally provide structural support of some form and must meet containment or pressure-tight requirements [44].

2.2.1.5 Permanent Mold Casting

Permanent molds are usually made of steel or steel alloys and are used to cast metals or alloys with a lower melting point than the matrix, although other materials such as graphite may also use. Due to

the high manufacturing cost of permanent metallic molds or matrixes, they are applied only in large-scale industrial production [45].

2.2.2 Solidification Process

Solidification is one of the oldest manufacturing processes in which the liquid phase of a material changed in to solid phase. These phase change processes are accompanied by either absorption or release of thermal energy. A phase can be defined as a physically distinct, homogeneous and mechanically inseparable portion of a substance [28], [46].

The solidification process is the critical stage in most metallurgical activities. This process is primarily driven by heat transfer from the liquid metal due to the difference in temperature between the liquid melt and its ambient environment. This extraction of heat from the liquid to the surrounding heat sink controls the metal's cooling rate [18].

The solidification process takes place through nucleation and growth of the solid phase under favorable boundary conditions. Generally, solidification occurs when the temperature of a liquid lowered below its melting point. Several examples of solidification can be found in everyday life: Freezing of water to form ice, Formation of snow, and Solidification of melted metals. From the industrial perspective, casting is the basic metallurgical process in which alloys and pure irons will be solidified in a mold [45].

2.2.3 Solidification of casting

Solidification of metal during casting after the molten liquid metal poured into a mold cavity is an essential phase in the casting process, significantly influencing product quality and yield. Solidification of the casting process involved a macroscopic and microscopic phenomenon. From the micro point of view, the solidification process involves the microstructure evolution during the solidification process. The solidification process as a whole includes three different steps: nucleation (an increase in the number of nuclei), growth (an increase in the volume of the grain) and impingement [47].

The macroscopic phenomenon included in the solidification of the casting process is heat transfer, fluid flow and mass transfer. Basic flow mechanisms during the casting process are filling the mold, residual flow due to the incoming momentum and the natural convection-driven flow in the mold. From the heat transfer point of view, the Solidification of casting encompasses the phase transition

from liquid metal to a solid-state due to heat removal by the mold and segregation during solidification [48].

The solidification of the casting of metals can encompass the casting of pure metal and alloys. During the solidification of binary and multi-component alloys, the physical phenomena become more complicated due to phase transformation over a range of temperatures [49]. Disordered atomic configuration in liquid phase changes to ordered arrangement of crystal in the solid phase [50].

2.2.4 Modelling Solidification Processing

Modelling of solidification systems is a problem of great mathematical and industrial significance. In recent years, computer simulation models have developed to simulate heat transfer in solidification processes. Numerical methods, mostly finite-difference or FEMs, are effectively used. However, accurate data on the thermo- physical material properties are also needed [51].

The modelling of the solidification process incorporates two modelling phenomena called micro and macro modelling. The macro modelling phase changes in terms of heat transfer and fluid flow, and stress distribution. In contrast, the micro modelling includes solidification kinetics and fluid flow in the mushy zone [52].

2.2.4.1 Heat Transfer Modelling of Solidification Process

Solidification is a classical moving boundary problem that includes the transfer of heat and mass. The heat transfer occurs between the mold and cast, the mold and the environment, and show up inside the cast material. The advancement of mathematical modelling tools to depict heat transfer during the solidification processes is becoming a vital tool to understand and predict the solidification process [53].

2.2.4.1.1 Pure Metal Solidification

Solidification of a pure substance described as isothermal phase change problems characterized mainly by two parameters: the material melting temperature and its latent heat [54], [55]. Solidification of pure metal is a distinct phase change at a discrete temperature called freezing point or melting point and is associated with the latent heat of fusion [56].

2.2.4.1.2 Alloy Solidification

In the case of alloys, melting or solidification takes place over an extended range of temperatures. A two-phase moving region separates the solid and liquid phases, the ‘mushy zone’. The fixed grid

method has widely used to solve phase change problems for such situations, which appear in most practical casting and solidification problems.[57]

Solidification of alloys is more common in industry than pure metal solidification. In alloy solidification, two-phase or mushy zone exists between the solid and the liquid regions. Liquid metals flow in this zone has also been studied by several researchers [14].

2.2.4.2 Numerical Methods to Model Solidification Process

The main problem in the numerical approach is to follow the phase boundaries through the domain as the phase transforms from liquid to solid. The numerical methods for solving this problem mainly classified into two types.

- Fixed grid method and
- Front tracking method [28], [58].

The fixed grid method allows the interface to move through a fixed mesh. The interfacial boundary conditions are satisfied by applying unique techniques. The location of the interface recovered afterwards. Whereas, in front tracking methods, the interface motion is followed explicitly (tracking boundary). The most common numerical scheme is the Finite difference method (FDM), Gradient Vector method (GVM), boundary element method (BEM), finite volume method (FVM), and FEM. The FEM is a powerful tool to handle irregular shapes and non-linear material properties. Front-tracking methods are accurate for isothermal phase change, and they are not suitable for 'mushy problems' where the phase change occurs over a temperature interval [49].

2.2.4.2.1 Casting Process Modelling Using FEM

The FEM solves differential equations by using piecewise continuous functions as approximations for continuous quantities in the domain. Variational, Galerkin or other techniques can use to obtain the integral formulation, which, after evaluation of the integrals, leads to a set of algebraic equations in matrix form for each element. Once equations formulated for all the elements, the global matrices assembled, and the final solution obtained. This technique is more complicated than the finite difference method; however, it can easily apply to irregular geometries [14], [27].

The element sizes for the two sides of the interface can be significantly different. Unequal element size at the interface is often useful as a relatively dense mesh is generally employed for the casting region compared to the mold region [8].

2.2.4.2.2 Finite Element Software's to Model Solidification

There are specific commercial solvers used to simulate the casting process utilizing FEM. The commercial software's are tabulated below in Table 2.1.

Table 2.1: Available commercial software to model casting process

Software	Vendor
Wincast	RWP GmbH, Germany
CAPCAST	EKK, Inc, Michigan, USA
Procast	ESI group, Paris, France

Source: [28]

Even if there are available commercial software for modelling the casting process, a basic general and well-known computational tool called ANSYS can model the casting process in different varieties.

2.2.5 Defects in Casting Process

There are many types of defects associated with the casting process. Defects in the casting process may arise from the chemistry of alloys, casting design, casting process, and casting environment. Defects can be related to thermodynamics, fluid flow, heat transfer, and stress. A defect may arise from a single clearly defined cause that enables the remedy to seek in one of these sectors. For most cases, all defects are interrelated. Since defects decrease the process yield, it is essential to study every aspect of defects encountered in the casting process [41], [59].

Defects in the casting process can be minimized by the understanding of their fundamental causes' defects. Common defects associated with the casting, their cause with a remedy to decrease defects, and modelling technique given in different literature [13], [41], [59]–[62], are discussed below.

2.2.5.1 Porosity

Porosity may arise from a combined effect of solidification shrinkage and gas evolution. The effects may arise simultaneously. One of the most effective ways to minimize porosity defects is to design a feeding system using porosity prediction modelling. There are many models which can predict shrinkage porosity and gas porosity. In such a way, the model can determine the location of porosity so that the feeding system can be redesigned. This process is repeated until porosity is minimized and not likely to appear in the critical areas of the castings.

The primary cause of porosity formation is pressure drop due to shrinkage and gas segregation in the liquid. The liquid densities of many alloys are lower than that of the solid phase. Hence solidification shrinkage happens due to the metal contraction during the phase change.

2.2.5.2 Hot tearing

Hot tearing is one of the most severe defects encountered in castings. Many studies have revealed ho tearing occurs in the late stage of solidification when the fraction of solid is close to one. The formation and propagation of the hot tearing have found to be directly affected by the cooling history, the chemical composition, and mechanical properties of the alloy, as well as the geometry of the casting.

2.2.5.3 Macro segregation

Macro segregation is another defect for alloy casting processes. Numerous factors can cause macro segregation during casting solidification processes. Those include thermal and solute induced buoyancy, forced flow, solid movement.

Inclusions and sand defects

Non-metallic inclusions in castings considered in two main groups. The first are the indigenous, or endogenous, inclusions, the product of reactions within the melt. This type of defect is a microscopic defect. The second group are the exogenous inclusions, which result from entrainment of non-metallic during pouring and concentrated at a particular region on the cast.

2.2.6 Parameters Affecting Solidification and Microstructure of Cast

Different parameters during the casting process affect the solidification process and then the microstructure and mechanical properties of the final product. The solidification process and the microstructure of the cast product can determine the mechanical strength and other properties of the final product [63]–[68].

2.2.6.1 Cooling Rate

The cooling rate and solidification time are essential parameters that determine the final cast product. When the molten metal pours in the mold walls of the mold provide a chilling effect to the regions around the mold wall hence the region have a higher cooling rate. There will be greater undercooling in regions with higher cooling rates and help in the increased formation of several nuclei during solidification. If there are many nuclei, the structure is finer and hence possesses better properties. On the other hand, if solidification time extended, the nuclei formed will be favored for growth, and hence

coarser grains formed. Additionally, a higher cooling rate will cause higher strength and hardness by refining the cast's graphite size and matrix structure, but the material's ductility will decrease. Therefore, the composition of the molten metal and the design of the casting process must be arranged so that the required graphitization influence for the required cooling rate [65].

The cooling rate of the solidification process has great importance, and the shape of the curve has excellent effects on the final microstructure [66] since different cooling rates produce different micro structures and hence a variety of thermo mechanical properties [49].

The cooling rate of casting solidification can be affected by different parameters. The basic parameters are:

- Pouring temperature.
- Mold size.
- Mold property.

2.2.6.2 Pouring Temperature

The pouring temperature of the melts is a typical operation when preparing molten metal to pour in the core. The material is melted in the respective furnace to ready it for pouring at the given pouring temperature. The pouring temperature is mostly the superheat temperature above the melting point of the melts for pure and alloy materials. The pouring temperature can affect the final structure of the cast. For example, for a commercial aluminum alloy, the pouring temperature is around 1073k because a high superheat temperature results in a structure coarsening, favoring a columnar grain structure. According to a study conducted by A. Ferreira et al. [63], “The thermal parameters (cooling rate, solidification speed, and local solidification time) are affected by pouring temperature. These, in turn, affects the microstructure arrangement and micro segregation profiles.”

2.2.6.3 Mold Size

The mold used in the casting process can significantly affect the cooling rate of the solidification of casting. The mold wall thickness affects the heat transfer from the melt since the heat transfer is inversely proportional to the wall thickness of the mold. Generally, when the size of the mold wall thickness decreases, the cooling rate increase [67].

2.2.6.4 Mold Sand Property

The property of mold material highly affects the cooling rate of the solidification process. The heat flux through the mold is high with a high thermal conductivity coefficient, and the temperature profile is also smooth for high thermally conductive material. Also, the higher heat capacity of mold material results in a higher cooling rate of the cast at the initial stage of the solidification [68].

2.3 Mathematical Modelling and Finite Element Formulation

2.3.1 Introduction

The problem is represented by a set of partial differential equations. An accurate representation of a physical system will generally require a complex system of equations. By using some assumptions, one may be able to simplify the model to a considerable extent.

2.3.2 Mathematical Modelling of Casting Solidification Process

The two-dimensional (2D) partial differential set of equation in Cartesian coordinates to govern the fluid flow for the initial mold filling stage can be written as. [22], [69], [70]

$$\rho c \frac{\partial T}{\partial t} = \frac{\partial}{\partial x}\left(k \frac{\partial T}{\partial x} \right) + \frac{\partial}{\partial y}\left(k \frac{\partial T}{\partial y} \right) + Q \qquad (2.1)$$

During casting solidification, the heat transfer process is accompanied by the release of latent heat of fusion at the solid/liquid interfaces. Different techniques have used to take account of the release/or absorption of latent heat. These methods generally divided into fixed and moving mesh methods. Fixed mesh methods involve the solution of a continuous system with an implicit representation of the phase change, while in the moving mesh, also known as front tracking methods, the solid/liquid regions are treated separately, and the phase change interface explicitly determined as a moving boundary. The fixed grid solutions offer a more general solution as they account for the phase change implicitly without attempting to establish the position of the front [69], [71]

2.3.3 Modelling Latent Heat Release through the Source Term

In what can see as the most general and straightforward treatment of Latent Heat, the source term in equation (eqn-3.15) written as

$$Q = \rho L \frac{\partial f_s}{\partial t} = \rho L \frac{\partial f_s}{\partial T} \frac{\partial T}{\partial t} \qquad (2.2)$$

The energy balance equation then can be written as

$$\rho c\frac{\partial T}{\partial t}=\frac{\partial}{\partial x}\left(k\frac{\partial T}{\partial x}\right)+\frac{\partial}{\partial y}\left(k\frac{\partial T}{\partial y}\right)+\rho L\frac{\partial f_s}{\partial T}\frac{\partial T}{\partial t} \quad (2.3)$$

$$\rho\left(c-L\frac{\partial f_s}{\partial T}\right)\frac{\partial T}{\partial t}=\frac{\partial}{\partial x}\left(k\frac{\partial T}{\partial x}\right)+\frac{\partial}{\partial y}\left(k\frac{\partial T}{\partial y}\right) \quad (2.4)$$

It is observed that the term in parenthesis on the left-hand side of the equation (Eqn. 3.18) can be treated as an 'equivalent specific heat (C_{eff}),' when compared with the original equation.

$$C_{eff}=\rho\left(c-L\frac{\partial f_s}{\partial T}\right) \quad (2.5)$$

This formulation of latent heat liberation during liquid-solid phase change can model several alloy solidifications processes, including the sand-casting process.[69], [70], [72]

2.3.3.1 Enthalpy Method

In a slight variation of the above treatment of latent heat, the net enthalpy of the alloy at any temperature written as:

$$H=\int_{T_O}^{T}\rho c dT+\left(1-f_S\right)\rho L \quad (2.6)$$

Differentiating the above equation with respect to T, we obtain

$$\frac{\partial H}{\partial T}=\rho\left(c-L\frac{\partial f_s}{\partial T}\right) \quad (2.7)$$

The energy equation (eqn. (3.17) becomes

$$\frac{\partial H}{\partial T}=\frac{\partial}{\partial x}\left(k\frac{\partial T}{\partial x}\right)+\frac{\partial}{\partial y}\left(k\frac{\partial T}{\partial y}\right) \quad (2.8)$$

The numerical solution of the above equation explained in a later section. This method assumes that a continuous function for enthalpy over the entire computational domain is available.

Among the fixed mesh methods, one of the earliest and the most commonly used method is the ***'effective heat capacity'*** method. This method is derived from writing equation (3.22) as follows

$$C_{eff}\frac{\partial T}{\partial t}=\frac{\partial}{\partial x}\left(k\frac{\partial T}{\partial x}\right)+\frac{\partial}{\partial y}\left(k\frac{\partial T}{\partial y}\right) \quad (2.9)$$

Where: $C_{eff}=\frac{\partial H}{\partial T}$

2.3.4 The Finite Element formulation

The governing differential equation (Eqn. 3.23) can be transformed into an element equation using Galerkin weight residual formulation.

The finite element formulation has a series of steps to solve the given problems. The step to formulate the finite element solution are: [16], [21], [22], [69], [73]–[75]

Step 1: Identifying the system governing equation for the liquid-solid phase change process.

The distribution temperature T within the element is assumed to be a linear combination of polynomials of the form,

$$T^e(x,y,t) = \sum_{i=1}^{m} N_i(x,y) T_i(t) \tag{2.10}$$

With the assumed distribution of the temperature over the element, the elemental equation becomes:

$$C_{eff}\frac{\partial T}{\partial t} = \frac{\partial}{\partial x}\left(k\frac{\partial T^e}{\partial x}\right) + \frac{\partial}{\partial y}\left(k\frac{\partial T^e}{\partial y}\right) \tag{2.11}$$

Step 2: Galerkin method of the weak formulation

Multiplying equation (Eqn. 3.25) by weight functions Ni, integrating over an element domain and equating the weighted residual to zero, we get

$$\int N_i\left[\frac{\partial}{\partial x}\left(k\frac{\partial T^e}{\partial x}\right) + \frac{\partial}{\partial y}\left(k\frac{\partial T^e}{\partial y}\right) - C_{eff}\frac{\partial T}{\partial t}\right]d\Omega = 0 \tag{2.12}$$

Reducing the order of differentiation by applying integration by parts to the first and the second terms of the integral equation,

For the first term by using integration by part

$$\int N_i\left(\frac{\partial}{\partial x}k\frac{\partial T}{\partial x}\right)d\Omega = uv - \int v\,du \tag{2.13}$$

let $u = N_i$ then $\frac{du}{dx} = \frac{\partial N_i}{\partial x}$

$$dv = \left(\frac{\partial}{\partial x}k\frac{\partial T}{\partial x}\right) \text{ then } v = \int\left(\frac{\partial}{\partial x}k\frac{\partial T}{\partial x}\right)dxdy = \int\frac{\partial}{\partial x}k\frac{\partial T}{\partial x}dy \tag{2.14}$$

Where:

$\int\frac{\partial}{\partial x}$ is the integral identity

$$\int N_i\left(\frac{\partial}{\partial x}k\frac{\partial T}{\partial x}\right)d\Omega = \int_{\Omega}\frac{\partial}{\partial x}N_i k\frac{\partial T}{\partial x}dy - \int_{\Omega} k\frac{\partial N_i}{\partial x}\frac{\partial T}{\partial x}dxdy, \tag{2.15}$$

but by using *Gradient Theorem*

$$\int_{\Omega}\nabla F dy = \oint_{\Gamma} n_y F ds \tag{2.16}$$

$$\int_{\Omega}\frac{\partial}{\partial x}N_i k\frac{\partial T}{\partial x}dy = \oint_{\Gamma} N_i\frac{\partial T}{\partial x}n_y ds \tag{2.17}$$

$$\int N_i \left(\frac{\partial}{\partial x} k \frac{\partial T}{\partial x} \right) d\Omega = -\int_{\Omega} k \frac{\partial N_i}{\partial x} \frac{\partial T}{\partial x} dxdy + \oint_{\Gamma} N_i \frac{\partial T}{\partial x} n_x ds \quad (2.18)$$

For the second term in the same way

$$\int N_i \left(\frac{\partial}{\partial y} k \frac{\partial T}{\partial y} \right) d\Omega = -\int_{\Omega} k \frac{\partial N_i}{\partial y} \frac{\partial T}{\partial y} dxdy + \oint_{\Gamma} N_i \frac{\partial T}{\partial y} n_y ds \quad (2.19)$$

Substituting the results in equation (Eqn. 26) yields

$$\int_{\Omega^e} \left[-\left(k \frac{\partial T^e}{\partial x} \frac{\partial N_i}{\partial x} \right) - \left(k \frac{\partial T^e}{\partial y} \frac{\partial N_i}{\partial y} \right) - N_i C_{eff} \frac{\partial T}{\partial t} \right] dxdy + \oint_{\Gamma} N_i \left(k \frac{\partial T^e}{\partial x} n_x + k \frac{\partial T^e}{\partial y} n_y \right) ds = 0 \quad (2.20)$$

Applying the boundary condition on the boundary Γ to split it in to Γ_1 and Γ_2 in the following way

$$\oint_{\Gamma} N_i \left(k \frac{\partial T^e}{\partial x} n_x + k \frac{\partial T^e}{\partial y} n_y \right) ds = -\oint_{\Gamma_1} N_i q ds - \oint_{\Gamma_2} N_i h \left(T^e - T_{\infty} \right) \quad (2.21)$$

Upon substitution

$$\int_{\Omega^e} \left[\left(k \frac{\partial T^e}{\partial x} \frac{\partial N_i}{\partial x} \right) + \left(k \frac{\partial T^e}{\partial y} \frac{\partial N_i}{\partial y} \right) + N_i C_{eff} \frac{\partial T}{\partial t} \right] dxdy + \oint_{\Gamma_2} N_i h T^e = -\oint_{\Gamma_1} N_i q ds + \oint_{\Gamma_2} N_i h T_{\infty} \quad (2.22)$$

Step 3: Discretizing the domain of interest into elements

For the general procedure, the total volume of the domain is discretized into finite Elements. In each element, the temperature distribution expressed in terms of the nodal values. The domain discretized into triangular elements.

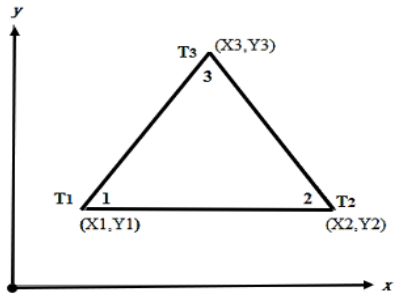

Figure 2.1 Three nodal linear Triangular elements in natural and global coordinate [43]

The linear triangular element in Figure 2.1, has three nodes at the vertices and the variable interpolation within the element is linear in x and y direction given as:

$$T = a_1 + a_2 x + a_1 y \quad (2.23)$$

Rewriting in matrix form:

$$T = \begin{bmatrix} 1 & x & y \end{bmatrix} \begin{Bmatrix} a_1 \\ a_2 \\ a_3 \end{Bmatrix} \quad (2.24)$$

Where a_i is a constant to be determined.

The interpolation function in equation (Eqn-3.38) should represent the nodal temperature at three nodes. Therefore, substituting the x and y values at each nodal point gives:

$$\begin{Bmatrix} T_1 \\ T_2 \\ T_3 \end{Bmatrix} = \begin{bmatrix} 1 & x_1 & y_1 \\ 1 & x_2 & y_1 \\ 1 & x_3 & y_1 \end{bmatrix} \begin{Bmatrix} a_1 \\ a_2 \\ a_3 \end{Bmatrix} \tag{2.25}$$

Inverting the matrix in equation (Eqn-3.39) and rewriting the equation gives

$$\begin{Bmatrix} a_1 \\ a_2 \\ a_3 \end{Bmatrix} = \frac{1}{2A} \begin{bmatrix} x_2y_3 - x_3y_2 & x_3y_1 - x_1y_3 & x_1y_2 - x_2y_1 \\ y_2 - y_3 & y_3 - y_1 & y_1 - y_2 \\ x_3 - x_2 & x_1 - x_3 & x_2 - x_1 \end{bmatrix} \begin{Bmatrix} T_1 \\ T_2 \\ T_3 \end{Bmatrix} \tag{2.26}$$

Where:

$$A = \frac{1}{2} \det \begin{bmatrix} 1 & x_1 & y_1 \\ 1 & x_2 & y_1 \\ 1 & x_3 & y_1 \end{bmatrix}$$

The magnitude of A is the area of the linear triangular element. However, its value is positive if the element node numbering is counter-clockwise and negative otherwise.

For finite element computation, the nodal element sequence must be in the same direction for every element in the domain.

Substituting equation (eqn-3.39) in to (3.40) yields

$$T = N_1(x,y)T_1 + N_2(x,y)T_2 + N_3(x,y)T_3 \tag{2.27}$$

Where:

N_i - the shape function for linear triangular element and it is given below.

$$N_1 = \frac{1}{2A}\left[(x_2y_3 - x_3y_2) + (y_2 - y_3)x + (x_3 - x_2)y\right]$$

$$N_2 = \frac{1}{2A}\left[(x_3y_1 - x_1y_3) + (y_3 - y_1)x + (x_1 - x_3)y\right]$$

$$N_3 = \frac{1}{2A}\left[(x_1y_2 - x_2y_1) + (y_1 - y_2)x + (x_2 - x_1)y\right]$$

Step 4: Introduce an approximation of field variable over an element

The approximation of field variable is done by applying interpolation function

$$T(x,y,t)^{(e)} = \sum_{i=1}^{m} N_j(x,y)T_j(t) = [N]^T \{T\} \tag{2.28}$$

Where m = 3 for triangular element.

Differentiating the field variable T with respect to other variables x, y, and t as follows

$$\frac{\partial T(x,y,t)^{(e)}}{\partial x}=\sum_{i=1}^{3}T_j(t)\frac{\partial N_j(x,y)}{\partial x} \tag{2.29}$$

$$\frac{\partial T(x,y,t)^{(e)}}{\partial x}=\left[\frac{\partial N_1}{\partial x}\frac{\partial N_2}{\partial x}\frac{\partial N_3}{\partial x}\right]\begin{Bmatrix}T_1\\T_2\\T_3\end{Bmatrix} \tag{2.30}$$

$$\frac{\partial T(x,y,t)^{(e)}}{\partial y}=\sum_{i=1}^{3}T_j(t)\frac{\partial N_j(x,y)}{\partial y} \tag{2.31}$$

$$\frac{\partial T(x,y,t)^{(e)}}{\partial y}=\left[\frac{\partial N_1}{\partial y}\frac{\partial N_2}{\partial y}\frac{\partial N_3}{\partial y}\right]\begin{Bmatrix}T_1\\T_2\\T_3\end{Bmatrix} \tag{2.32}$$

$$\frac{\partial T(x,y,t)^{(e)}}{\partial t}=\sum_{i=1}^{3}N_j(t)\frac{\partial T_j(t)}{\partial t} \tag{2.33}$$

Where: N_j-is the weights function.

Step 5: Evaluate the integral form over each element

The integral for each element is calculated by substituting equations (Eqn. 3.44-3.47) in to (Eqn. 3.23)

Substituting the above interpolation functions and rearranging gives:

$$[C]^e\left\{\frac{\partial T}{\partial t}\right\}+[K]^e\{T\}^e=\{F\}^e \tag{2.34}$$

Where:

$$C_{ij}=\int_{\Omega^e}C_{eff}N_iN_jd\Omega$$

$$K_{ij}=\int_{\Omega^e}\left[k\frac{\partial N_i}{\partial x}\frac{\partial N_j}{\partial x}+k\frac{\partial N_i}{\partial y}\frac{\partial N_j}{\partial y}\right]d\Omega+\oint_{\Gamma_2}hN_iN_jd\Gamma$$

$$F_i=\oint_{\Gamma_1}qN_id\Gamma+\oint_{\Gamma_2}hT_\infty N_id\Gamma$$

Step 6: assemble the global matrix equation

The global matrix of the problem is given as

$$[C]\left\{\frac{\partial T}{\partial t}\right\}^t+[K]\{T\}^t=\{F\}^t \tag{2.35}$$

Step 7: Solution techniques

Element equations and iterative time marching schemes are required to solve system of matrix equations (3.49), and results in a set of nodal temperature for every time step is calculated.

Time Stepping Schemes

Forward difference method: the time derivative of this method is expressed as

$$\left\{\dot{T}\right\}^{t} = \frac{\{T\}^{t+\Delta t} - \{T\}^{t}}{\Delta t} \tag{2.36}$$

Substituting equation (3.50) in to (3.49) and re arranging gives

$$[C]\{T\}^{t+\Delta t} = \Delta t\left(\{F\}^{t} - [K]\{T\}^{t} + [C]\left\{\frac{\partial T}{\partial t}\right\}^{t}\right) \tag{2.37}$$

The above equation (3.51) can be solved from the given initial condition $\{T\}^{t}$ and the general boundary condition $\{F\}^{t}$ as:

1. Setting $t = 0$ in equation (3.51) to solve $\{T\}^{\Delta t}$ from $\{T\}^{0}$ and $\{F\}^{0}$
2. After computing $\{T\}^{\Delta t}$ by repeating the previous step to solve $\{T\}^{2\Delta t}$ by setting $t = \Delta t$ in equation (Eqn. 3.51).
3. The step repeated until the solution reaches the final time.

This method is conditionally stable so that a proper size of time step Δt used to have a stable solution.

Backward difference method

For this method equation (3.50) can be re written as

$$[C]\left\{\frac{\partial T}{\partial t}\right\}^{t+\Delta t} + [K]\{T\}^{t+\Delta t} = \{F\}^{t+\Delta t} \tag{2.38}$$

The time derivative of this method if expressed a

$$\left\{\dot{T}\right\}^{t+\Delta t} = \frac{\{T\}^{t+\Delta t} - \{T\}^{t}}{\Delta t} \tag{2.39}$$

Substituting equation (3.52) in to (3.53) yields

$$\left([C] + \Delta t[K]\right)\{T\}^{t+\Delta t} = \Delta t\left(\{F\}^{t+\Delta t} + [C]\{T\}^{t}\right) \tag{2.40}$$

Crank-Nicolson method

For this method equation (3.50) can be re written as

$$[C]\left\{\frac{\partial T}{\partial t}\right\}^{t+\frac{\Delta t}{2}} + [K]\{T\}^{t+\frac{\Delta t}{2}} = \{F\}^{t+\frac{\Delta t}{2}} \tag{2.41}$$

The time derivative of this method if expressed a

$$\left\{\dot{T}\right\}^{t+\frac{\Delta t}{2}} = \frac{\{T\}^{t+\Delta t} - \{T\}^{t}}{\Delta t} \tag{2.42}$$

on the other hand, the other terms are computed as average like

$$\{T\}^{t+\frac{\Delta t}{2}} = \frac{1}{2}\left(\{T\}^{t} + \{T\}^{t+\Delta t}\right) \tag{2.43}$$

$$\{F\}^{t+\frac{\Delta t}{2}} = \frac{1}{2}\left(\{F\}^{t} + \{F\}^{t+\Delta t}\right) \tag{2.44}$$

Substituting equation (3.56) through (3.58) into (3.55) yields

$$\left(2[C]+\Delta t[K]\right)\{T\}^{t+\Delta t} = \Delta t\left(\{F\}^{t} + \{F\}^{t+\Delta t}\right) + \left(2[C]-\Delta t[K]\right)\{T\}^{t} \tag{2.45}$$

This method is unconditionally stable.

The solution procedure for this method is the same as the forward difference method, but this method is unconditionally stable. Therefore, any size of Δt is used without worrying about stability. However, the time step size is an essential parameter for controlling the accuracy of the solution.

2.4 Empirical Review

In the ’60s and ’70s of the twenty-century different scholars [24], [76], [77] shows the use of FEM or the analysis of transient heat transfer in solid media, and they investigated the nature of temperature profile in the object, and they validate the FEM with the experimental result. Those works show the advantage of FEM for transient heat transfer analysis over other numerical methods available during that time. Nevertheless, the works focused on the phase change problem like solidification.

J. A Dantzig and S. C. Lu (1985) [49] probed the generally applicable methods for representing the heat flow in the mold surrounding three-dimensional casting by boundary conditions applies at the surface of the casting by using a commercial FEM solver named ANSYS. They use the method to systematically represent the local suface geometry by a plane, sphere, or cylinder based on local heat flow enviroment and then use the methode to solve the heat flow problem in various sand molds. Then they present the solutions used to construct the boundary condition and implement it in a FEM program. The FEM program presented the temperature distribution at the different surfaces of the geometries. However, the researchers do not show the transient nature of temperature using a time-stepping scheme.

R. W Lewis and P.M. Roberts (1985) [78] investigated the modelling of heat transfer modelling numerically using a heat transfer analysis program. The development of a non-linear heat conduction simulator that uses the FEM presented in their study. The paper focuses on the appllication of FEM

to model solidification problems by giving more attention to the industrial casting process. Although convective heat transfer analysis and thermal stress coupled to predict mechanical behaviour, including crack formation. Finally, they present the temperature versus time graph by using Various time-stepping methods considered for use in conjunction with the Galerkin semi-discrete weighted residual (FEM) form of the differential equation for aluminum- bronze and sand

M. Samonds et al. (1985) [27] presented an experimental and numerical analysis of solidification in sand-casting using implicit-explicit schemes to predict the time-dependent solidification process. In their study, they use a single layer of the quadratic element in the sand. They use an implicit-explicit formulation with an appropriate solver by taking the sand element as explicit. Applying the conservation of energy principle to the problem and applying the Galerkin method of FEM saves 79% of computer modelling time due to an appropriate solver and a 39% reduction in computing time due to an explicit, implicit algorithm. Finally, they show the FEM is acceptable, with the result obtained by the numerical method for high conductive sands for tapered and un tapered Aluminum-Bronze slab.

R.W. Lewis et al. (1990) [22] developed a self-contained computer-aided design system capable of analyzing foundry casting processes by introducing adaptive remeshing in phase change zones of sand and gravity dies to study the heat transfer during solidification of casting by FEM. In the study, an interfacial heat transfer model was introduced to improve the simulation of the casting process, and advective heat transfer in the liquid was modelled. The temperature and velocity contour are presented in die and gravity casting. The entire package can be used for solidification analysis in castings, including the effects of natural convection. The numerical results show the possibility of applying this package to practical use on the foundry floor.

A. K. Tieu and L. S. Kim (1997) [40] assessed a three-dimensional heat transfer nature analysis of a continuous cast slab to determine the temperature profile and solid shell thickness. The authors study a non-linear thermo-physical property of the slab during the solidification process by using a general thermo-fluid mechanics computer program called PHOENICS, to solve the problem numerically. The model then validated with the experimental data from the foundry, and the prediction of the numerical solution is quite close to the experimental value. Finally, they predict the process parameter on casting flow, cooling rate and water flow rate.

Sulaiman and Hamouda (2001) [79] conducted a study to investigate the thermal history of an aluminum alloy casting inside the sand mold during 1200 seconds using a FEA and experimental

study. Result of the study depicted that the solidification of the molten metal takes 11 seconds to solidify at a point on runner and takes 2 seconds at products. The heat was transferred from the casting to the sand and from the sand to the surroundings. The experimental temperature curves are generally higher than for modeling for the mold. This is because of trapped air and the porosity of the sand mould.

Pariona and Mossi (2005) [45] studied numerical simulation of a two-dimensional heat transfer during the solidification of an L-shape non-linear pure iron in industrial greensand molds, AI 50/60 AFS, and mullite to compare a comparative study. The study presented the cooling curve and local solidification at different locations in the cast and heat flux, thermal gradient, and heating and cooling curves at different points in the mold by using a finite element tool ANSYS 9. The study shows molding process affects the process and the microstructural quality, and the mechanical properties of the cast. During a one and half hour solidification, a five-second increment of each sub-step employed, a convection phenomenon between the mold and the environment but radiation heat transfer ignored. The maximum and minimum temperature in the sand mold is 1321K and 555K, but in the mullite mold, 886K and 827K at the upper right corner and lower bottom of the mold. The result shows the Colling rate is fast in the mullite mold since its density and thermal conductivity is higher than the green mold; this causes more significant thermal flow and thermal gradient in the sand mold. The simulation did not consider the positioning of the feed head, the hot top and the conventional mold model used.

Krabbenhoft, K et al. (2006) [80] investigated the use of fixed mesh FEM using implicit mixed enthalpy–temperature method for phase-change problems to show the temperature versus time graph. In this work, the advantage of using the implicit method over the explicit method briefly described. In this study, enthalpy and temperature interpolated separately and subsequently linked by using the proper relationship in the mesh nodes during the solution phase. An algorithm is used to model the efficient and robust problem and is further easy to implement and generalize to arbitrary finite elements. The study shows the capability of an implicit finite element procedure for handling phase-change problems with a mushy zone. The study does the method on two-dimensional problems only the three-dimensional analysis not considered.

Diego J. Celentano et al. (2006) [81], investigated the effect of natural convection and different heat transfer condition on the thermal-microstructural evolution in gray cast-iron solidification during the cylindrical casting. The FE simulation of the problem utilizes five different cases by varying heat transfer parameters. The temperature distribution and liquid fraction evolution graph at a point shows

the pattern of alloy solidification nature during alloy solidification. The simulation validated with experimental study with good agreement.

Chang Li et al. (2011) [82] studied the temperature field of the casting process of rectangular steel with a liquidus temperature of 1943 K and sand temperature of 298 K by using ANSYS to analyze temperature field distribution and the variation inside the cast and the mold According to the temperature field thermal analysis of casting process, it concludes that the temperature of casting core reduces gradually with time. The temperature of casting and sand mold ends reduce more slowly. The isothermal line presented on the cast and sand mold during the 600-second of simulation. However, this study shows only the temperature distribution, the cooling load, the thermal flux and thermal gradient.

Petr Kotas et.al, (2012) [83] conducted a computational study to eliminate hot tears in steel casting using solidification pattern optimization. The transient thermal analysis of a 3-Dimentional original casting layout were simulated using a thermal-fluid model employing FE based software called MAGMASOFT. The multi objective optimization problem of choosing the proper riser and chill designs has been investigated using genetic algorithms while simultaneously considering their impact on centerline porosity, the macro segregation pattern, and primarily on hot tear formation. The original casting after were carried out using process parameters resulting in excess hot tears and other defects on the surface of the cast. The optimized layout of casting resulting in eliminated hot tears and porosity formation in the casting.

B. Patel et al. [84] analyzed the transient heat transfer analysis of solidification of L-shaped steel in the sand-casting process across the mold by finite element analysis using ANSYS software. The study considers the mode of heat transfers as conduction occurs between the steel and the sand mold, and convection occurs between the sand mold and the ambient air. Then the problem is modelled on the ANSYS applying the procedures step by step, and the analysis proceeds convergence test. Finally, the simulation result of thermal flux presented on the post-processing of ANSYS. Vector plot of thermal gradient and two-dimensional temperature distribution in casting. The study showed only the temperature distribution over the casting, so the temperature distribution between the mold and casting is not considered.

Recently T. Skrzypczak et al. [10] probed the numerical models of the solidification process during the casting of Fe-C alloy by considering the phenomena of defect called shrinkage cavity formation by using FEM. The study conducted by a written Visual C++ environment to simulate the described

process and predict where and when the shrinkage cavity is formed. This research models the solidification process by FEM and gives an algorithm for shrinkage cavity formation based on the assumption that the shrinkage cavity is due to a gravitational effect. Numerical examples were given in the paper to show the model in terms of the given material property. Finally, the simulation result shows the shrinkage cavity is formed on the top surface of the object and the authors suggest using an appropriate design of the riser and cooling conditions to assure the high probability of obtaining casting products of good quality. As a gap, the study does not consider the effect of mold on the formation of shrinkage cavities.

2.4.1 Empirical studies at ABMI

Few studies have been published on the study of casting process at ABMI. Various approaches have been proposed to minimize the defects encountered in the foundry. The proposed methods in the literatures mostly focus on experimental and theoretical approaches. Taguchi method of numerical experimentation and design of experiment method are the most well-known approaches in local foundries. Numerical modeling of casting in ABMI were studied in two studies presented as follow.

Kidu and Asmamaw (2017), [85] conducted a simulation based process parameter analysis of manganese alloy trash plate casting inside the sand mold. The main objective of the study was to analyze parameters affecting the specific casting and to provide standard to produce quality casting in ABMI. Numerical experimentation and computational simulation method were carried out in the study. The computational simulation carried out using ANSYS Mechanical software. Simulation result shows the total time required to complete solidification of molten metal in the mold cavity which was 769.05 seconds. The transient thermal simulation model of casting process has not shown the methodology to model the process, initial and boundary conditions, nodal results, solidification front and cooling curve of the heat transfer analysis for the problem.

Tegegn and Balkeshwar (2019), [86] studied the casting of roller mill in ABMI using design of experiment and simulation method. Computational simulation of a three-dimensional roller m ill model was carried out by using ProCAST software for 50000 seconds. Taguchi method of numerical experimentations has been carried out for parameter optimization and analysis of variance (ANOVA). The casting process parameters such as permeability, pouring temperature, and moisture content identified using cause and effect diagram. Based on the numerical results of the study, their interpretation and the optimal values of the parameters have been determined. It has been found that the casting defects are minimized by 2.98%. The total solidification time using simulation software,

shrinkage porosity has been observed in both gating system and roller part. The cooling curve, cooling rate and effect of different parameters were not considered in the study.

2.5 Research Potential

All the authors listed above have been addressed numerical modelling of the casting process, prediction of solidification, use different FEM techniques, and recommend improving the casting process to minimize the defects.

Since the casting process has a complex shape, non-linear nature and tremendous effort to conduct experiments, the numerical analysis has received intensifying acceptance in the foundries in a different country. However, numerical simulation for the casting process in ABMI does not get much courtesy, and there is no available comprehensive work related to it. Available studies in case of ABMI to model the solidification of casting for specific case do not give an attention for numerical modeling. Studies conducted and listed above do not consider the variation of different parameters on the solidification of casting in one study. Hence, this study will address transient heat transfer analysis of solidification during the sand-casting process using FEM. The lack of attention to computational modelling of the sand-casting process in local foundries, including ABMI, is motivation to undertake this study.

Chapter 3: Research Methodology

3.1 Introduction

In this chapter methodologies utilized for fulfilling the specific objectives of the study presented step-by-step. Selecting particular sand casting as a case study; determination of thermophysical properties for the cast and mold material; mathematical modeling of the solidification process by utilizing FEM; and computational modeling of the chosen sand-casting processes utilizing ANSYS program performed to achieve the primary objective of the study. Methodologies used within the study presented in detail via the following subsections.

This section introduces the method employed for the study and details of numerical expressions of the overall modelling of solidification of material by sand-casting to achieve the research objective mentioned above. Figure 3.1 show the schematic diagram of the conceptual framework of the applied methodologies. The main sections of the methodologies are:

(1) Process Selection and Data collection.
(2) Thermophysical property determination of the selected sand-casting process.
(3) Computational modelling of the sand-casting process by using ANSYS software.
(4) Validation of the study with Experimental studies from work of Literatures.

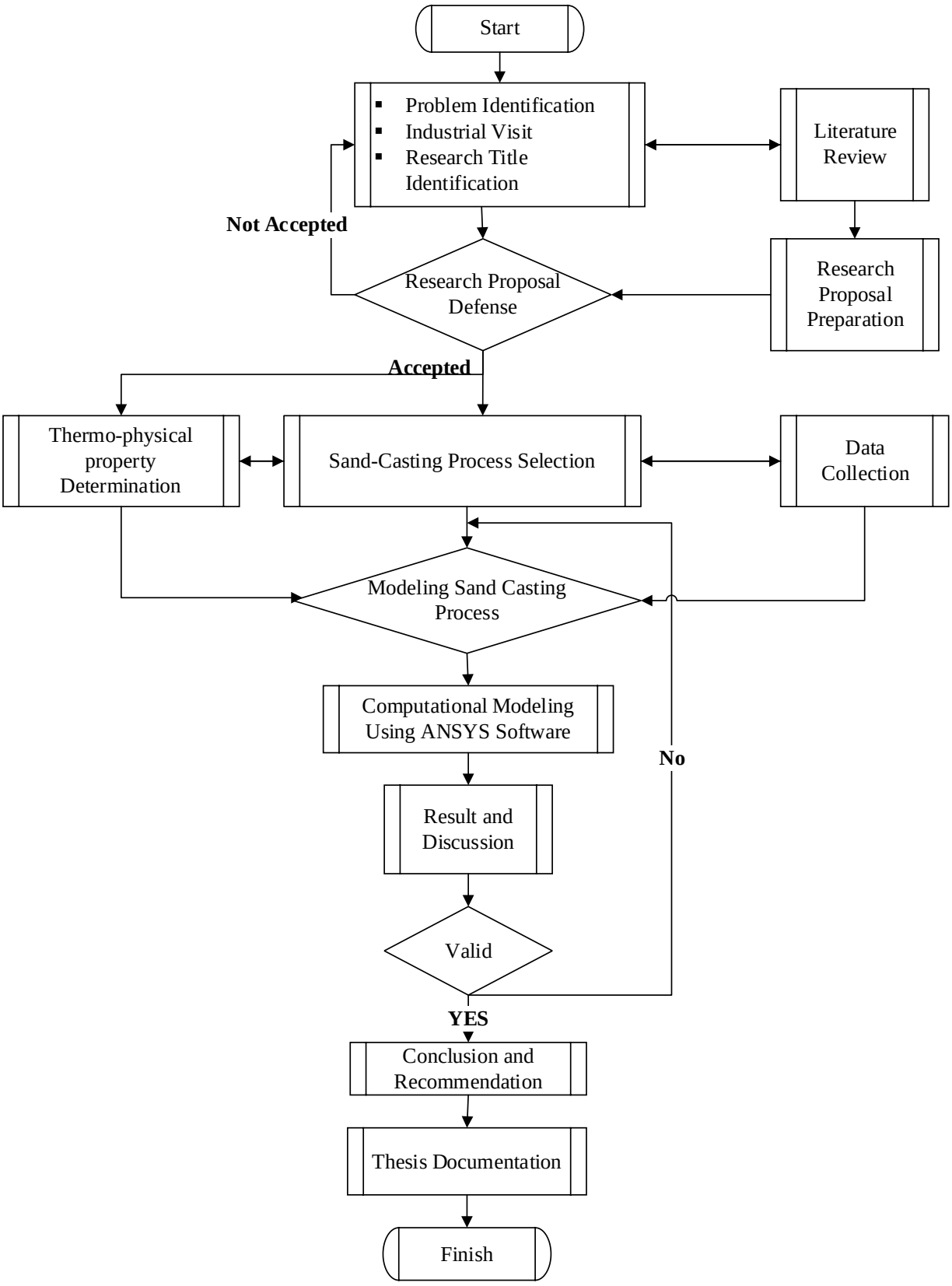

Figure 3.1 Methodology Flow chart of the study

3.2 Process Selection and Data Collection

3.2.1 Case Study and Process Selection

In this study, a case study carried out in the local metal products manufacturing industry called ABMI. The study conducted based on primary data from the sand-casting process, for the case study different process was selected with interest to model the sand-casting in pure metals and alloys in the industry to perform modelling of the sand-casting process.

In ABMI, there are many metals manufacturing processes. Metal casting, heat treatment, and mechanical workshop is the basic departments in the industry. The metal casting shop includes sand preparation and reclamation, metal melting furnaces, mold design, and making units. Centrifugal casting plant is not operational due to maintenance and foundry personnel problems in the industry. The sand-casting shop in the shop utilizes ferrous and non-ferrous molten metals to get the desired shape.

From the sand-casting foundry operation, for this study, the casting of ash cleaner door (case 1) and manhole frame (case 2) from cast alloy (grey cast iron); and casting of a flywheel (case 3) from pure metal (aluminum); is selected for the study. The cases selected based on different factors. The production capacity of products, the simplicity of geometry, and encompassing different types of metal solidification, and recommendations from the foundry personnel. The geometry of the models and its overall dimensions are given in appendix B.

3.2.2 Data collection

Available data for the simulation collected from the company. During the study, the following thermal data used for the study gathered.

Ambient temperature = 293.15k recorded by the company
Mold temperature = 298.15k recorded by the company
Pouring temperatures for the casting process in the foundry for the selected cases tabulated below.

Table 3.1: Pouring temperature of different casting material at ABMI

Material	***Pouring temperature (K)***
Grey cast iron	1673
Pure Aluminum	1073

Source: data from ABMI

3.3 Thermophysical Property Determination

In order to study the solidification process of the sand-casting process, determining the thermo-physical property of the sand and metal is a vital task. However, the availability of accurate and reliable thermophysical data in the simulation of the solidification process is a severe problem [87]. Experimental determinations of thermo-physical properties are reliable, and it is also tricky. In ABMI, there is no data related to the thermophysical properties of sand and metal since the thermophysical properties are rely depend on the composition of the metal. Different authoritative and comprehensive compilations of critically and systematically evaluated thermo-physical property data are presently available.

Juan J. and Peter N. [88] suggest using reliable sources of thermophysical sources of data's. The sources of data listed in the American Society of Metals (ASM) handbook is:

- Recommended Values of Thermophysical Properties for Selected Commercial Alloys by K.C. Mills. Experimental determination, estimation, and validation of the thermophysical properties in the solid and liquid states [89].
- The ASM International Materials Properties Database Committee publishes a comprehensive thermal properties database of most commercially available metals [90].
- The Center for Information and Numerical Data Analysis and Synthesis (CINDAS) generated and recommended reference values for diverse materials [29, 47, 50].

3.3.1 Thermophysical Property of the selected processes

The selected process is the casting of ash door cleaner for the boiler furnace of the sugar factory and automotive flywheel. The material type used for the casting process gathered from the foundry. The mold material is silica sand. The material to be cast is grey cast iron and Aluminum, which has non-linear nature in which the properties changed with varying temperatures.

3.3.1.1 Property of the casting material

Grey Cast Iron

The grey cast iron used to cast is a grade of G-25. The chemical composition of the cast alloy is measured in the laboratory and listed in the following table. The chemical composition measured in the laboratory of the company by using a Spectro meter.

Table 3.2: chemical composition (%) of the grey cast material

Grade	C	Cr	Mg	Mn	Si	S	P
Gr25	3.4-3.8	< 1.15	<0.002	< 0.6	1.7-2.2	< 0.1	< 0.15

The exact chemical composition of the grey cast iron not given in the data of the company. The chemical composition of grey cast iron used in this study is selected accordingly from the resources above listed by ASM. The chemical composition used for the study presented in Table 3.3 below. The values are given in the recommended data's [89].

Table 3.3: chemical composition of grey cast iron.

C	*Cr*	*Fe*	*Mg*	*Mn*	*Mo*	*Ni*	*P*	*S*	*Si*
3.72	0.95	91.9	<0.002	0.6	0.59	0.19	0.09	0.032	1.89

The melting and pouring temperature of the material listed in the references. The melting temperature is given as 1080 K- 1190 K [2][89]. The pouring temperature of the material specified in the manual of the company as 1340 ^{o}C - 1430 ^{o}C, the pouring temperature for grey cast iron is given as 1673 K in the ASM handbook [2], the pouring temperature for the cast iron given as value is 1613 K – 1755 K [91]. From the given data is the value of the melting and the pouring temperature used for this study is;

Melting temperature range: $T_m = 1353K - 1463K$

Pouring temperature: $T_p = 1673K$

Nonlinear thermophysical properties grey cast and Aluminum presented in Appendix A. The enthalpy of the cast metals during solidification can be calculated as follows. [92]

The average specific heat given as:

$$C_{avg} = \left(\frac{C_S + C_L}{2} \right) \tag{3.1}$$

Where:

$C_S = 660 \ J / Kg.k$

$C_L = 950 \ J / Kg.k$

$$C_{avg} = \left(\frac{660 + 950}{2} \right) J / Kg.k$$

$$C_{avg} = 805 J / Kg.k$$

The calculation for the specific heat at the transition region can be given as:

$$C^* = C_{avg} + \frac{L}{(T_L - T_S)} \quad (3.2)$$

$L = 220\ KJ / Kg$

$L = 220\ KJ / Kg * density\ of\ the\ material$

$l = 220 KJ / Kg * 7200 Kg / m^3 = 1.584 * 10^6 KJ / m^3$

$$C^* = 0.805\ KJ / Kg.k + \frac{220\ KJ / Kg}{(1463 - 1353)k}$$

$C^* = 2.805\ KJ / Kg.k$

The enthalpy below the solidus temperature for the casting metal is given as follow

$$H_{-} = \rho * C(T - T_o) \quad (3.3)$$

The reference temperature is 273 K.

Applying equation (3.3) at the reference temperature 273 K gives

$H_{@273k} = \rho * C(273 - 273)$

$H_{@273k} = 0\ J / m^3$

The enthalpy at the solidus temperature is calculated by the following equation

$$H_s = \rho_s C_s (T_s - T_o) \quad (3.4)$$

$H_s = 6964\ \text{Kg/m}^3 * 660\ J / Kg.k\ (1353 - 273)k$

$H_s = 4.96E09\ J / \text{m}^3$

The enthalpy at the liquidus temperature is calculated as follow

$$H_l = H_s + \rho_l C^* (T_l - T_s) \quad (3.5)$$

Substituting the corresponding values in the given equation as

$H_l = 4.96E09\ J / m^3 + 6764\ Kg / m^3 * 2805\ J / Kg.k * (110k)$

$H_l = 4.96E09\ J / m^3 + 2.09E09\ J / m^3$

$H_l = 7.05\ E09\ J / m^3$

The enthalpy at a temperature above the liquidus temperature calculated by the equation below

$$H_{+} = H_l + \rho C_l (T - T_l) \quad (3.6)$$

At a temperature above the liquidus temperature (1773 K) the value of the enthalpy is gives

$H_{@1773k} = 7.05 * 10^9\ J / m^3 + \left(950 kg / m^3 * 6609 J / kg.k (1773 - 1463)k\right)$

$H_{@1773k} = 13.8 * 10^9\ J / m^3$

Aluminum

The enthalpy value of Aluminum also calculated using the above methods and the result is tabulated below

Table 3.4: Enthalpy data for pure Aluminum

Temperature (K)	***Enthalpy (J/m^3)***
0	0
968	$1.6857*10^9$
970	$2.7614*10^9$
1273	$3.6226*10^9$

Source: [92]

Thermal conductivity of cast materials

The thermal conductivity used in the study gathered from an available relevant literature review. The data presented in the following tables

Table 3.5: Thermal conductivity of grey cast iron used for the study

Temperature (k)	293	298	373	473	673	973	1353	1463	1673	1773
Thermal conductivity $(W/m.k)$	52	49	48	46	42	35	29	26	28	29

Source: [89]

Table 3.6: Thermal conductivity of pure Aluminum iron used for the study

Temperature (k)	0	273	473	573	673	803	1073
Thermal conductivity $(W/m.k)$	206	208	215	228	249	268	290

Source: [92]

3.3.2 Property of Mold Material

In the company's history, ABMI used a mold material called Isomer that imported from Italy, German and other European countries. The mold material used currently for the process is silica sand (SiO_2). The sand locally available and comes from Merhabete, Northern Shewa, Ethiopia.

The property used for this study is linear with temperature. Some of the characteristics of silica sand is used in the company and given in the following table.

Table 3.7: Properties of silica sand

Characteristics	**Value**
Color White	light brown
Grain fineness number (mesh)	45-60
Fusion point	(1700K-1800K)

Source: company data sheet

Resin and catalyst used as binders in molding system. Resin acted as a bonding material and a catalyst used to facilitate the reaction of resin and sand. The chemical name of catalyst and resin are Sulphonic acid Furfural alcohol, respectively, in proper composition.

The property of the silica sand as a mold material is not temperature-dependent. Most works of literature used the value of the mold as not dependent on temperature [45], [20]. The ASM handbook of casting [2], suggests using non-linear data for the mold material. However, Pariona et.[45], [93], [94] did the numerical simulation to predict the filling and solidification process in a sand mold. The study's material is non-linear for the former and linear for the second study, but the result shows no tangible difference in the temperature profile. So, in this study, the silica sand property does not vary with temperature.

3.3.2.1.1 Measuring Density of Silica Sand

The value of density of silica sand used in any analysis in ABMI used as 1800 kg/m^3. The density of the silica sand used for molding application is not measured. To get the actual density of the sand with the bonding materials, experimental measurement of the density in the laboratory is the best approach. The density of the silica sand with the bonding material conducted on an apparatus called analytical balance.

Figure 3.2- Sample silica sand bonded with risen

The machine has five-digit readability. To determine the specific gravity of the silica sand, a 50 cm^3 specification pycnometer used to put the silica sand.

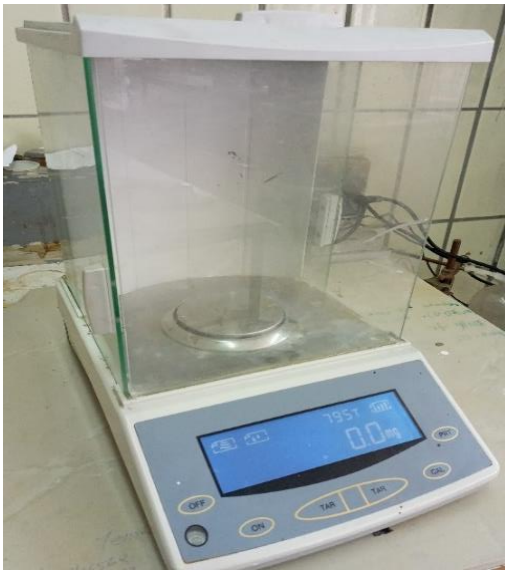

Figure 3.3 Digital balance.

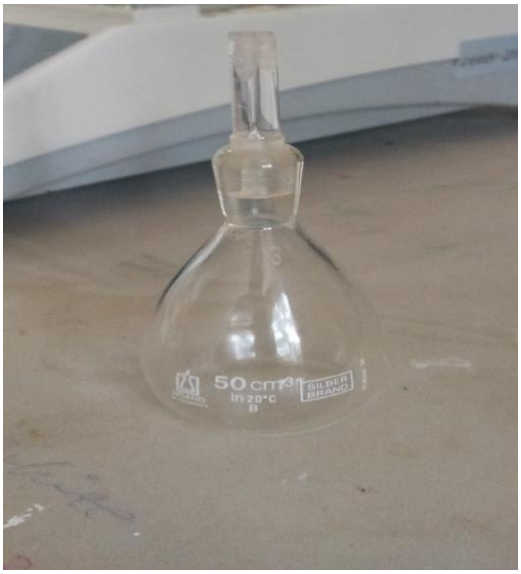

Figure 3.4- Pycnometer

The procedure of the test is starting with cleaning the pycnometer. Initially, a mass of the pycnometer measured in the digital balance; secondly, the silica sand is put into the pycnometer in the proportion of one-third of the pycnometer's volume to measure the mass of the silica sand. Thirdly the mass of the silica sand plus distilled water is measured, and finally, the mass of the distilled water only measured.

After conducting all four measurements, test values recorded. To check the reputability of the test, four trial tests taken. The mean value of the trials taken as a value of the measurement.

Table 3.8: Experimental result of density measurement

Description	***Sample***	***Trial 1***	***Trial 2***	***Trial 3***	***Trial 4***
Mass of empty flask	$m_1\ (g)$	28.5499	28.6642	28.5742	28.6351
Mass of flask with sample	$m_2\ (g)$	50.9795	47.2180	47.2294	51.6605
Mass of flask with sample and water	$m_3\ (g)$	92.2035	89.8512	89.9553	92.4832
Mass of flask and water	$m_4\ (g)$	78.6243	78.6313	78.6372	78.6289

To calculate the density of the silica sand the following equation used.

$$\rho_{sand} = \frac{m_{sand}}{V_{sand}} \qquad (3.7)$$

To determine the density, first, the exact value of the volume of the pycnometer calibrated. The process calibrated according to checking the pycnometer's volume by using the measured mass of

distilled water. Since the density of distilled water and air known at a given temperature, the pycnometer's volume calculated using the following equation.

$$V_{flask} = \frac{m_4 - m_1}{\rho_{water} - \rho_{air}} \tag{3.8}$$

At room temperature, 293 K, the density of air and distilled water are.

$$\rho_{air} = 0.0012466\ g/cm^3$$
$$\rho_{water} = 0.99820\ g/cm^3$$

Using the equation above (Eqn. 3.8), volume of the silica sand for the first trial.

$$V_{flask} = \frac{(78.6243 - 28.5499)\ g}{(0.99820 - 0.0012466)\ g/cm^3} = 50.2274\ cm^3$$

The volume of the pycnometer is varying with its actual volume due to repetitive using the flask for different tests. Due to the chemical and temperature effect on the flask, the volume increased. Thus, measuring of the volume during the test is a necessary task.

The specific gravity of the distilled water known at a given temperature. The density of distilled water during the test calculated by using the following formulae.

$$\rho_{water} = \frac{m_{water}}{V_{flask}} \tag{3.9}$$
$$\rho_{water} = \frac{m_{water}}{V_{flask}} = \frac{m_4 - m_1}{V_{flask}} = \frac{(78.6243 - 28.5499)g}{50.2274 cm^3} = 0.9970\ g/cm^3$$

The standard density of distilled water at 20°c is $0.99978\ g/cm^3$. The error estimated for the known density calculated as

$$\%error = \frac{\rho_{\text{measured}} - \rho_{\text{standard}}}{\rho_{\text{standard}}} \tag{3.10}$$
$$\%error = \frac{\rho_{\text{measured}} - \rho_{\text{standard}}}{\rho_{\text{standard}}} = \left(\frac{0.9970 - 0.99820}{0.99820}\right) * 100\% = 0.125\%$$

The measurement error is within an acceptable range. From this estimated error, the test is acceptable.

To calculate the density of silica sand, first, let us evaluate the volume of the sample inside the pycnometer during the test. The volume of the sample is the value of the volume of distilled water subtracted from the total volume of the pycnometer with sample and distilled water.

The mass of distilled water in the flask with the sample is calculated as

$$m_{water} = m_3 - m_2 \quad (3.11)$$
$$m_{water} = (92.2035 - 50.9795)\ \text{g} = 41.224\ \text{g}$$

The volume of the distilled water in the flask with the sample is to be

$$V_{water} = \frac{m_{water}}{\rho_{water}} \quad (3.12)$$
$$V_{water} = \frac{41.224\ g}{0.99695\ g/cm^3} = 41.2983\ cm^3$$

The volume of the sample inside the flask is to be

$$V_{sample} = V_{flask} - V_{water} \quad (3.13)$$
$$V_{sample} = (50.2274 - 41.3501)\ cm^3 = 8.9291\ cm^3$$

Finally, the density of the sample is determined by using equation (eqn. 3.9)

$$\rho_{sample} = \frac{m_2 - m_1}{V_{sand}} \quad (3.14)$$
$$\rho_{sample} = \frac{50.9795 - 28.5499\ g}{8.8974\ cm^3} = 2.512\ g/cm^3$$

The density of the silica sand to use in this first trial is $2512\ kg/m^3$.

In the same way, the value of density in the remaining three trials is tabulated below.

Table 3.9: Density measurement data and statistics

Trial	*Mass of sample (grams)*	*mass of water (grams)*	*Volume of flask (cm^3)*	*Density of water (grams/cm^3)*	*Standard water density (gram/cm^3)*	*Percentage error (%)*	*Volume of water (cm^3)*	*Volume of silica sand (cm^3)*	*Density of silica sand (gram/cm^3)*
1.	22.430	50.0744	50.227	0.9969	0.9982	0.12489	41.298	8.929086	2.5120
2.	18.550	49.9671	50.119	0.9969	0.9982	0.12489	42.710	7.409717	2.5040

3.	18.662	50.0730	50.226	0.9969	0.9982	0.12489	42.803	7.423073	2.5165
4.	23.030	49.9897	50.142	0.9969	0.9982	0.12489	40.896	9.246151	2.4903
$\bar{X}$	41.851	50.0235	50.176	0.9969	0.9982	0.12489	41.926	8.249499	2.5057
SD	0.9708	0.05314	0.0533	0	0	0	1.1912	1.195836	0.014104

From the data tabulated above with a standard deviation of 0.014, the mean density of the silica sand is 2.506 g/cm^3 or 2506 kg/m^3.

3.3.2.1.2 Specific Heat and Thermal Conductivity of Silica Sand

It is difficult to determine the thermophysical properties of silica sand experimentally since laboratories are not available locally. The thermophysical properties required for the study collected from available literatures. The thermal conductivity and the specific heat of the silica sand are given in different literature [20] [45]. The values given in different researches are different depending on the property of the silica sand. The thermal conductivity and specific heat values used in this study selected by referring actual density of the sand used in ABMI. The values extracted from a study [95]. The density value stated in the given literature is 2700 kg/m^3. Relative to other values of thermophysical properties in the literature, the value used has a relatively slight difference. Values are:

$k = 0.83\ w/m.k$
$Cp = 674$ J/kg.k

Even though experimental measurement of the sand density performed in a laboratory, the thermal conductivity and specific heat of the silica sand used in ABMI foundry is not measured. To accommodate the stated problem in the study's different thermophysical properties, the silica sand used as a scenario. The cases selected from available relevant previous studies on solidification modelling. The data from the literatures given below:

Scenario One:

The ASM handbook gives a thermophysical property correlation for silica sand with different mesh (grain fineness number). The grain fineness number, the mesh of silica sand in ABMI, ranges from

45-60. According to a couple of studies conducted in ABMI, the grain fineness number is 50.81 and 53.8 [37], [86]. For silica sand of mesh size ranging from 50-70 is given as follows.

$\rho = 1634\ kg/m^3$

$Cp = 1.066 + 8.676*10^{-5}\mathrm{T}$ (J/kg.k)

At the mold temperature which is 298k the value of specific heat for silica sand is

$Cp = 1091.9$ J/kg.k

Besides the thermal conductivity of silica sand is given as

$k = 0.676 - 0.793*10^{-3}\mathrm{T} + 0.556*10^{-6}\mathrm{T}^2$ (W/m.k)

At the mold temperature of 298k the thermal conductivity value is to be

k=0.49 $W/m.k$

Scenario Two

Most studies on modelling solidification of sand-casting use a property of the mold as temperature independent. In this study, one case seen for temperature-dependent thermophysical property for the silica sand. The thermophysical properties are taken from a study by Diego J. Celentano et al., [96]. The density in their study used is 1550 kg/m^{3,} and the thermal conductivity and specific heat values given in the following table.

Table 3.10: Non-linear thermal conductivity and specific heat of silica sand

Temperature (K)	*Thermal conductivity (W/m K)*	*Specific heat (J/kg K)*
293	0.54	1827
573	0.57	1980
773	0.65	2000
973	0.79	2000
1173	1.00	2100
1373	1.26	2150
1573	1.59	2200

Scenario Three

The study conducted on modelling of casting [12] gives a thermophysical property of silica sand as follows.

$\rho = 1400\ kg/m^3$
$k = 0.8\ w/m.k$
$Cp = 800$ J/kg.k

Scenario Four

Pariona et al. [45] probe the solidification of pure iron in sand and mullite mold using FEM. In this study, the thermophysical properties were assumed as linear with temperature and given as below:

$\rho = 1474.3\ kg/m^3$
$k = 0.52\ w/m.k$
$Cp = 1172.3$ J/kg.k

3.4 Computational Modelling of the Sand-Casting Process

3.4.1 Introduction

Different numerical methods used to computationally model solidification heat transfer of the casting process. The finite volume method (FVM), finite difference method (FDM), FEM, boundary element method (BEM) are the best known in solving the problem. [3],[27]. The numerical simulation of any FEM problem solving adopted a common methodology as presented in flowchart diagram below.

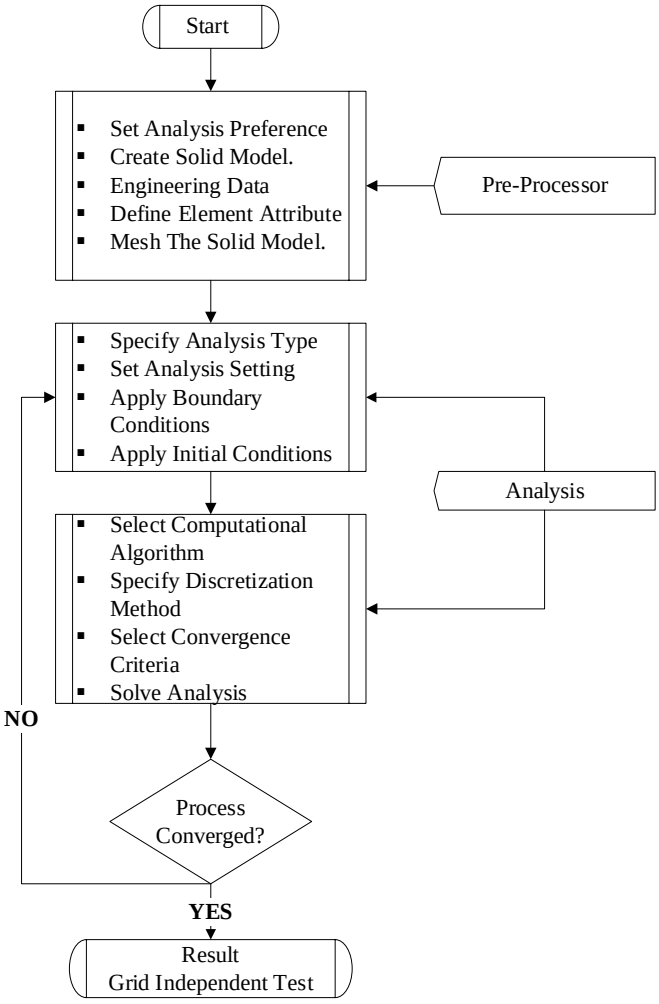

Figure 3.5- Methodology flow diagram of computational modelling of the process

3.4.2 Boundary Condition and Initial Conditions of the Process

3.4.2.1 Boundary conditions

The boundary conditions for the solidification simulation are the convective heat transfer between the ambient air and the mold applied on the vertical and horizontal edge. The convective heat transfer with the surrounding is set as a constant throughout the process since the effect of temperature dependent convective heat transfer coefficient is not significant. Most of the related works used constant heat transfer coefficient for sand casting process.

3.4.2.1.1 Convective Heat Transfer Coefficient

The convective heat transfer coefficient between the ambient and the sand mold box determined by the empirical relation. The average free convection coefficient can be determined based on the dimensionless parameters on the film temperature [97].

$$T_f = \frac{T_\infty + T_w}{2} \qquad (3.15)$$

The ambient temperature in the foundry is 293 K. The wall temperature of the mold immediately after pouring is taken as 1673 K for grey cast iron and 1000 K so that the film temperature is

$T_f = \frac{1673 + 293}{2} = 993k$ for case 1 and case 2

$T_f = \frac{1000\ K + 293}{2} = 646.5k$ for case 3

For the case of the study, the geometry selected for simulation is a two-dimensional section of the cast and mold assembly. The section is taken at a purposely selected plane to include all the necessary parts of the cast body. Therefore, the heat transfer coefficient can be determined for the horizontal and vertical surfaces since the two-dimensional model has an edge on the horizontal and vertical surfaces.

The convective heat transfer coefficient (h) correlation determined from the dimensionless parameters, namely the Nusselt number, Grashof number, Prandtl number, and Rayleigh number. Different correlations are given in different conditions cited in [97].

The Grashof number is found using

$$Gr = \frac{g\beta(T_w - T_\infty)L^3}{\upsilon^2} \qquad (3.16)$$

The property of the air at the film temperature tabulated in different textbooks in reference [97]–[100].

The Rayleigh number is the product of the Prandtl and Grashof number.

$$Ra = Gr * \Pr \qquad (3.17)$$

The value of the Prandtl number for the air and the calculated Grashof number can give the Rayleigh number as follow

The average Nusselt number given

$$Nu = 0.68 + \frac{0.67Ra^{1/4}}{\left[1 + (0.492/pr)^{9/16}\right]^{4/9}} \quad \text{for } Ra < 10^9 \qquad (3.18)$$

$$Nu^{1/2} = 0.825 + \frac{0.387Ra^{1/6}}{\left[1 + (0.492/pr)^{9/16}\right]^{8/27}} \quad \text{for } 10^{-1} < Ra < 10^{12} \qquad (3.19)$$

The value of convective heat transfer coefficient (h) can be determined from the following basic equation

$$h = \frac{Nu * k}{L} \qquad (3.20)$$

Heat transfer coefficient on the horizontal surface.

Since the models are two-dimensional, the horizontal surface's heat transfer coefficient is different from a vertical surface. The heat transfer coefficient on the horizontal surface heated from the bottom can be calculated as follows.

The Nusselt number can be given by

$$N_u = 0.27 R_a^{1/4} \quad (3.21)$$

The characteristic length calculated as follows

$$L = \frac{As}{p} \quad (3.22)$$

P is the perimeter of the horizontal length

Computing equation (3.15) through equation (3.22) to get the heat transfer coefficient on the vertical and horizontal surface of the mold in all three cases are presented below in Table 3.11.Table 2.1

Table 3.11: Results of heat transfer coefficient calculation

Case	*Height (m)*	*Length (m)*	$T_a(k)$	$T_w(k)$	$T_f(k)$	G_r	R_a	N_u	h_v $(W/m^2.k)$	h_h $(W/m^2.k)$
1	0.4	0.187	293	1673	993	$3,720,634,148$	$2.717*10^9$	168.2	***10.6***	***8.3***
2	0.1	0.0405	293	1673	993	$930,158,537$	$6.539*10^8$	83.2	***21.1***	***27***
3	0.2	0.0556	293	1073	783	$1,860,317,074$	$1.308*10^9$	166.23	***21.1***	***23.2***

3.4.2.2 Initial conditions

The initial condition for the process is the initial mold temperature, the ambient temperature, and the initial pouring temperature of the metal. The ambient temperature in the foundry for a specific casting measured as 293k. The pouring temperature for the grey cast iron is 1673k, and the initial temperature of the mold body found 298k.

3.4.2.3 Pouring Temperature

The pouring temperature of metals used in the study were used as the solidification starting temperature. According to Cruchaga et al. cited in Celentano et.al.,[81] there is non-uniform temperature distribution during filling of the mold cavity. However, for simplicity, an instantaneous filling of the mold cavity is assumed in the present analysis considering a stagnant liquid alloy with a uniform initial (pouring) temperature distribution. This approximation is justified by the short filling

times usually found in many applications that, as a consequence, lead to relatively small temperature differences in the alloy. The approximation is also justified in ABMI [86].

3.4.3 Modelling of the Solidification on ANSYS Workbench Mechanical Solver

The computational modelling of the solidification process carried out using a FEM tool called ANSYS Mechanical Workbench. The alternatives in the software Transient Thermal Analysis, a part of ANSYS Mechanical package used for modelling thermal analysis of problems.

In the ANSYS workbench package, there are two options to solve thermal analysis of a process: transient thermal analysis and steady-state thermal analysis. Since the thermal load of the sand-casting process is time-dependent, its analysis is carried out by transient thermal analysis. ANSYS customer training manual [92] strongly suggests using transient thermal analysis to solve the solidification process.

The basic procedure used in the ANSYS Mechanical Workbench to solve the problem is presented in the following methodology flow chart.

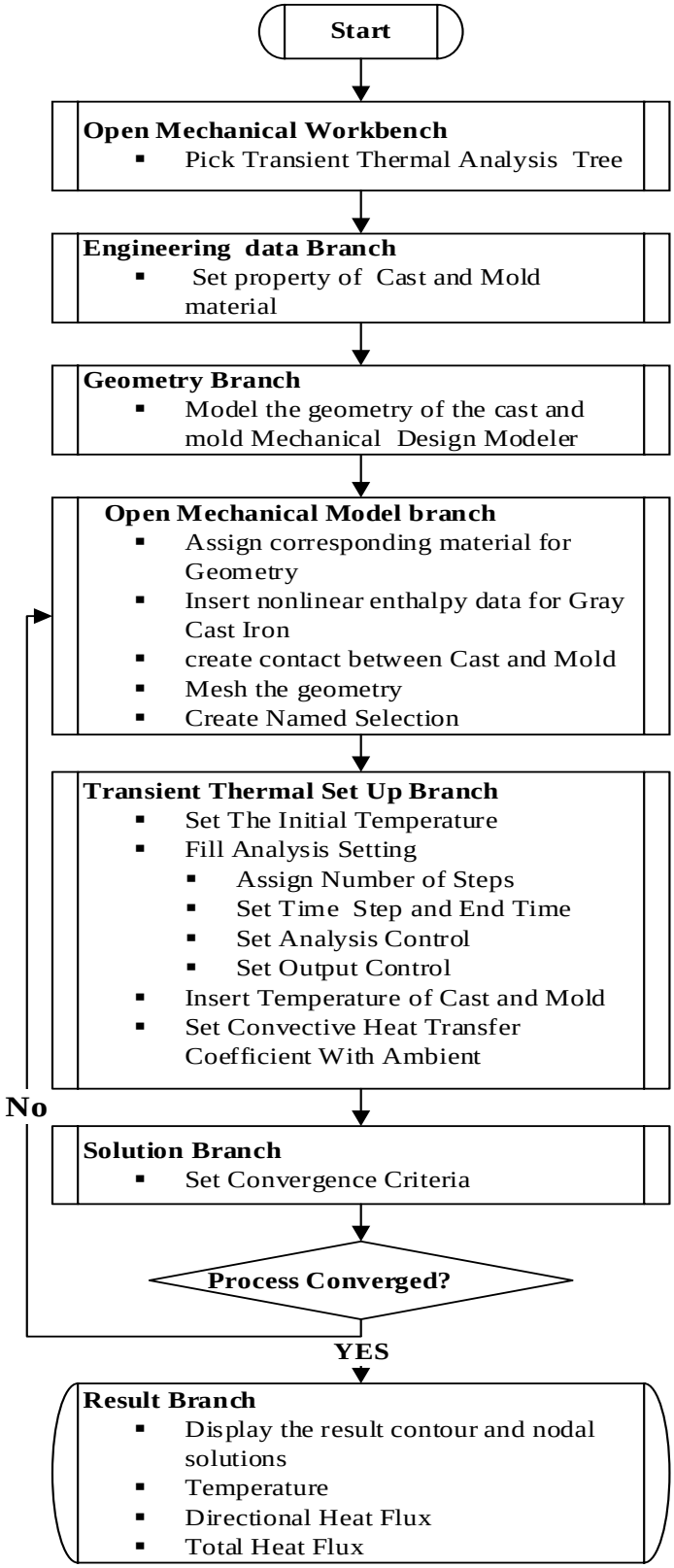

Figure 3.6: Steps used on ANSYS Mechanical Workbench

3.4.3.1 ANSYS Transient Thermal Setup

The ANSYS Transient Thermal setup used to simulate a model of a problem with non-linear temperature boundary conditions. The setup utilizes FEA to calculate temperatures and heat flux, based on given initial and boundary conditions and material properties, at discrete nodes generated by a discretization process performed by the software. As for all FEM, the transient thermal analysis has three main steps to solve any problem: preprocessor, analysis, and post-processor.

Pre-processor

Set the Analysis Preference.

The analysis preference for modelling the sand-casting process selected in the ANSYS mechanical workbench tree. The transient thermal analysis set as a preference analysis for the solidification process. The setup tree comprises six-step ladders: Engineering data, Geometry, Model, Setup, Solution and Results.

Engineering Data

Engineering data consists of material selection. ANSYS has the physical properties of many materials built into the system. However, grey cast iron and Aluminum material properties used for the simulation formatted in engineering data.

The mechanical project schematic gives default material data for any analysis. The default material data should be formatted by the material properties used in the study. The material used for the cast and mold is grey cast iron and silica sand mold. The property of the materials used for the grey cast iron is nonlinear, while the material property used for silica sand is linear since the nonlinear effect for the silica sand is negligible.[45], [92].

In the thermal analysis of solidification of the sand-casting process, there are four critical properties: density, specific heat, enthalpy, and thermal conductivity. The isotropic thermal conductivity of grey cast iron and pure aluminum as a function of temperature used in the study is presented in the figure below.

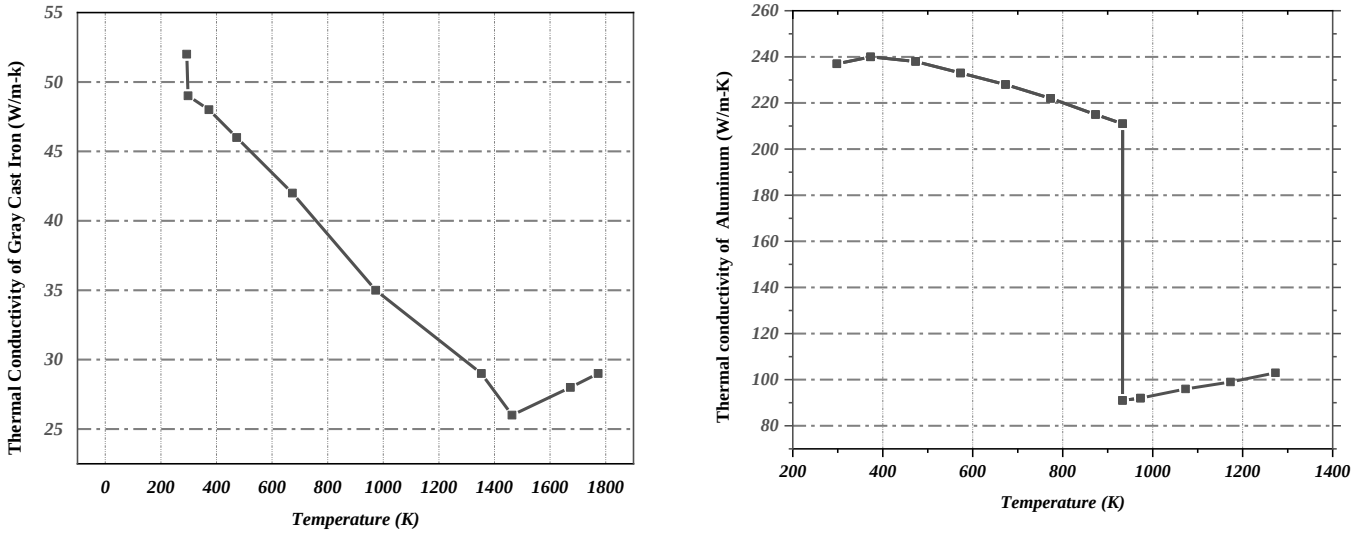

(a) (b)

Figure 3.7: Thermal conductivity of casting metals used in the study (a)-cast iron, (b) Pure-Aluminum

The enthalpy of the cast metals used in the study can be inserted via a command on the mechanical solver. Since the enthalpy property derived from both density and specific heat, those properties are overwritten in engineering data.

Geometry Modelling

Geometry is where the model is specified. The geometry model for all cases modelled in ANSYS Design Modeler. The geometries shown in the following figures.

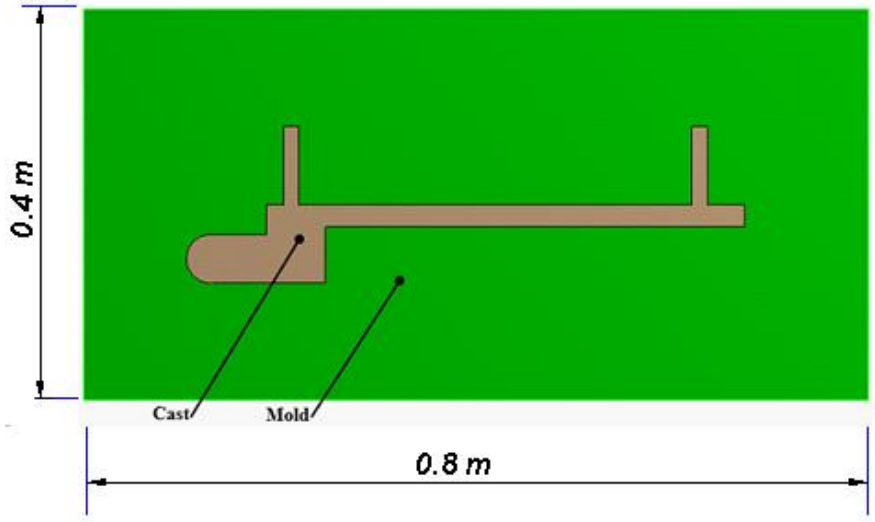

(a)

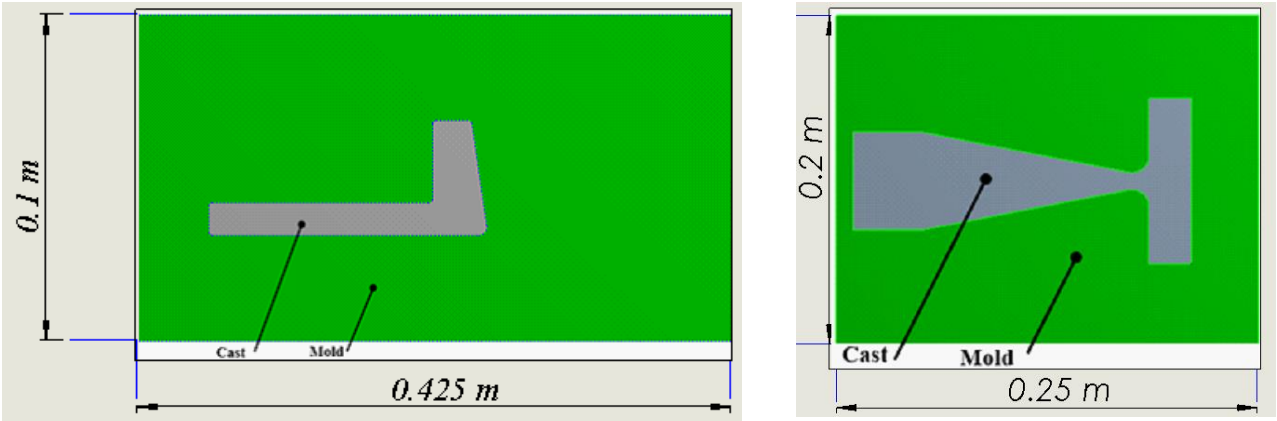

(b) *(c)*

Figure 3.8: Geometry of the cast and mold for (a); case one, (d); case two and (c); case three

Model

In this part ("model") of transient thermal set up, parameters that control the simulation are selected: Model, Transient Thermal, and Solutions. Transient Thermal comprised of Initial Temperature and Analysis Settings. This section is where the boundary conditions are specified as well. Solutions where the output values such as temperature and heat flux are specified.

The model part consists of Geometry, Coordinate System, Connections, and Mesh. The material assignment is performed in the geometry part according to the filled engineering data. The local and global coordinate systems also set for the given analysis as default or user-defined options. Contact regions between the cast and the mold bodies specified in the connection part of the setup. Finally, the meshing of the bodies performed by using appropriate meshing techniques for the problem. Named selection can also set in this section of the simulation of the setup. The simulation outline is shown in the following figure.

In the geometry part, the material is assigned for the cast body is Grey Cast Iron for cases one and two, while Aluminum is for the third case. The mold material used for all the cases in the study is Silica Sand.

Coordinate system

The coordinate system at specific locations was set for simulation. This option is used to define an x, y coordinate location and the orientation of the coordinate system. These locations later used to place objects known as "Probes" throughout the model that collects specific information at areas of interest. In the simulation, this was used to place the temperature and heat flux probes at specified locations on the cast and mold body.

Meshing Solid Models.

The selection of element size is critical since the accuracy of the simulation rests on it. A large number of small elements give more accurate results than fewer elements. However smaller element increases the computation time. The size of the elements selected after the grid-independent test performed for all cases. Element size and mesh statistics for all cases presented in Table 3.12 below.

Table 3.12: Mesh statistics

Models	***Element size***		***Number of Elements***	***Number of nodes***
	Cast	***Mold***		
Case 1	1.5 mm	2 mm	84,212	255,661
Case 2	1 mm	2 mm	11,454	35,223
Case 3	1.5 mm	2.5 mm	10,448	32,243

The result of the meshing process is presented graphically in Figure 1.1. The mesh type used in the study were quadrilateral mesh (quad-mesh) since this type of mesh is regular quad-mesh, which can be applied for surfaces with general topologies and has higher regularity.

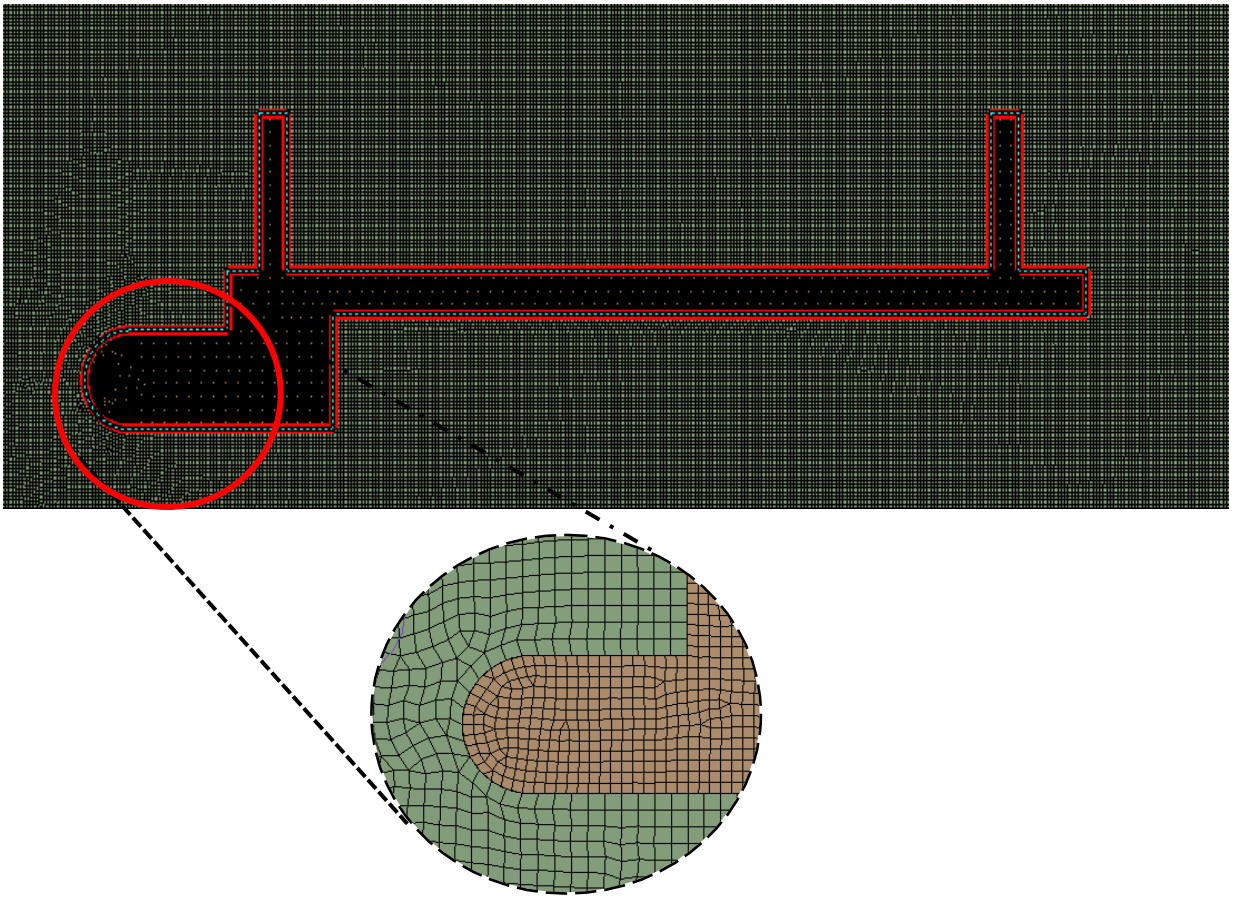

(a)

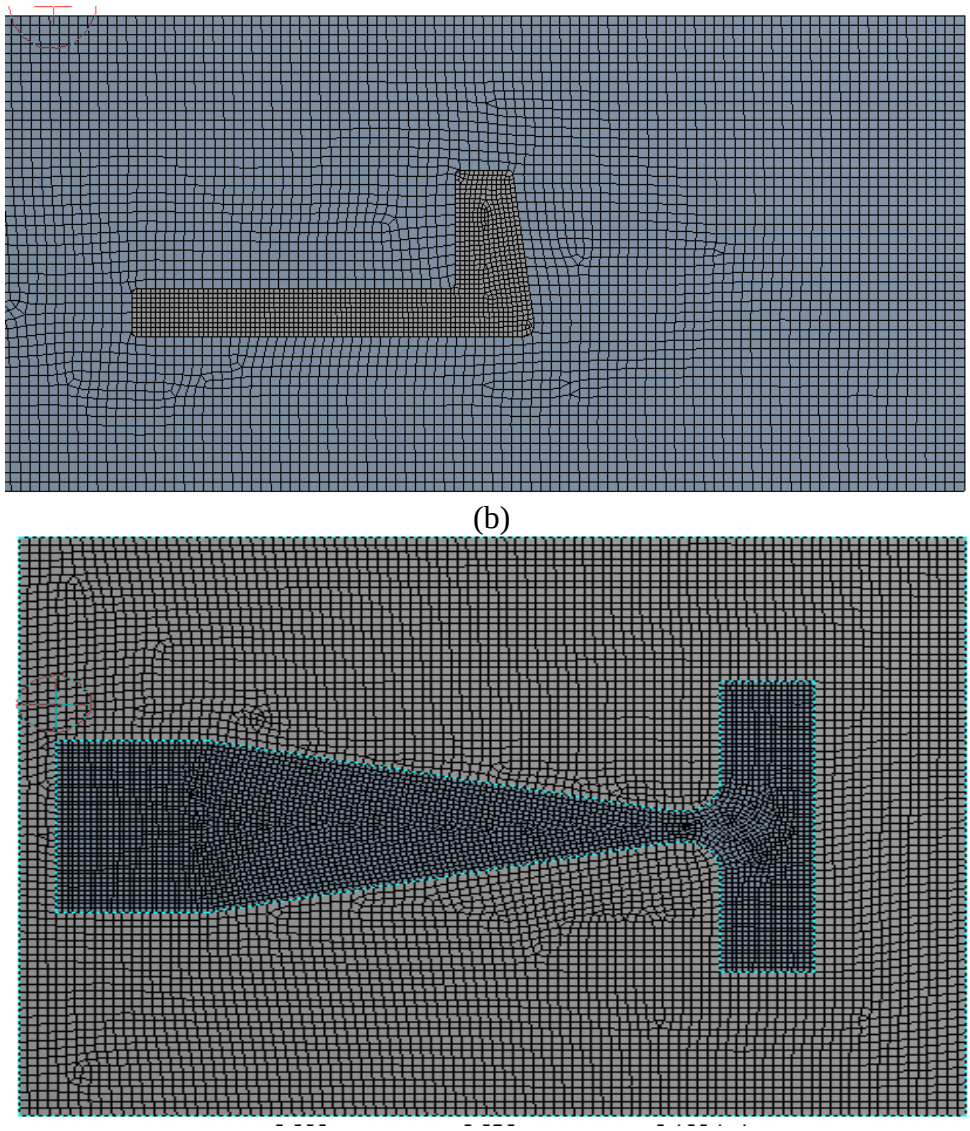

(b)

(c)

Figure 3.9: Meshing of the solid model for (a) case one, (b) case (2) and (c) case 3

Transient Thermal Analysis

In this section of the set-up, the initial conditions and analysis setting of the simulation is specified. The initial temperature, analysis setting, initial cast and mold temperature, convective heat transfer coefficient for the horizontal and vertical edge is assigned as calculated.

In the analysis, settings are several steps for the simulation are stated. Two steps are given for the solidification process. Parameters such as; End of the time step, minimum time step, maximum time step, solver control, non-linear control, and output control for two steps in each case were assigned in the simulation setup section.

For phase change problems a small minimum and initial time step is recommended, in the study the minimum and maximum time step value used for the first step number is 0.001 and 0.01, so the maximum iteration number per time steps were 100 in all cases since the first step end time set to be 0.1 seconds in all cases. For the three cases, the end time step for their cases is 2700, 500 and 1500 seconds. The minimum time step for the second step number used as 0.0001 in all cases. Hence the maximum iteration number per time steps in the three cases were 27,000,000; 5,000,000; and 15,000,000.

The ambient and initial temperature for mold and cast material as measured in ABMI were set. The boundary conditions, initial conditions and solver set up are presented in the following figure.

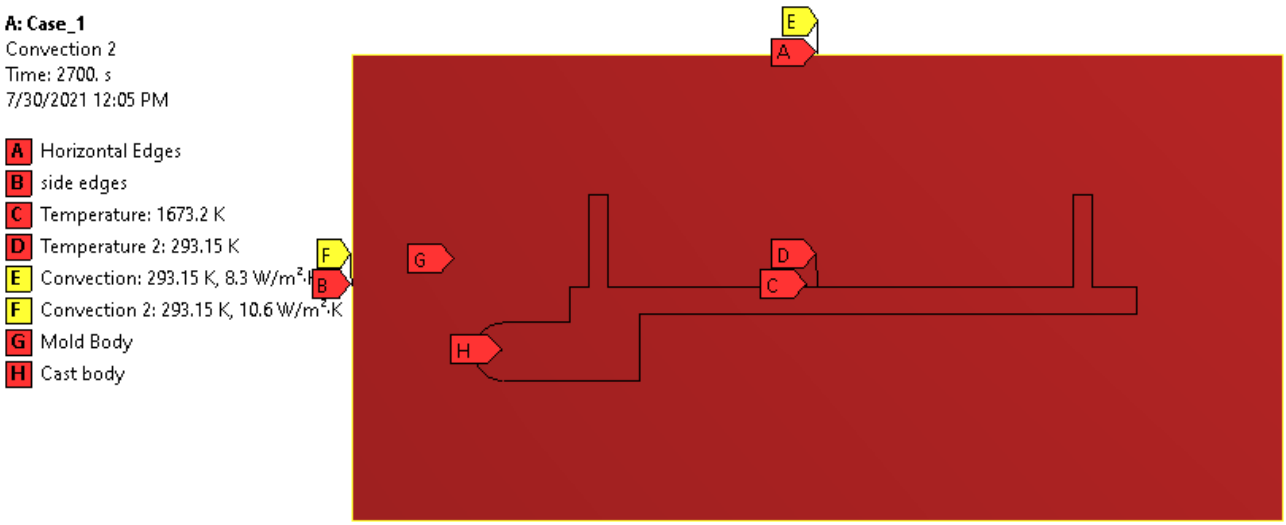

Figure 3.10: ANSYS model set up of case 1

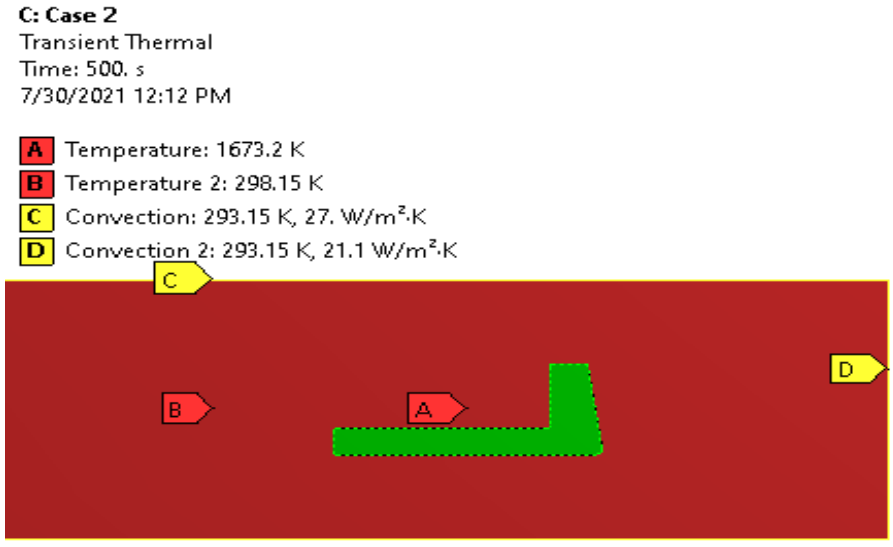

Figure 3.11: ANSYS model set up of case 2

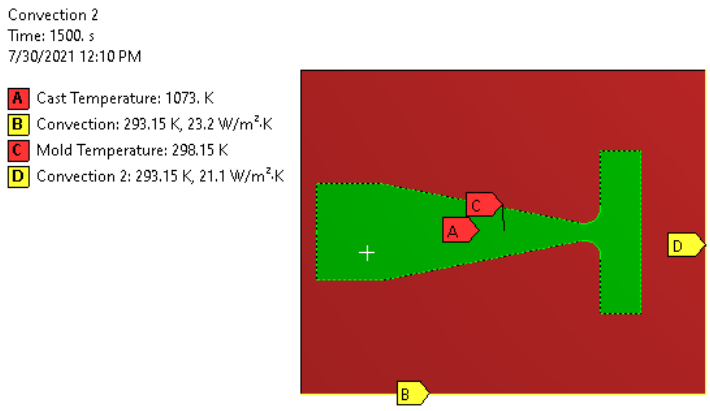

Figure 3.12: ANSYS model set up of case3

Solution

In this section of the simulation set up the model is executed to give a solution. The global maximum and global minimum temperature plots function as a function of time presented in the solution information section. Besides, the heat convergence checked in this section of the simulation set-up. In all the problem simulations, heat convergence with cumulative iteration is given as a graph, and the solution information shows the solution convergence at each time step of the analysis.

3.4.4 Mesh Independent Test

Finite element numerical methods are is a potent tool for simulating a variety of challenging real-world problems. However, the success of finding a solution does not guarantee numerical accuracy. When the number of finite elements in the model is more, the solution is more accurate. Nevertheless, how accurate is it? Is there a rule to decide the level of accuracy in the solution? How can we achieve accuracy? Those questions must get an answer to determine the minimum grid size or mesh resolution required to solve the problem by using FEM.

To show the problem's solution in the study is accurate adaptive mesh convergence techniques were performed in all the study cases. This technique allows the minimization of errors and uncertainties in the predicted results. Adaptive convergence requires the problem to be solved multiple times with different mesh discretization sizes, namely starts with coarse mesh move to finer mesh.

Table 3.13: Mesh dependent test for a different case shows the result of maximum nodal temperatures at 2700 seconds for case one, 500 seconds for case two and 1500 seconds for case three for different models of the sand-casting process with different element discretization. The time of display selected intentionally because the solidification already finishes before that time.

Table 3.13: Mesh dependent test for a different case of casting Models

Case 1			Case 2			Case 3		
Num. of Element	***Num. of Nodes***	***Max. Nodal Temp. (K)***	***Num. of Element***	***Num. of Nodes***	***Max. Nodal Temp. (K)***	***Num. of Element***	***Num. of Nodes***	***Max. Nodal Temp. (K)***
95,663	290,562	1282.55	35,223	11,454	1310.55	76,472	232,091	740.18
84,212	255,671	1282.55	33,190	10,805	1310.55	10,418	32,243	740.39
54,073	165,122	1282.55	15,267	4,908	1310.45	6,774	21,095	738.59
38,528	117,701	1282.55	8,654	2,753	1309.55	3,566	11,271	736.44
23,990	73,755	1282.45	5,646	1,777	1309.35	2,161	6,928	720.86
9,713	30,174	1282.25	4,038	1,257	1309.65	1,550	5,019	725.59
5,259	16528	1282.15	2,909	894	1307.15	1,149	3,770	721.65
3,363	10,686	1281.85	2,187	664	1302.25	883	2,928	725.65
2,342	7,517	1281.75	1,815	546	1304.85	736	2,457	726.35
1,704	5,529	1281.55	1,540	459	1306.85	564	1,929	733.9
1,312	4293	1281.95	1,247	366	1304.55	504	1,729	727.37
1,019	3,374	1281.05	1,050	305	1305.15	440	1,525	728.58
831	2,276	1281.45	-	-	-	-	-	-
705	2,376	1281.55	-	-	-	-	-	-

The maximum nodal temperature variation curve of the three cases of sand-casting solidification obtained using different element discretization also presented in Figure 3.15 via Figure 3.15.

It is seen that; the value of maximum temperature for the last models become the same. The relative error used to determine the per cent change of temperature between the consecutive mesh densities. In this case, the relative error is measured as zero. This phenomenon gives a clear insight that the FEM implemented is independent of the mesh size in all cases.

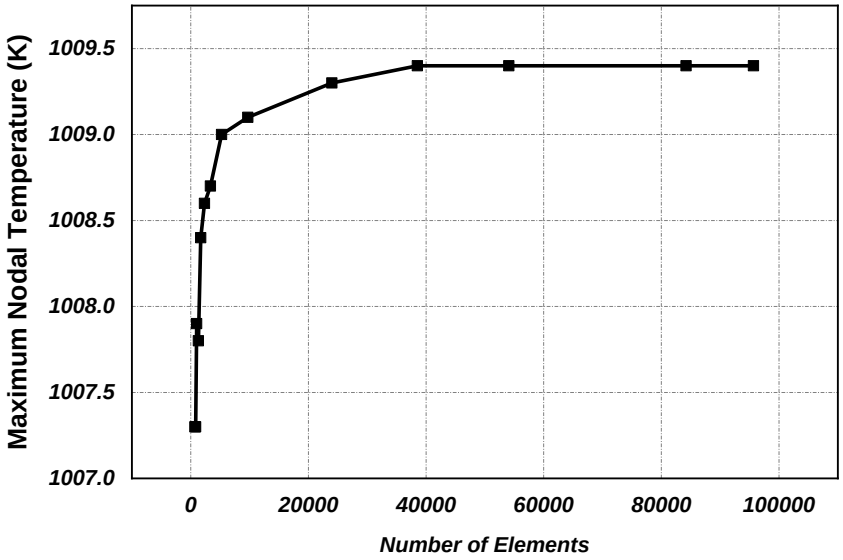

Figure 3.13: Mesh Independent Test for case 1

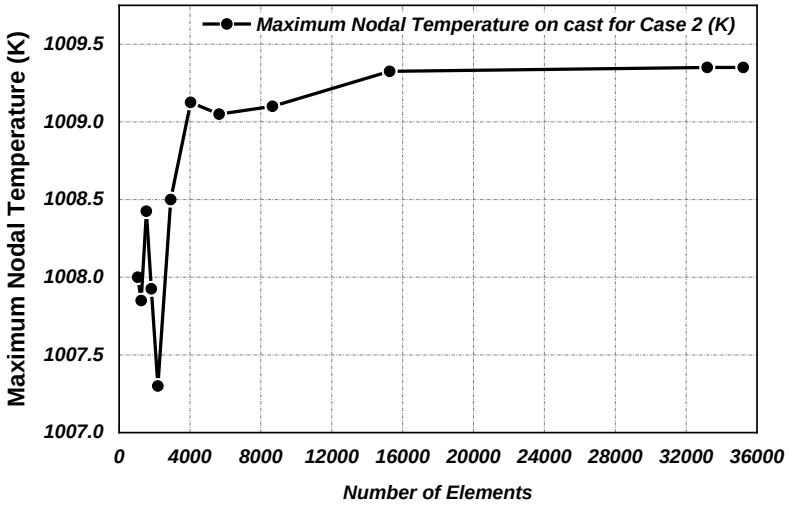

Figure 3.14: Mesh Independent Test for case 2

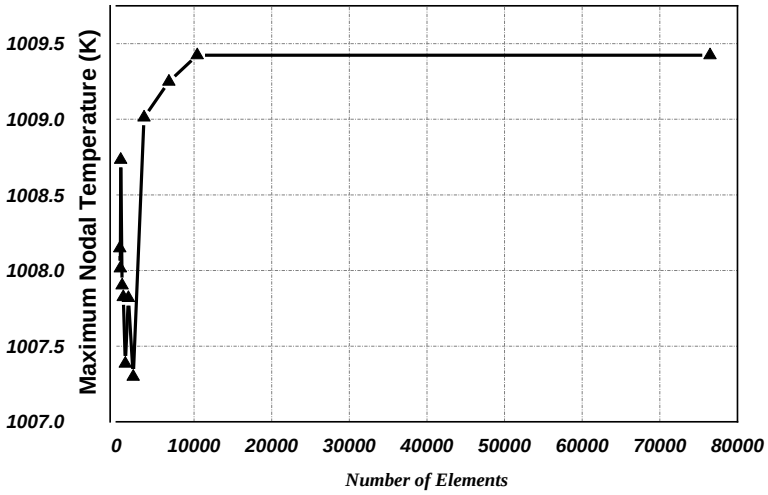

Figure 3.15: Mesh Independent Test for case 3

Chapter 4: Result and Discussion

4.1 Simulation Results

Based on the solution, solved results for all models obtained. The simulation results were presented temperature and heat flux at nodes, elements, and bodies of the selected interest on the problem domain at all-time steps. The result graphs from the simulation give insight into temperature distribution and heat flux distribution on the cast and mold.

4.1.1 Temperature Contour

The temperature contour plot on the cast and mold part for all cases is shown Figure 4.3 to Figure 4.6. The plot shows the temperature contour at different times, starting from the initial melt pours in the mold cavity to complete solidification of the melt inside the mold. The temperature in the cast decreases while the temperature contour in the mold part increases as the heat transfer occurs from the molten metal cast part to the mold part. The simulation result of temperature contour shows the nodes in which the temperature is maximum and minimum inside the selected part.

Figure 4.1 via Figure 4.4 shows the contour of temperature during the solidification of the grey cast iron at 2700 seconds of casting process. It can be seen from the graph the maximum nodal temperature inside the cast is reached at 1673.1 K at initial stages (5 seconds), 1282.6 K at last stage 2700 seconds. The blue color shows the lowest temperature region while the red color shows the maximum temperature region.

It can also be observed during the initiation of solidification process the temperature of the melt drops drastically around the contact region with mold walls. Hence, the minimum temperature is exhibited in the upper corner area of the cast part since the place is where the metal contacts with the mold first and the material thickness in this place is the smallest in the cast part. Besides, the maximum temperature in the mold part is encountered in the inner wall of the mold part around the geometry of more molten metal is introduced.

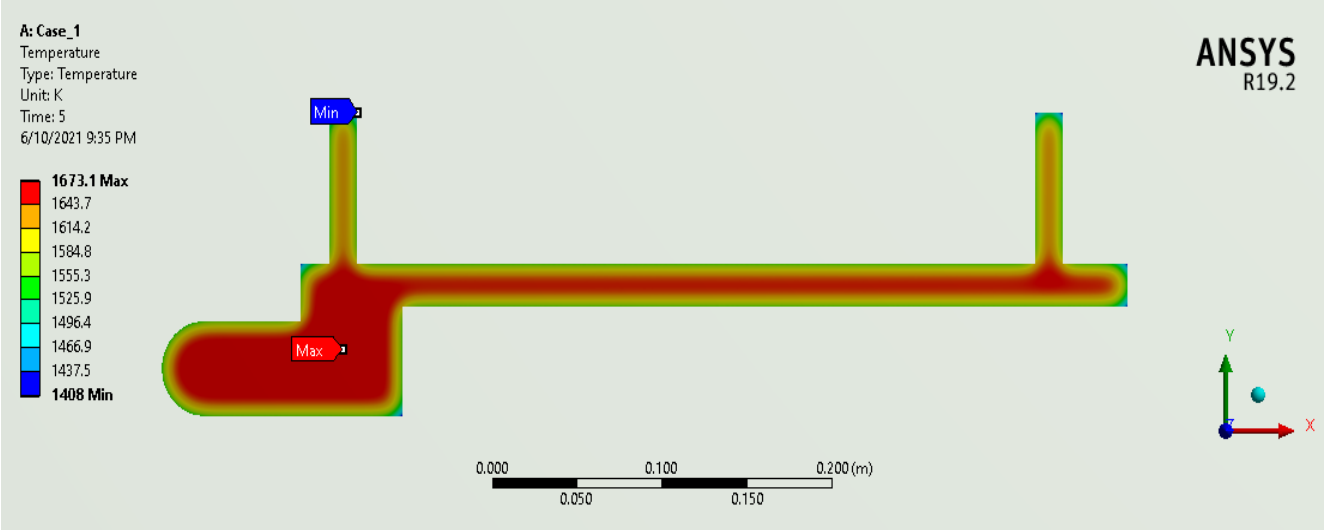

(a) Temperature contour on cast at 5 seconds

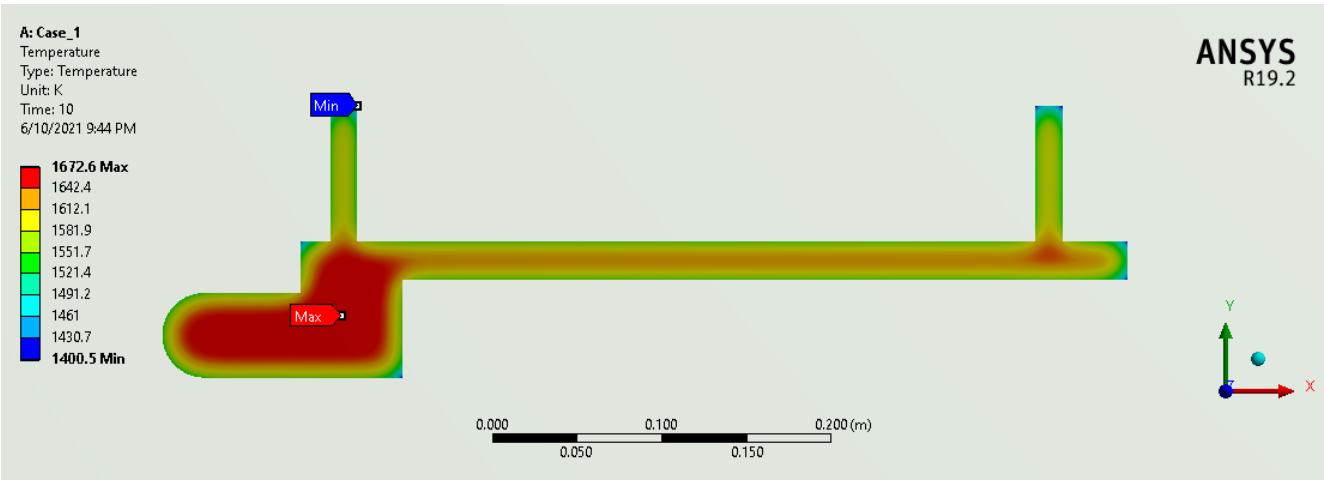

(b) Temperature contour on cast at 10 seconds

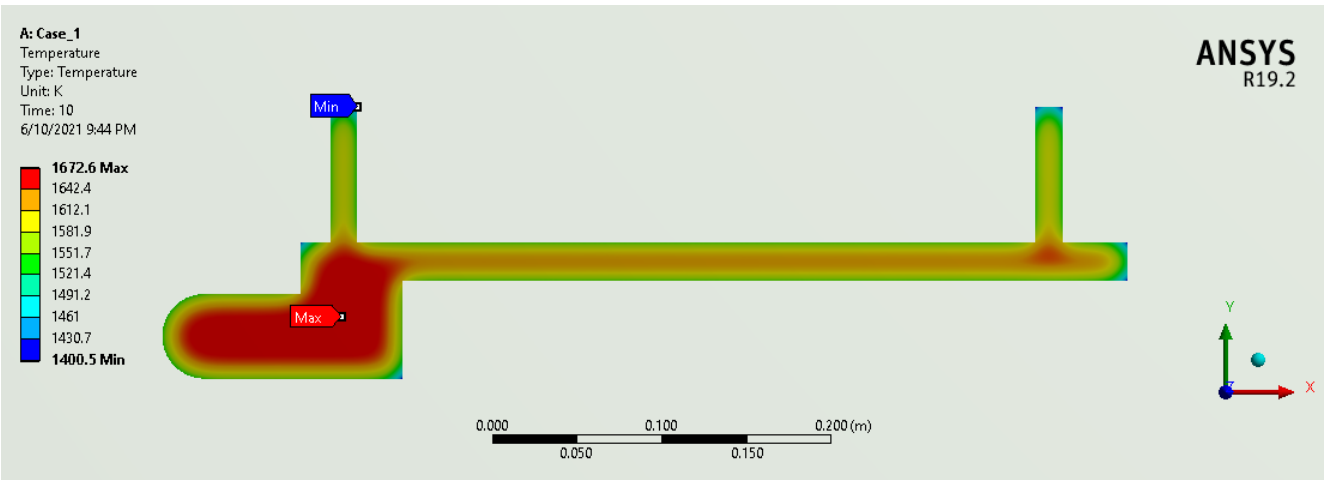

(c) Temperature contour on cast at 15 seconds

Figure 4.1: Temperature contour of grey iron casting inside cast part at 5, 10, and 15 seconds

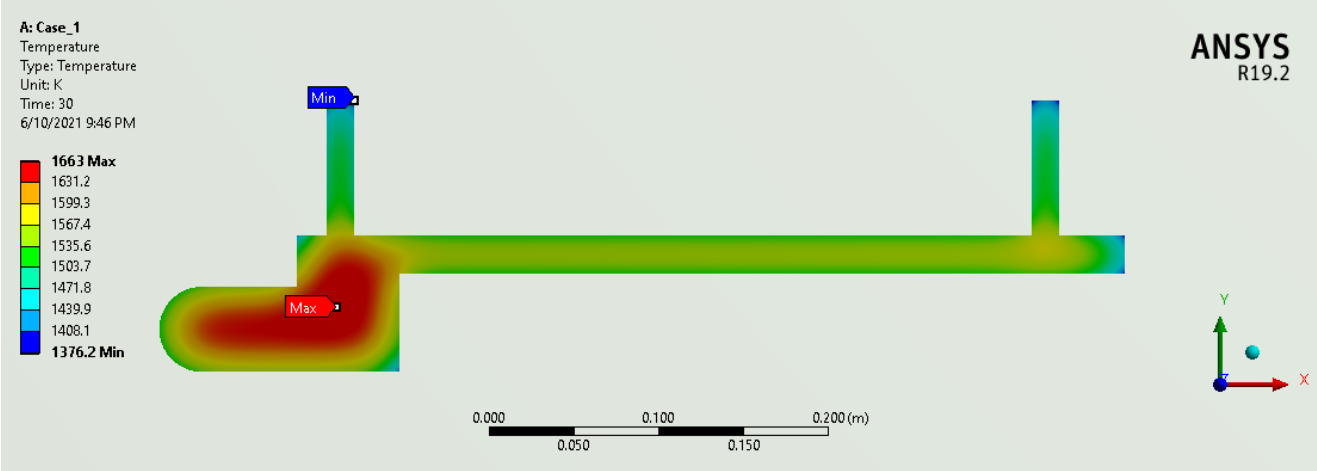

(d) Temperature contour on cast at 30 seconds

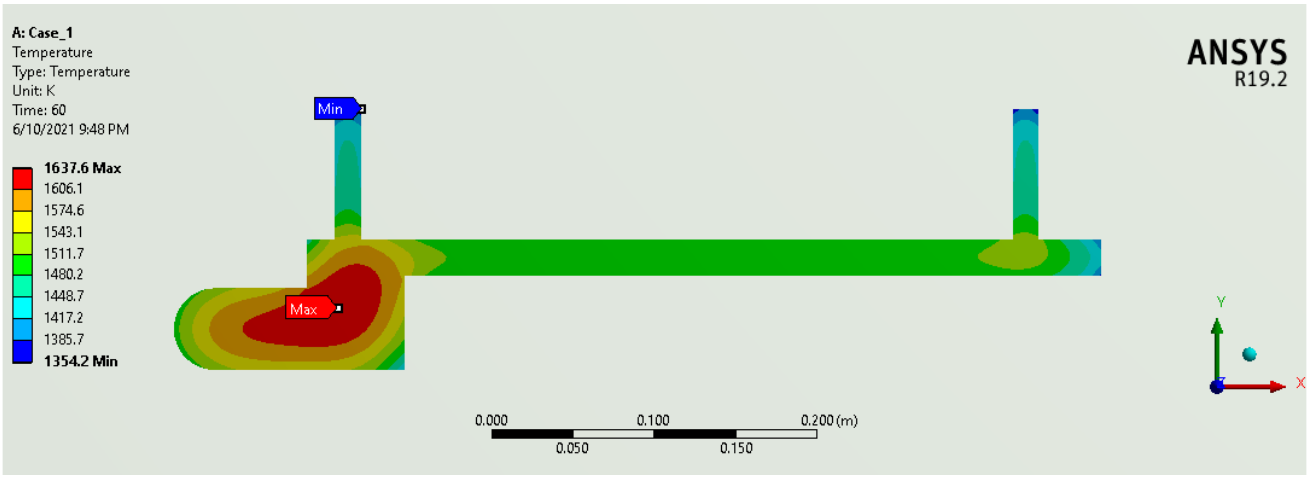

(e) Temperature contour on cast at 60 seconds

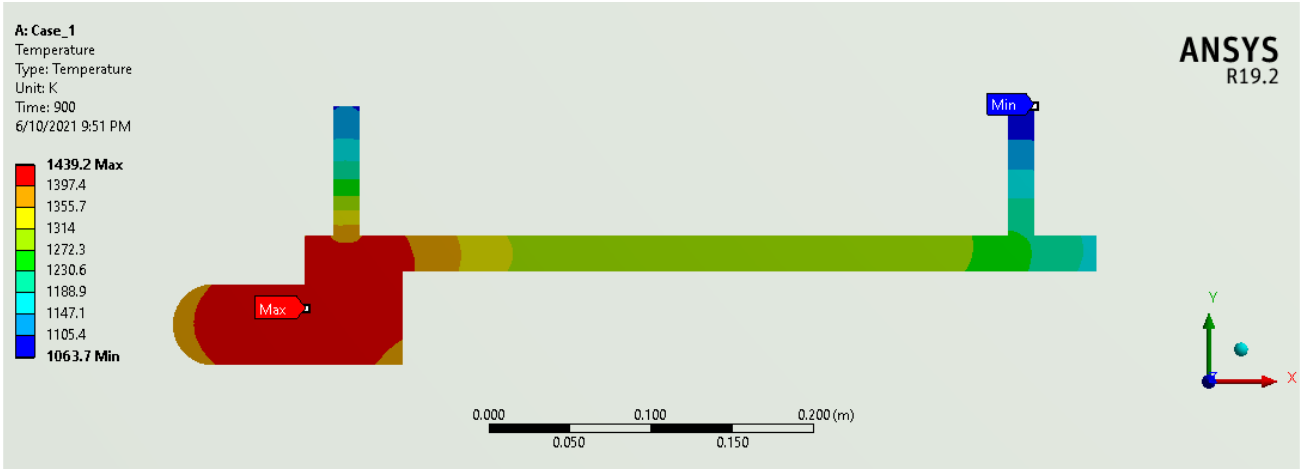

(f) Temperature contour on cast at 900 seconds

Figure 4.2: Temperature contour of grey iron casting inside cast part at 30, 60, and 900 seconds

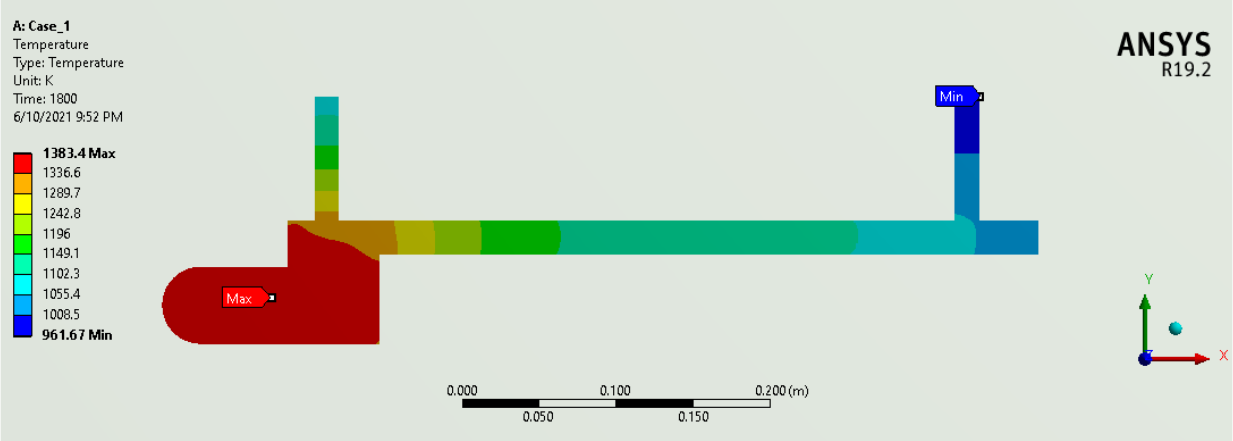

(g) Temperature contour on cast at 1800 seconds

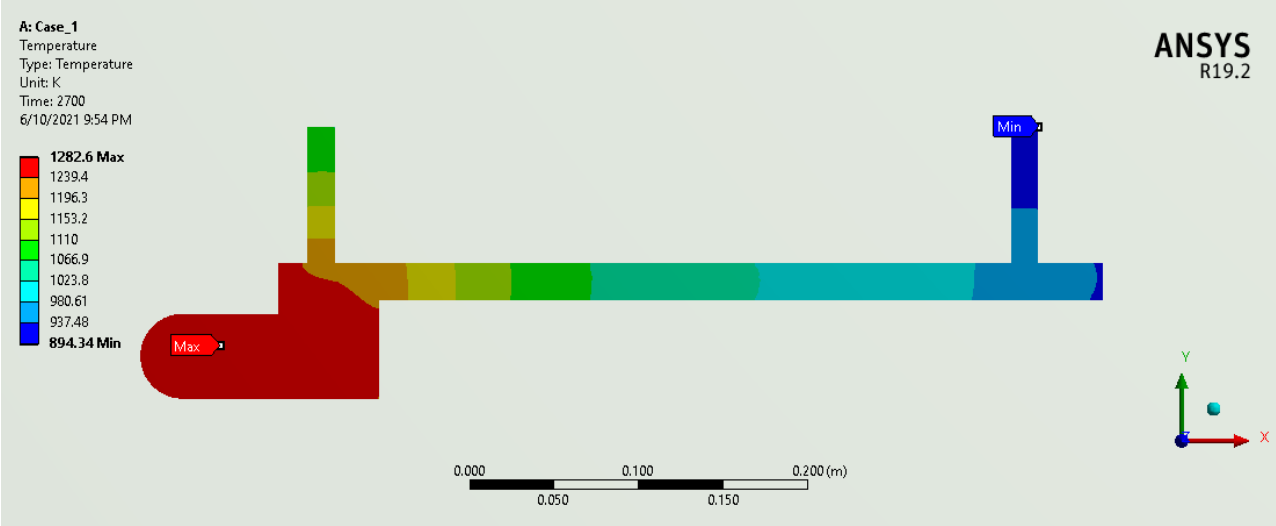

(h) Temperature contour on cast at 2700 seconds

Figure 4.3: Temperature contour of grey iron casting inside cast part at 1800 and 2700 seconds

Figure 4.5 below shows the temperature contour inside the mold at different time steps. The sand mold temperature profile shows increased pattern of temperature distribution due to extraction of heat from the molten metal introduced inside the cast. In contrast temperature profile in the cast part presented in above Figure 4.1, the temperature is significantly increase around the contact region with the cast part at the initiation of the initial filling of the molten metal on the mold cavity. It can be observed the maximum nodal temperature reaches 1619.8 K at initial stages (5 seconds), 1281.1 K at the final stage of simulation (2700 seconds). The temperature distribution shows there is an increase in the maximum nodal temperature and then drops down since the latent heat release of the molten metal drops when time is increased. The temperature contour displays the outward heat flow from the inner most wall of the mold to the outer most part.

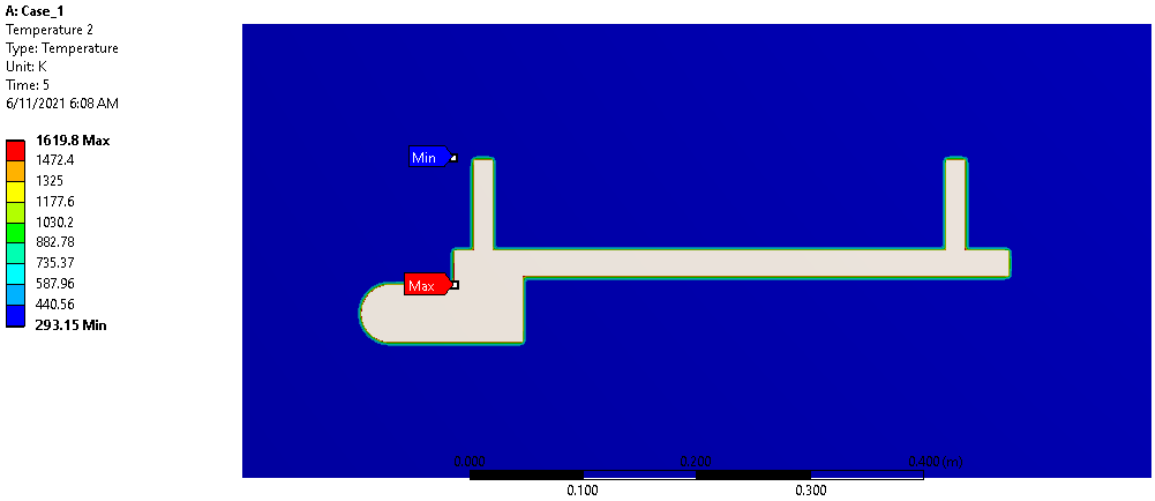

(a) At 5 second

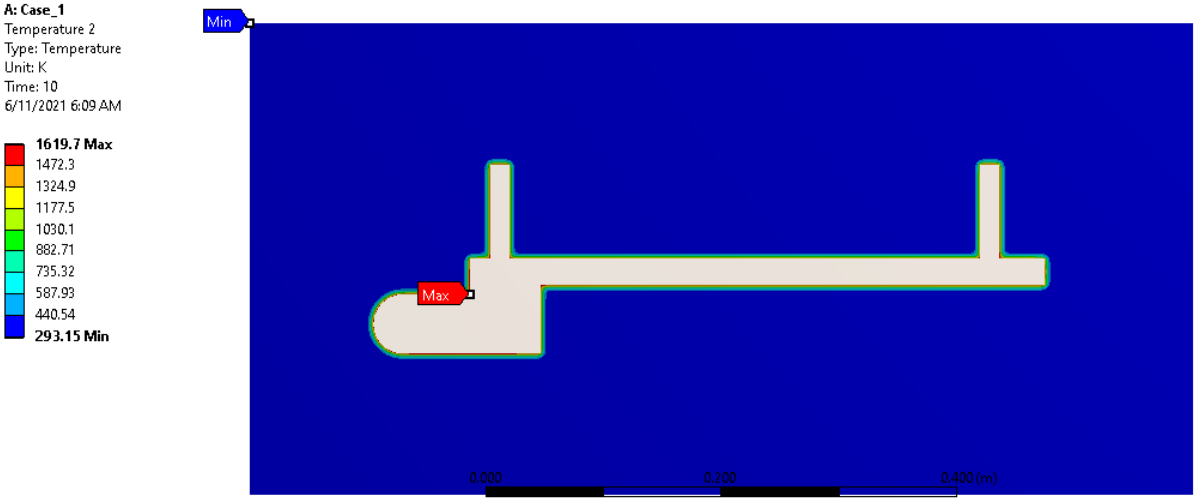

(b) At 10 second

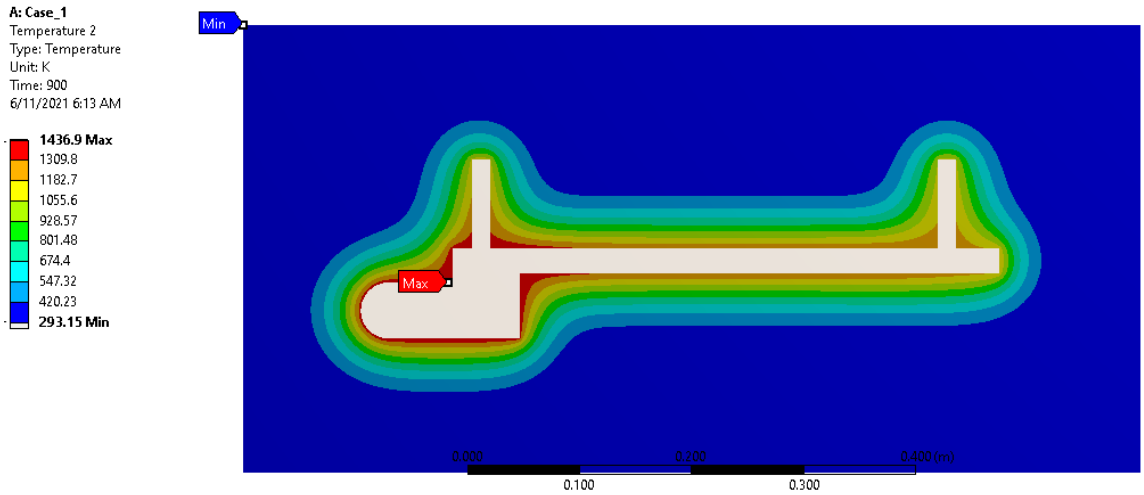

(c) At 900 second

Figure 4.4: Temperature contour of Ash cleaner door casting inside mold part at 5, 10, and 900 seconds

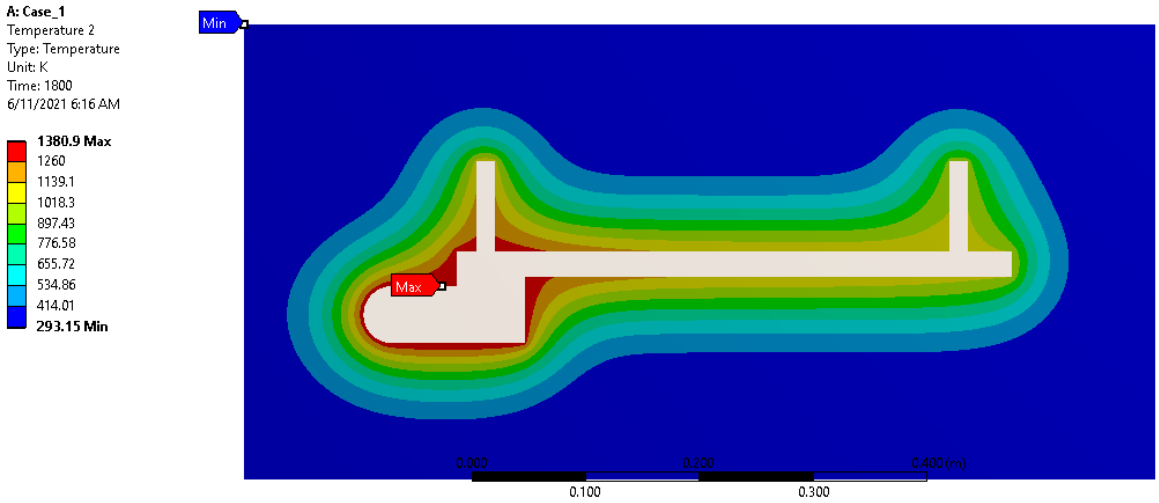

(d) At 1800 second

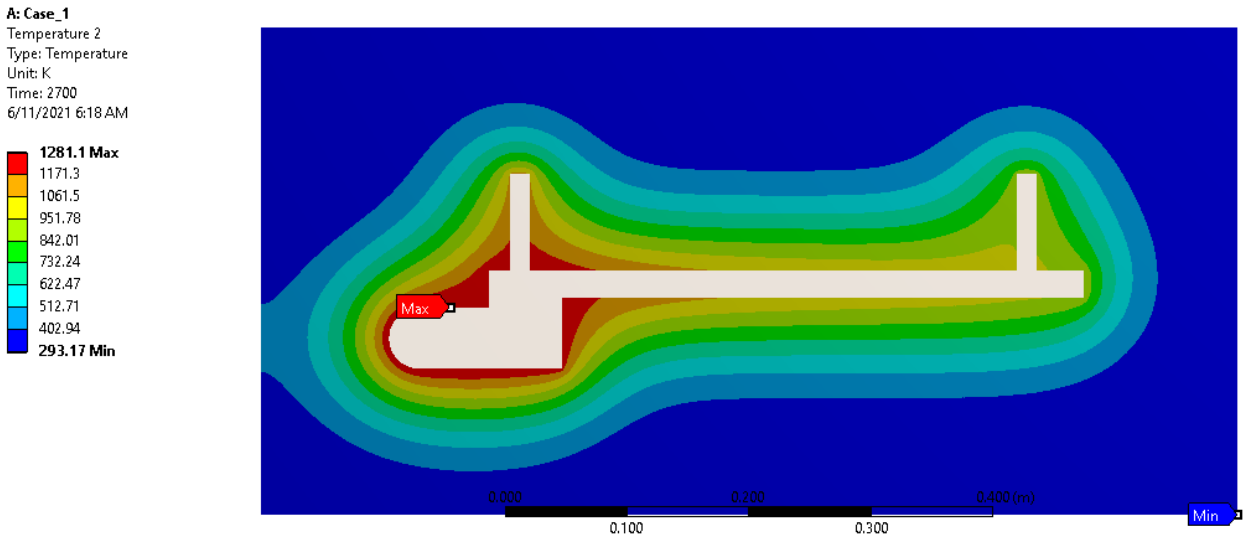

(e) At 2700 second

Figure 4.5: Temperature contour of Ash cleaner door casting inside mold part at discrete time point

Figure 4.6 shows the temperature contour inside the casting of the manhole frame (case 2) from the grey cast iron during 500 second simulation. As observed from the graph, the maximum nodal temperature reaches 1308.3 K during the initial period of solidification process (2 seconds), 764.43 K at the last time step (500 seconds). The cooling rate is high since the wall thickness is small, resulting to decrease heat transfer. The temperature gradually decreases when the time increased; hence the heat transfer is transient. The distribution of temperature inside the cast material shows there is high temperature value around the corner region since the material volume is high.

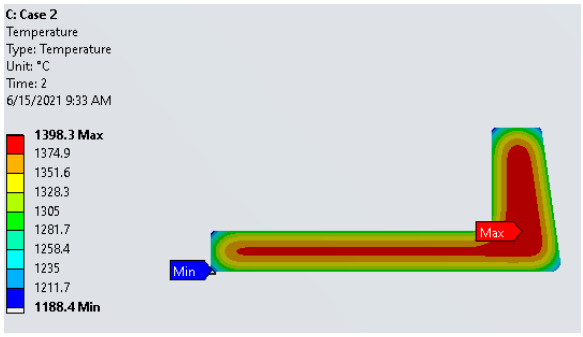

(a) At 2 second

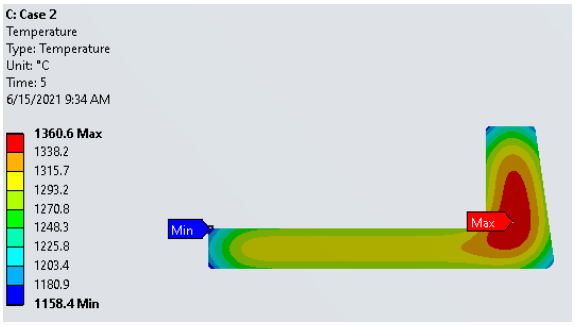

(b) At 5 second

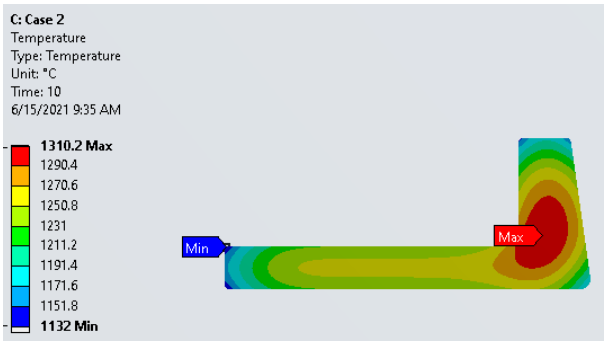

(c) *At 10 second*

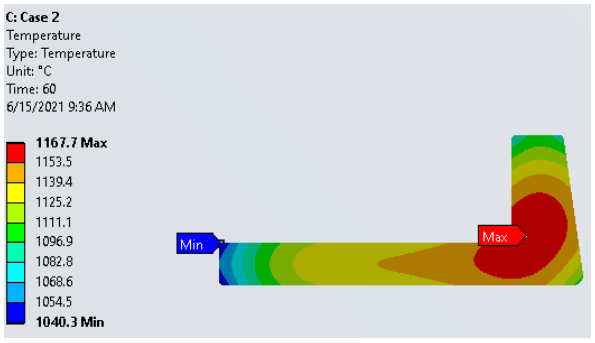

(d) *At 60 second*

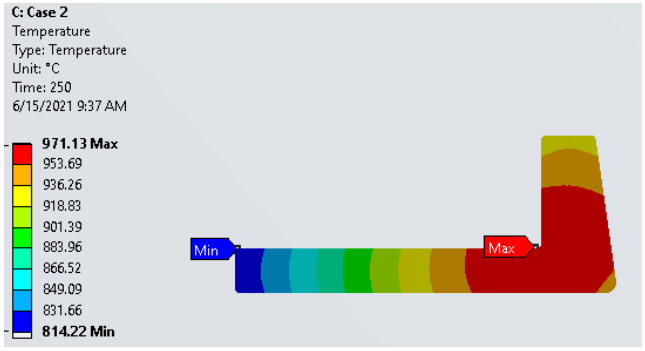

(e) *At 250 second*

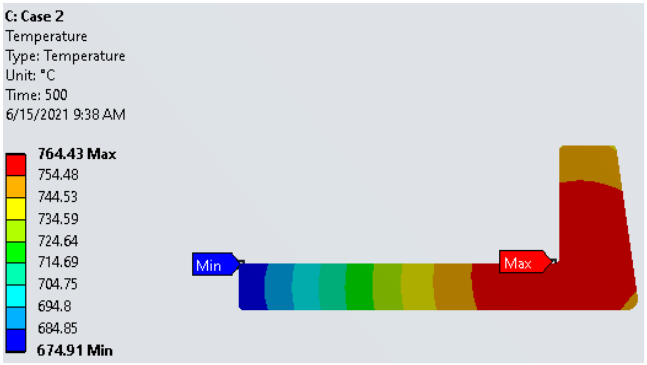

(f) *At 500 second*

Figure 4.6: Temperature contour inside casting of the frame at discrete time point

For the casting of the Aluminum flywheel, the temperature distribution inside the cast material 1500 seconds of simulation is presented in temperature contour plot in Figure 4.7 below. The plot shows the temperature decrease on the cast surface through time. Relative to the casting of gray cast iron as presented previously, the pouring temperature of aluminum is small. It is observed that during the initial stage of solidification the maximum temperature inside the cast is 797.37 K at 1 seconds, 465.59 K at the final stage of the simulation. Even though the pouring temperature of aluminum is small, the cooling of molten metal is also fast inside the mold cavity. The minimum nodal temperature inside

the cast observed on the outer most edge of the cast material with a value of 729.8 K and 452.66 K at 1 second and 1500 seconds respectively.

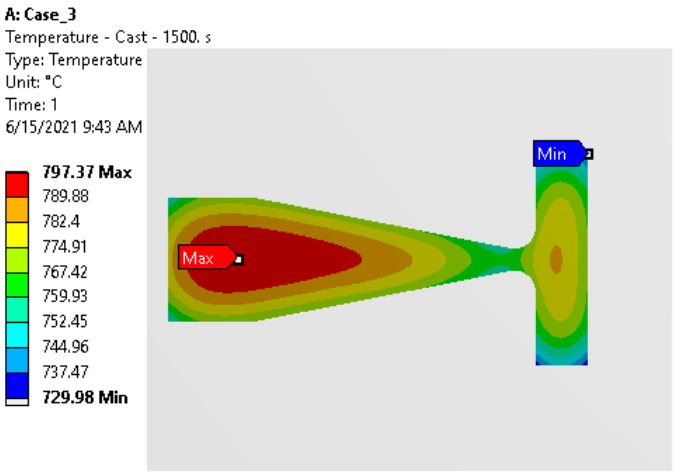

(g) At 1 second

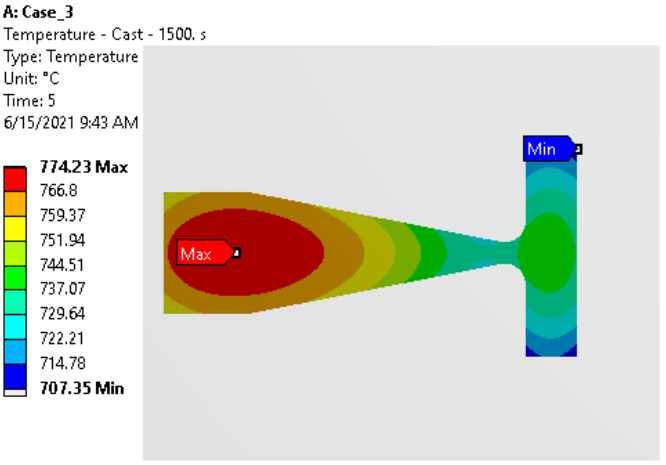

(h) At 5 second

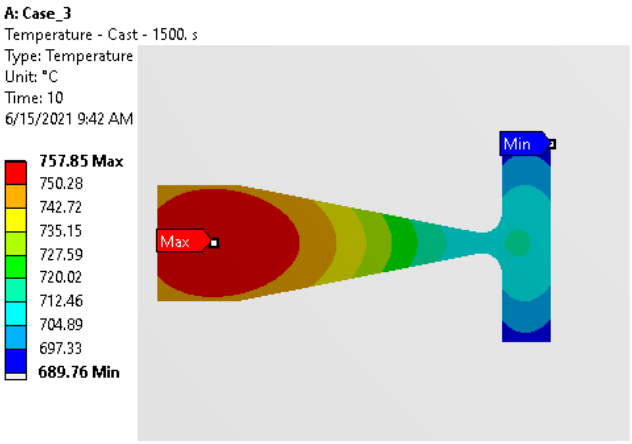

(i) *At 10 second*

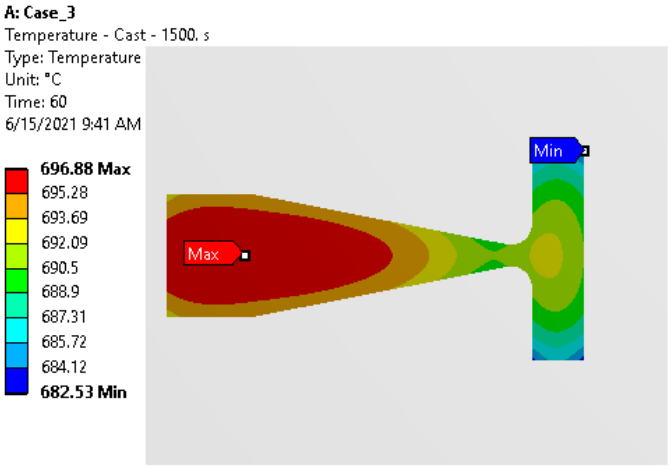

(j) *At 60 second*

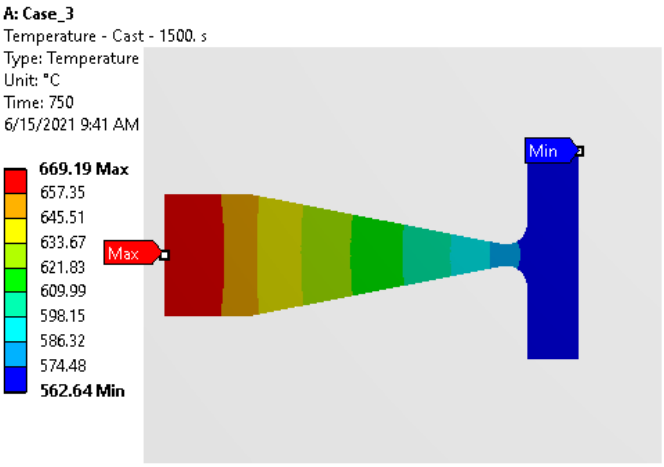

(k) *At 750 second*

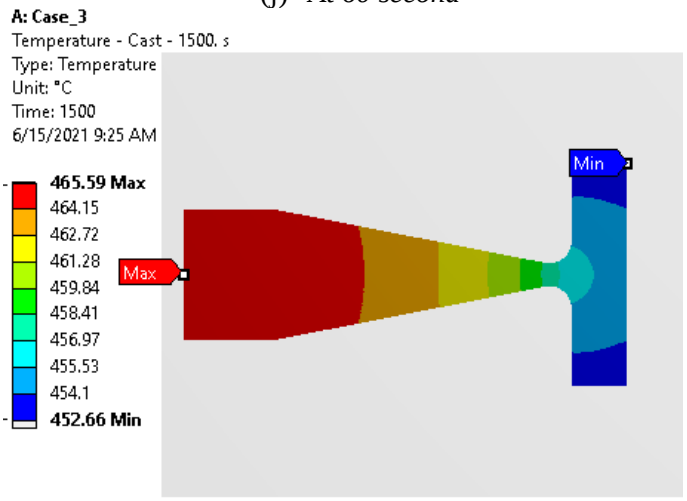

(l) *At 1500 second*

Figure 4.7: Temperature contour of Aluminum flywheel casting inside cast part at discrete time point

4.1.2 Simulation Result of Solidification pattern

The phases encountered during the solidification process, namely liquid phase and solid phase for pure iron. While for the solidification of alloy metals, there is a transition phase called the mushy zone in which liquid and solid metal presents simultaneously according to a solid fraction. The pattern of solidification can be plotted by applying a temperature range for the result grid. In this case the red color grid shows the temperature above the liquidus temperature which shows the liquid phase inside the cast material; the green color grid presents the mushy zone; and the blue color shows the solid phase inside the cast region.

Prediction of solidification pattern is vital process in modeling the solidification process since the place in which the solidification starts and ends may encounter a number of defects associated to solidification as presented in the literature review in chapter two. Specifically predicting the solidification of the casting process shows the nature of solidification process. The patterns of solidification for three cases presented next in graphs at discrete time.

The solidification phenomenon in case 1 is presented in Figure 4.10 at different discrete time. The range of mushy zone is presented between temperatures of 1463 K and 1353 K the values above and below those temperatures are shows the liquid and solid phases respectively. While the mushy zone presented in between the two values. The graph plots show the solidification pattern inside the cast during the casting of case one of the studies, as observed from consecutive graphs the only liquid phase presented inside the mold cavity until the time step reaches 62 seconds in which the transition region begins to exist. The liquid phase stays up to 515 seconds as presented in Figure 4.10 *(f)*. The solidification starts from the upper and right edges and goes directionally to the lower and left edges of the mold wall. Besides the mushy zone (transition) las longs until the time reaches 2249 seconds as presented in Figure 4.10 *(j).*

The phase transitions from the liquid to solid via mushy zone fulfilled by releasing latent heat from the molten metal. This rate of heat removal from molten cast iron is an essential factor that controls the solidification process. When the molten metal is fully solidified inside the sand mold. The place of last solidified metal is located in which the wall thickness is maximum and volume of metal is large relative to other places in the cast. Therefore, around the place that solidifies last there is most probably shrinkage, porosity and hot spot defects.

(a) 5 seconds

(b) 30 seconds

(c) 62 seconds

Figure 4.8: Solidification front of Case 1 casting at 5, 30 and 62 seconds

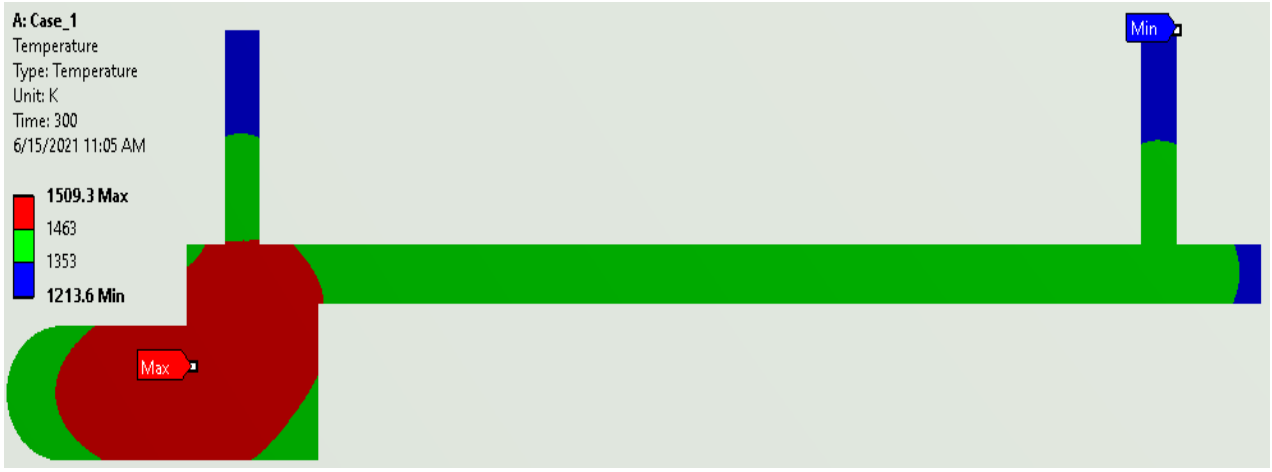

(a) 300 seconds

(b) 480 seconds

(c) 515 seconds (last liquid phase exist)

Figure 4.9: Solidification front of Case 1 casting at 300,480 and 515 seconds

(a) 900 seconds

(b) 1800 seconds

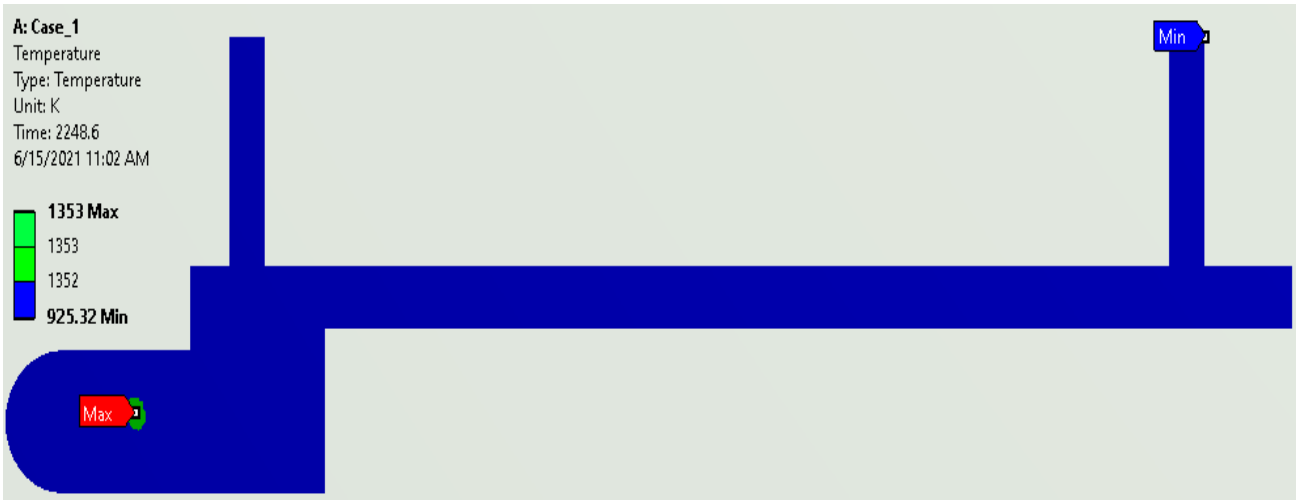

(c) 2248.6 seconds (solidification ends)

Figure 4.10: Solidification front of Case 1 casting at 900, 1800 and 2248.6 seconds

As presented in Figure 4.120 and Figure 4.12 ; the molten metal is inside the cavity is fully liquid until the time reaches 35 seconds as presented in Figure 4.12 *(d);* after the temperature gradually decreases below the liquidus temperature (1463k), a simultaneous phase presents inside the mold until the time reaches 90 seconds in which there is no liquid metal available inside the mold as depicted in Figure 4.12 *(f)*. The casting becomes fully in solid state at a time of 177 second as presented in Figure 4.12 *(h)*. The place lately solidifies as obvious, located where there is maximum thickness inside the cast. In the maximum thickness region, the cooling rate become slow and the metal solidifies slowly relative to a location with small wall thickness.

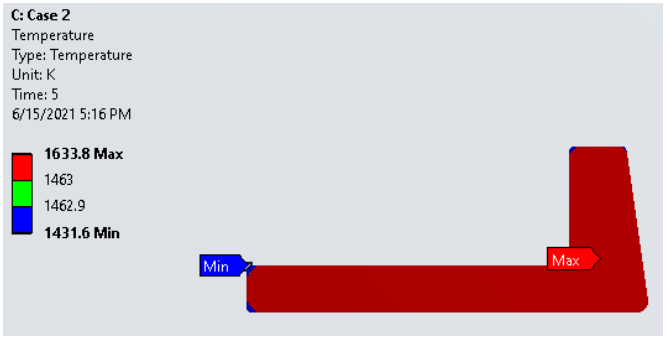

(a) At 5 second

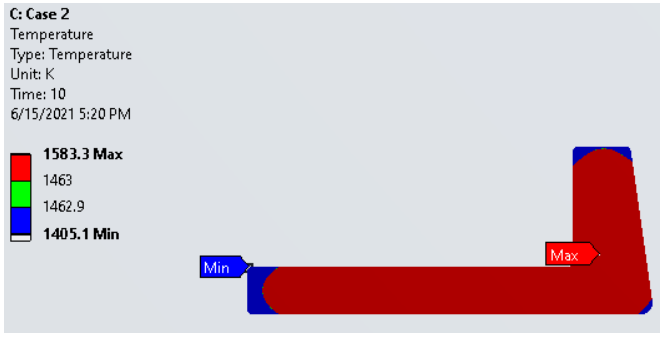

(b) At 10 second

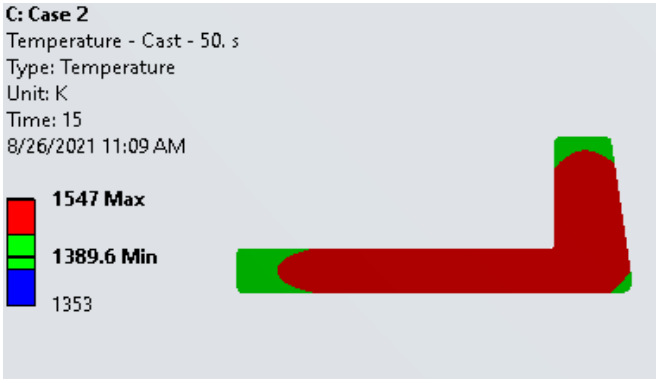

(c) At 15 second

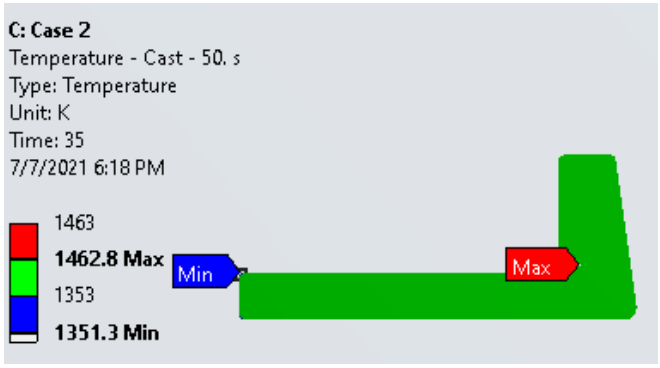

(d) At 35 second

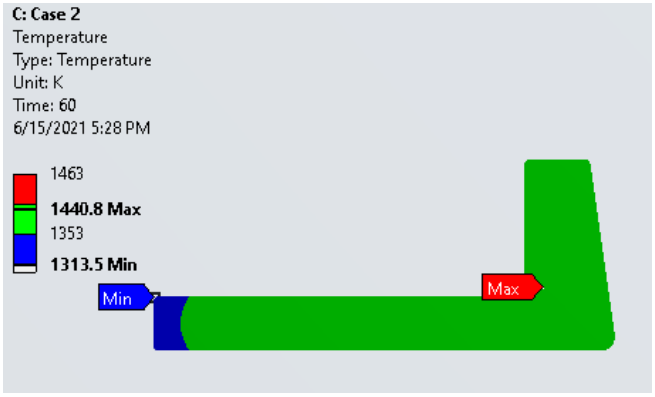

(e) At 60 second

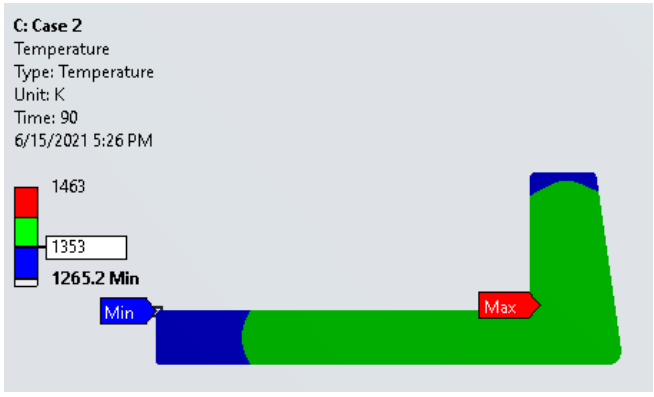

(f) At 90 second (no liquid phase)

Figure 4.11: Solidification front of Case 2 casting at discrete time point

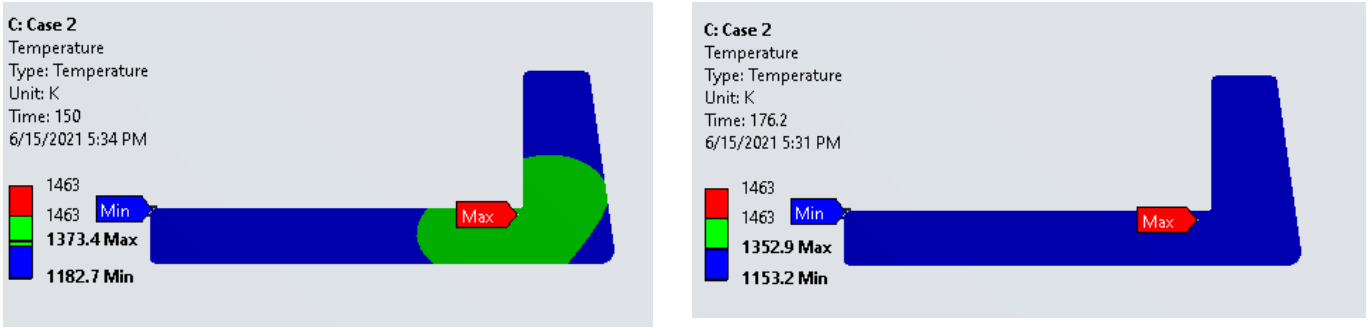

(a) At 150 second *(b) At 176.2 second (solidification end time)*

Figure 4.12: Solidification front of Case 2 casting at 150 and 176.2 seconds

The solidification phenomenon during the simulation of the manhole cover casting from grey cast iron shows non-directional pattern. The solidification starts from the inner left and upper write edge of the part as the thickness is small and there is direct contact of molten metal with the sand mold.

Figure 4.13 presents the solidification front for Aluminum casting (case 3). For this case, the transition range for the mushy zone is short; this signifies the truth that the solidification of pure metal occurs isothermally.

By Figure 4.13, the solidification of Aluminum attained in a short time. In this simulation, the solidification range is with is 2 kelvins from the melting temperature. The melting point of the Aluminum used in the study was 969 k. the liquidus temperature of 970 k presented inside the cast at around 53 seconds, which is the instant of time where the solidification begins. Since the transition range is short, the mushy zone inside the mold cavity presented until 133 seconds, in which the solidification of molten aluminum completed. As presented in the above plot, during the solidification of Aluminum, the cooling is fast, so latent heat release is prominent during the process.

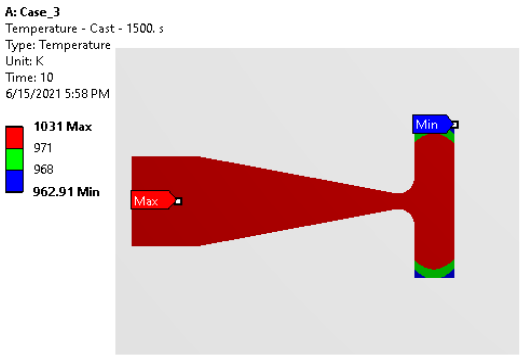

(a) At 10 second

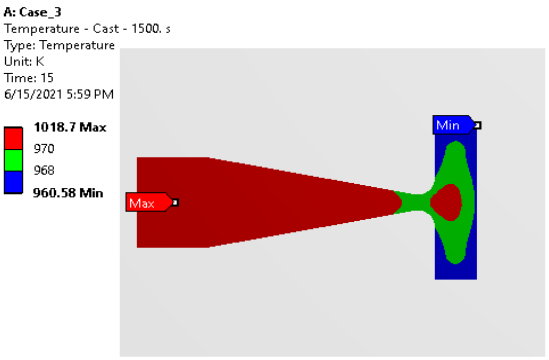

(b) At 15 second

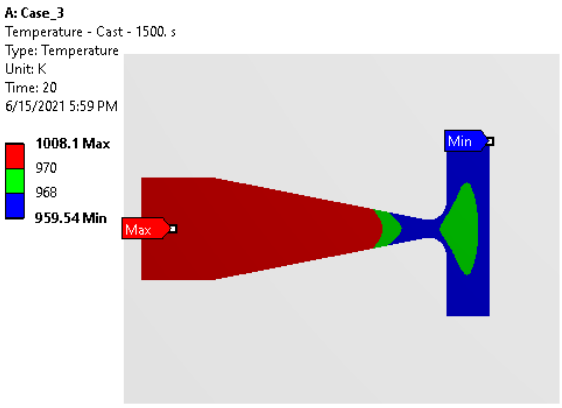

(c) At 20 second

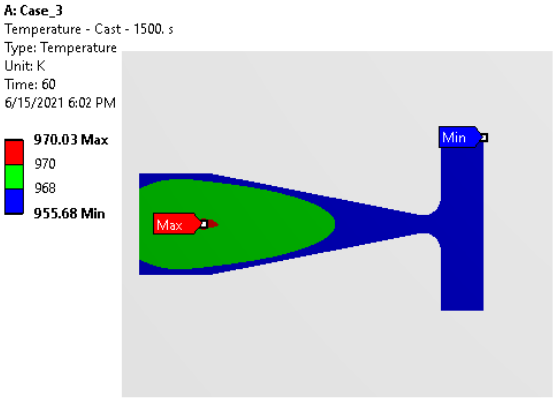

(d) At 60 second

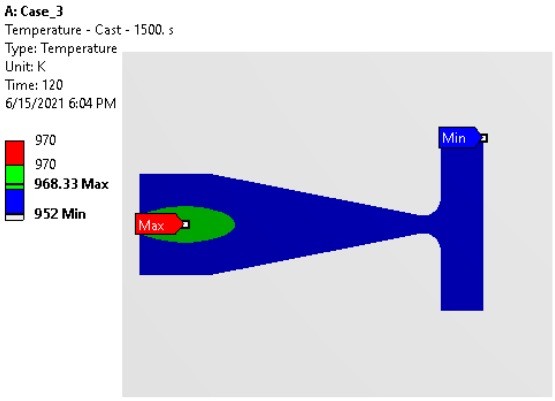

(e) At 120 second

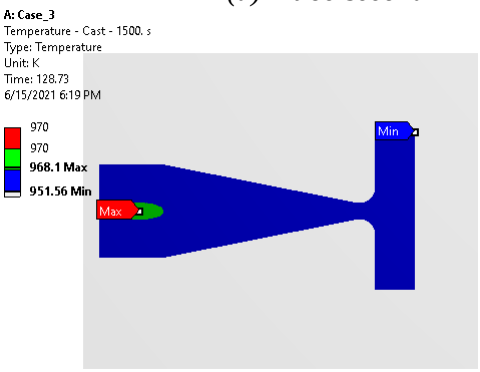

(f) At 128.73 second

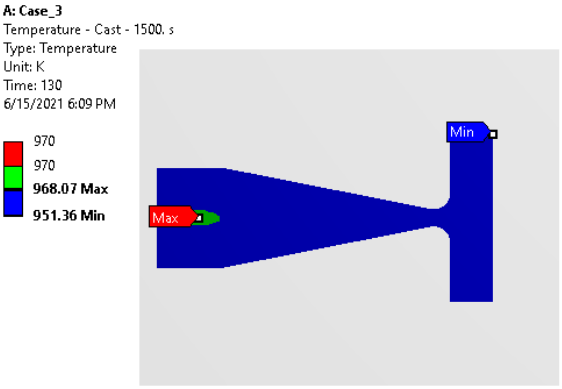

(g) At 130 second

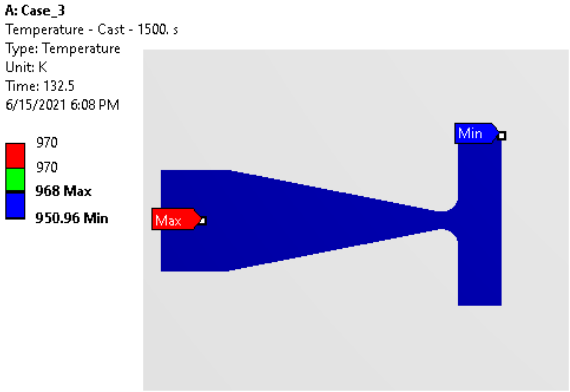

(h) At 132.5 seconds (solidification end)

Figure 4.13: Solidification front of Case 3 casting at discrete time point

4.1.3 Simulation Result of Cooling Curve

The temperature variation with time on cast and mold body during the solidification has plotted for all cases. The plot is known as cooling curve. The cooling and heating/cooling curve gradient during casting reflects the release of latent heat from the molten metal to the sand mold. Actual results of the cooling curve obtained at different locations inside the cast bodies.

An illustration of the cooling curve for all cases during the simulation presented. The plot shows the maximum nodal temperature result during the simulation. Figure 4.14 shows the cooling curve for the 2700 second simulation solidification during the casting of case 1. As presented in the graph, the temperature drastically decreases in the first 515 seconds until liquidus temperature (1463 k) inside the mold presents at point A. After the solidification starts, the molten metal inside the mold cavity presents both liquid and solid phases simultaneously in a mushy zone. After the transition from the liquid to solid ends at point B (1353 K) at 2249 seconds, the metal completely solidifies. After the solidus temperature, the metal further solidifies until shakeout time.

Steep slope at the beginning of solidification indicates a rapid solidification (high cooling rate) where a great amount of heat is released while shallow slope indicates slow cooling (low cooling rate). The cooling rate is maximum at the beginning of solidification, hence during the pouring liquid metal cast into the mold cavity and occupies it, the liquid metal mixes thoroughly and releases heat to the sand mold due to the high temperature difference. Complete thermal contact is observed between the cast and the mold which causes the heat transfer to be purely conduction, where the resistance offered by this liquid metal is negligible since the entire fluid flow is the superheated cast metal. Once the cast metal reaches the liquidus point on cooling, the cast shrinks and releases latent heat and also a number of metal oxides are released which causes an air gap between the cast and the mold. Due to this air gap the heat transfer phenomenon now changes to a complex one where all modes of heat transfer can be observed simultaneously.

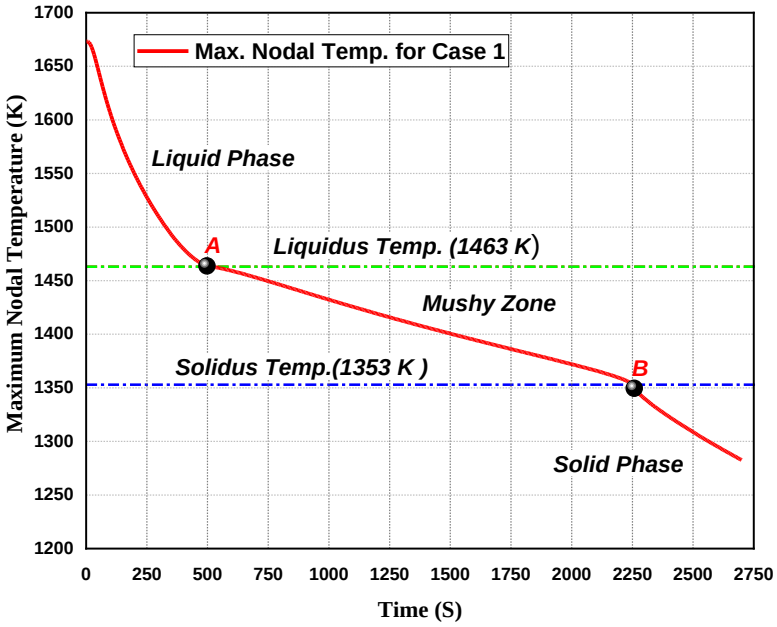

Figure 4.14: Cooling curve inside cast body for Ash cleaner door casting (case 1)

As shown in Figure 4.15, the cooling curve for the casting of manhole cover (case 2) with 500 second simulation, the cooling rate recorded as in the liquidus region reflects high release in latent heat of fusion from the molten grey cast iron until the temperature reaches 1463 K. The temperature further decrease with time in the transition region until the molten metal completely solidifies at a temperature of 1353 K. The cooling rate is faster as the liquid metal starts to change in to transition then the cooling rate slower in the transition period. The high cooling rate during the initial time signifies large amount of latent heat release from the molten metal.

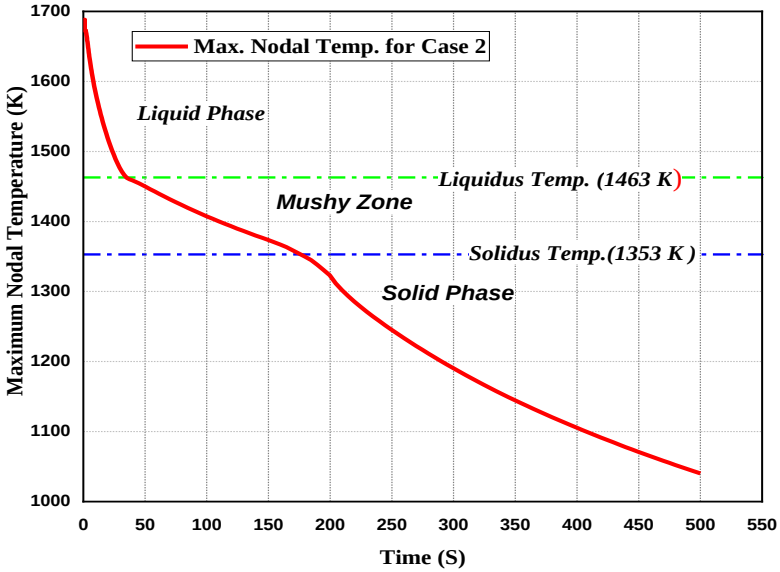

Figure 4.15: Cooling curve inside cast body for frame casting (case 2)

Figure 4.16 shows a clear trend during the solidification of pure metals during the casting of the Aluminum flywheel for case 3. The solidification occurs at an almost constant temperature from 970 K to 968 K (2 K solidification range). The solidification of aluminum completed in less time compared to alloy solidification; hence the latent heat fusion is small for this small compared to cast alloys. The temperature reaches 750 K after 1500 seconds of solidification simulation.

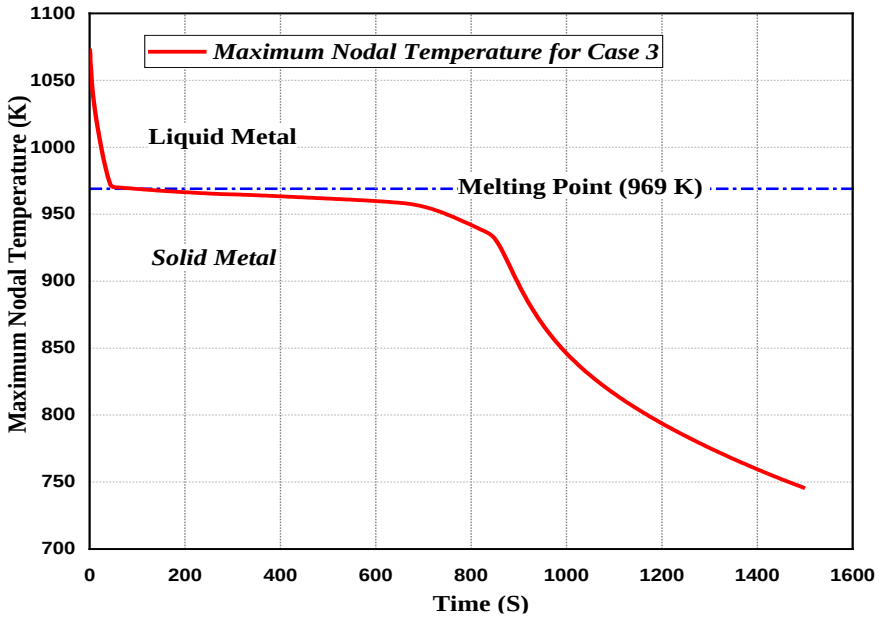

Figure 4.16: Cooling curve inside cast body for flywheel casting (case 3)

4.1.4 Nodal Results

The cooling curve solutions at the exact node points obtained in ANSYS on the cast presented using the probe created at different location of interest. By using a probe, a new coordinate system was created at a location of interest, to incorporate the thick wall section, thin wall section, at center, and at the edges around the mould wall. The result of cooling curves shows the release in latent heat, resulting in a gradual decrease in nodal temperature. The coordinate of nodes in each case is tabulated below in Table 4.1.

Table 4.1: Coordinate of nodes inside cast for all cases

	Case 1		***Case 2***		***Case 3***	
Location	***x-coordinate***	***y-coordinate***	***x-coordinate***	***y-coordinate***	***x-coordinate***	***y-coordinate***
1.	0.18811 m	0.145 m	0.317 m	-2.071e-4 m	3.5e-002 m	2.5e-002 m
2.	0.11661m	0.145 m	0.261 m	-2.071e-4 m	0.2 m	2.5e-002 m

3.	0.23811 m	0.145 m	0.32859 m	-3.424e-3 m	6.8384e-2 m	-1.147e-4 m
4.	0.46031 m	0.189 m	0.29105 m	-7.072e-4 m	0.1967 m	-1.05e-3 m
5.	0.62786 m	0.24 m	0.32402 m	1.506e-2 m	0.1942 m	-3.605e-2 m
6.	0.6465 m	0.189 m	0.3199 m	3.9004e-3 m	0.1817 m	9.5036e-4 m
7.	0.21186 m	0.24 m	0.32049 m	2.729e-2 m	0.1467 m	-4.05e-3 m
8.	0.21636 m	0.21636 m	0.27903 m	-7.072e-4 m	4.5e-002 m	-1.5e-002 m

Figure 4.17 shows the cooling curves within the solidification range for the selected nodes. The graph shows the temperature comparison about eight points inside the cast region. From the plot it can find that the temperatures of casting various points reduce gradually with time, while the nearer to casting core the slower of cooling speed. It is observed from the graph that at node 1 the solidification is slow and the solidification time is recorded as largest one from all nodes (498 seconds), Since the node locates in region there is larger accumulation of molten metal. The fastest solidified node, as presented in the same figure, is at node 5 and node 7. Geometrically the locations are in the upper left and right thin section with same y coordinate value (as shown in table 4.1). The transition region starts to present at 53 seconds in both cases. Their cooling curve appears in good agreement until complete solidification temperature occurs on the cast. The last solidification time shows a slight difference for node 5 and node 7 at 293 seconds and 308 seconds, respectively. The cooling curve for this case at other nodes shows higher cooling rate until the temperature reaches to liquidus temperature and slightly slower cooling rate in transition range.

Nodal temperature decrease drastically after the complete solidification presents at node 4,5,6 and 7, due to the presence of high temperature gradient in the location around wall thickness is small. The cooling pattern at node 2,3, and 8 exhibits high cooling rate during the initial cooling and slower cooling rate at mushy zone and slight decrease in under cooling stage.

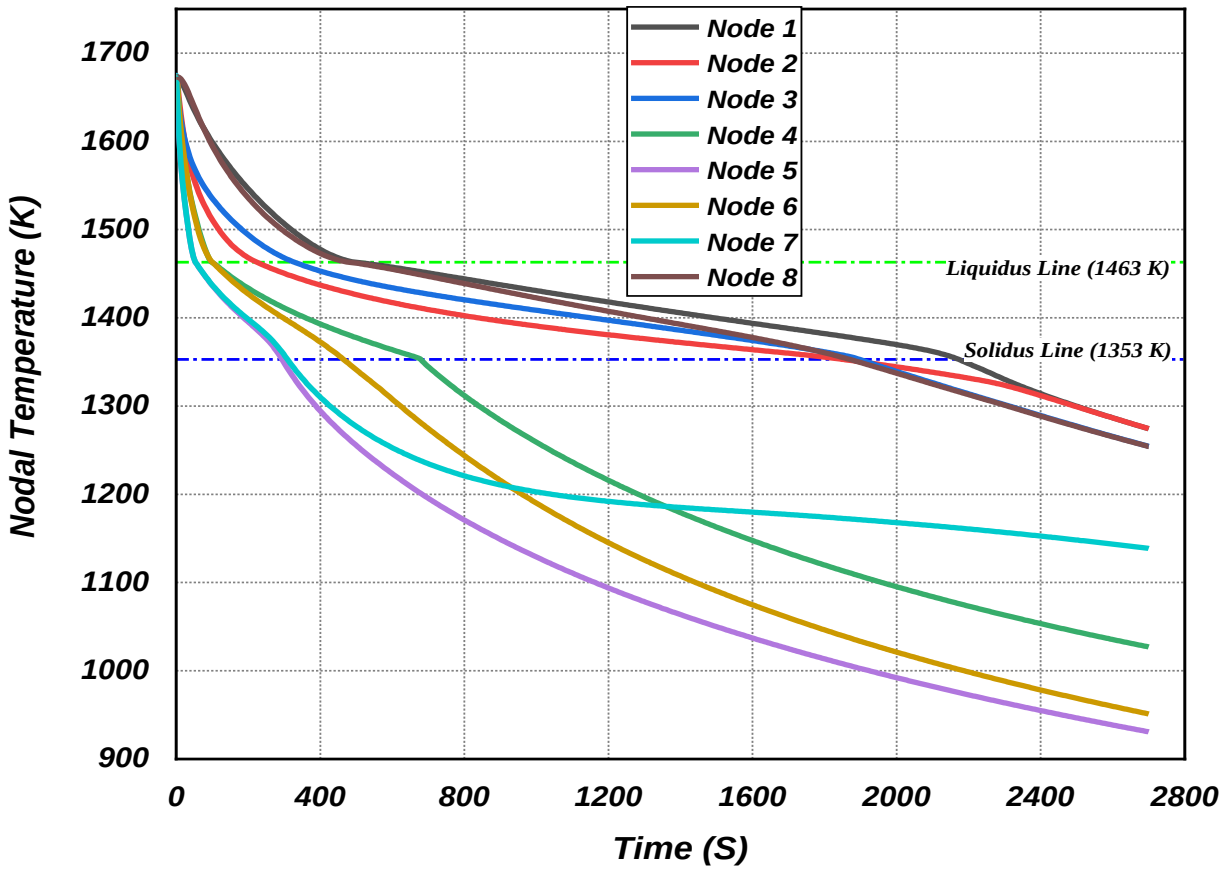

Figure 4.17: Cooling curve at different nodes inside the cast during Casting of Grey iron for case 1

Figure 4.18 presents the graphical representation of cooling curves inside the casting of case 2 at eight different locations. The node coordinates given in table 4.1 above. The result depicted that the time takes first node to start solidification is node 7 at 11 seconds. The node located around the upper edge of the cast. The last node to start the solidification is number node 6 at 34 seconds. All the cooling curve shows a fast cooling until the solidification starts and it takes much time to stays in the transition range. Further cooling stage shows a maximum heat loss around the wall near to wall with small wall thickness.

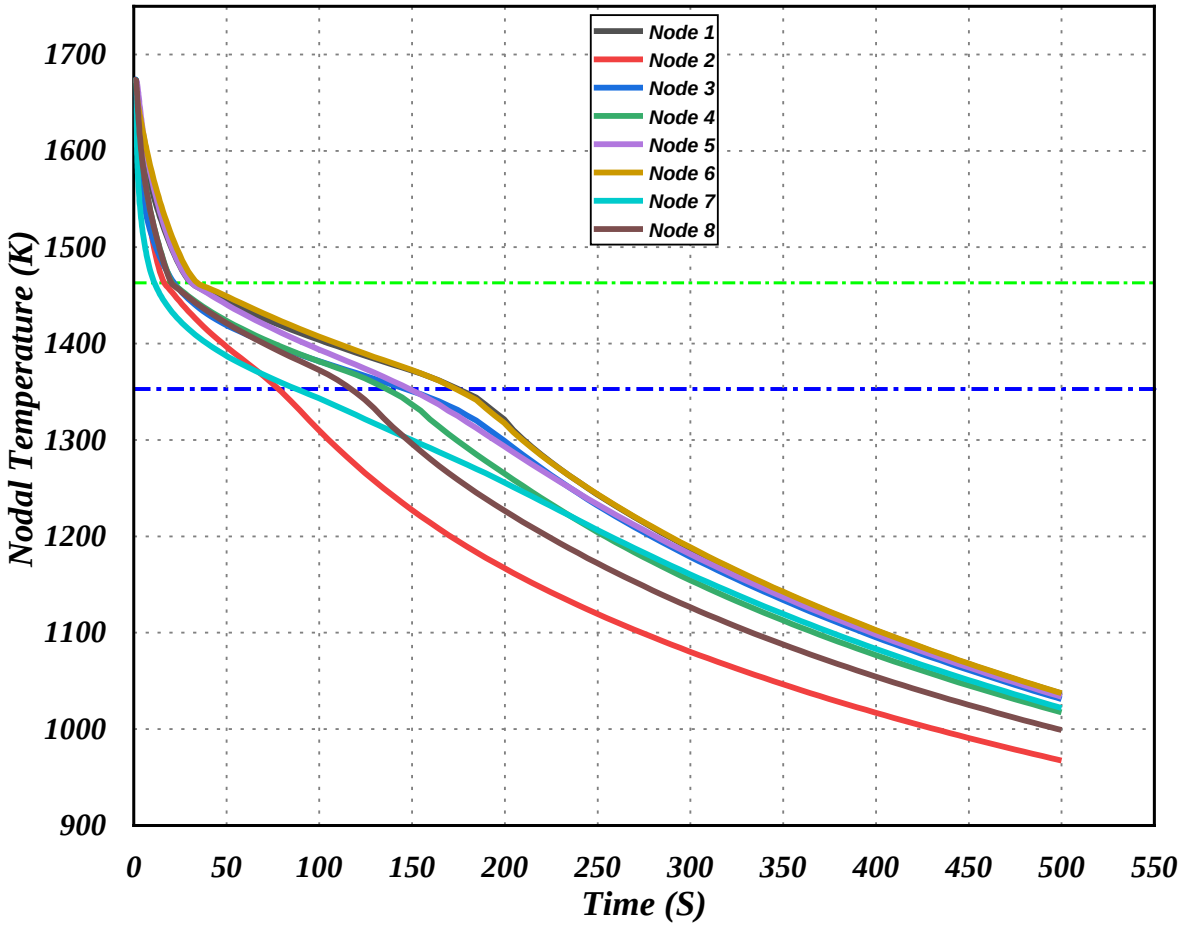

Figure 4.18: Cooling curve at different nodes inside the cast during Casting of Grey iron for case 2

Cooling curve of Aluminum casting presented in Figure 4.19 depicted that there is significant temperature gradient occurs during the cooling of liquid aluminum until the melting temperature. After the molten metal is solidified inside the mold cavity the trend of cooling curves shows an agreement and difference between nodes depending on their location on the cast. Nodes near the mold wall has large cooling rate and their temperature appears low at final time step. The nodes around the core of the cast shows a small Colling rate and takes larger time to cool down during the simulation.

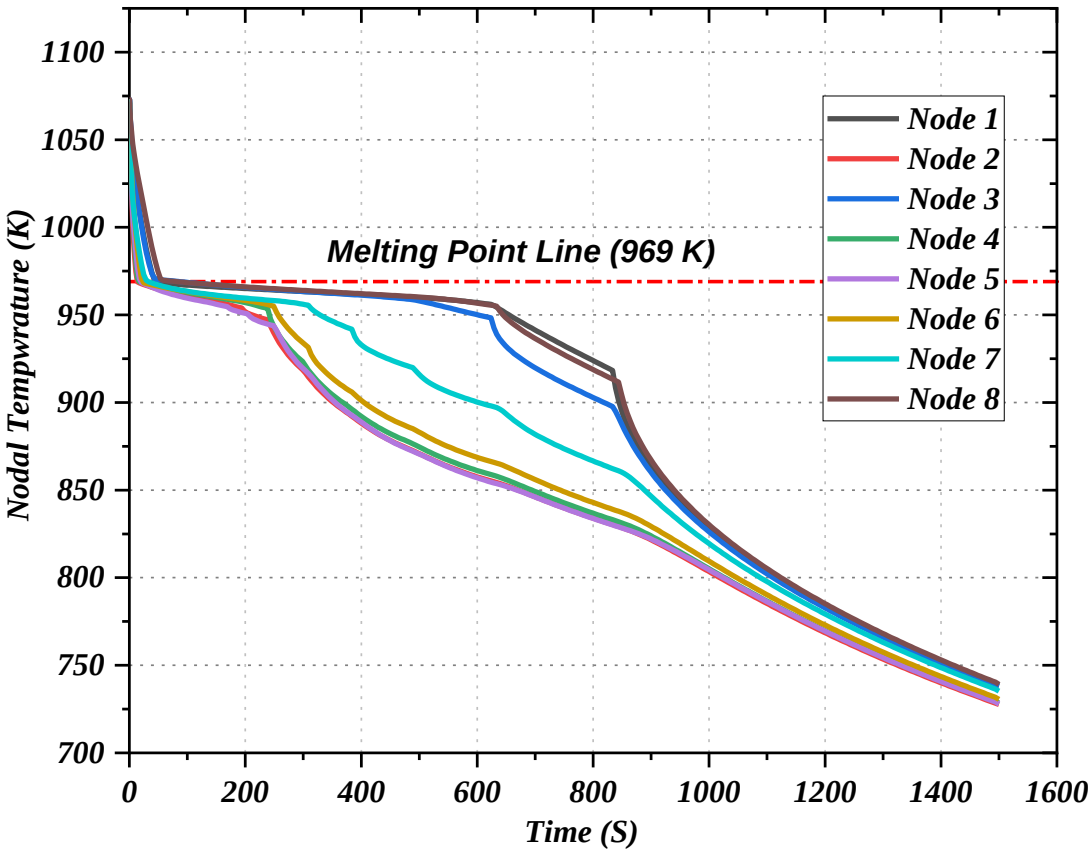

Figure 4.19: Cooling curve at different nodes inside the cast during Casting Aluminum for case 3

4.1.5 Heat Flux Contour

The energy change per unit time per unit area called heat flux throughout the cast and mold has computed in the simulation. The output of heat flux value displayed as a total heat flux contour plot. The total heat flux contour on the cast and mold material for all three cases plotted in Figure 4.20 via Figure 4.22.

Per Figure 4.20, the maximum and minimum total heat flux values at 2700 seconds are displayed on the cast and mold body. The maximum total heat flux located on a high heat transfer region occurs around the mold and cast contact wall. The maximum heat transfer occurred at the mold and wall contact since there is a high difference in initial molten metal temperature and mold wall temperature. At the given instant time, the maximum heat flux resulted on the cast and mold is 128.76 kW/m^2 and 39.86 kW/m^2. The result shows that the heat transfer rate from the cast to the mold.

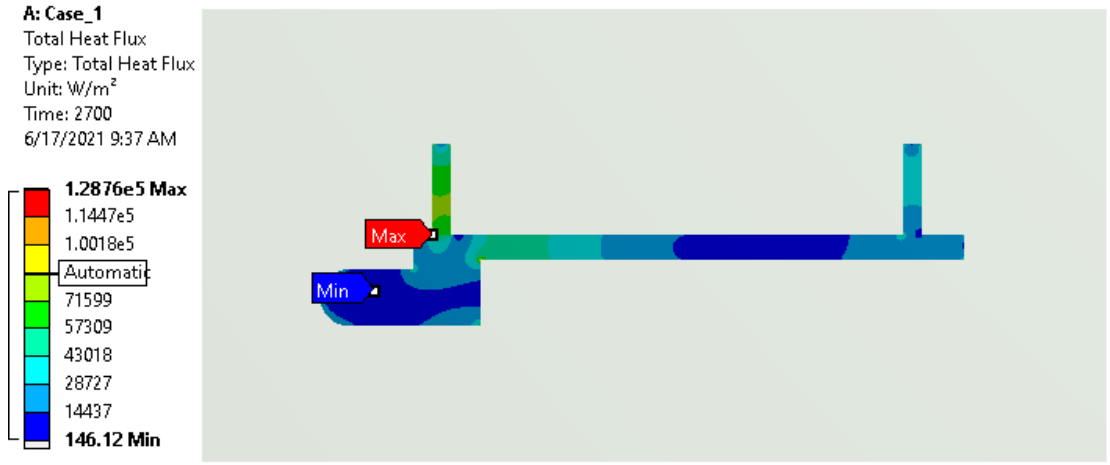

(a)

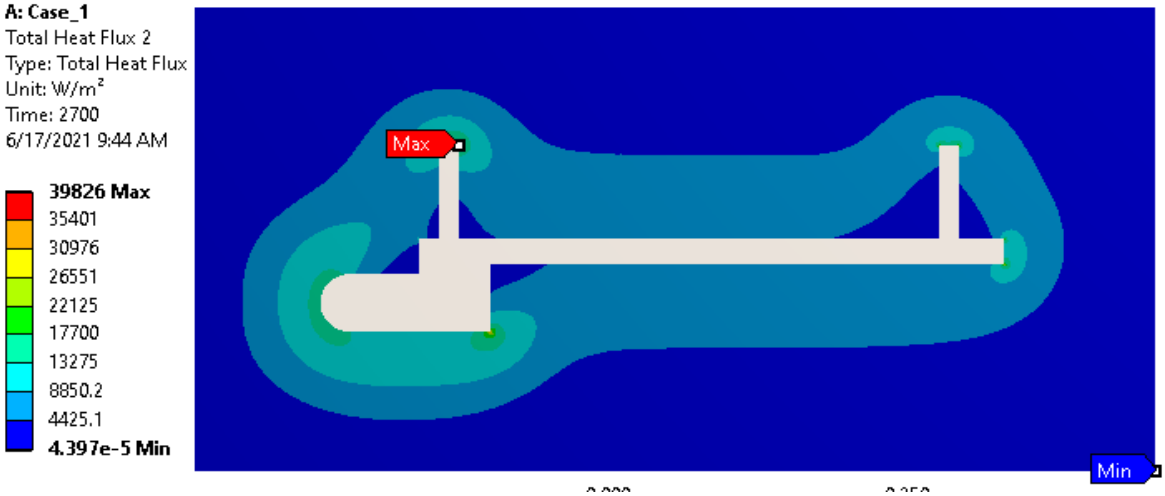

(b)

Figure 4.20: Total heat flux contour in (a) cast and (b) mold for case 1

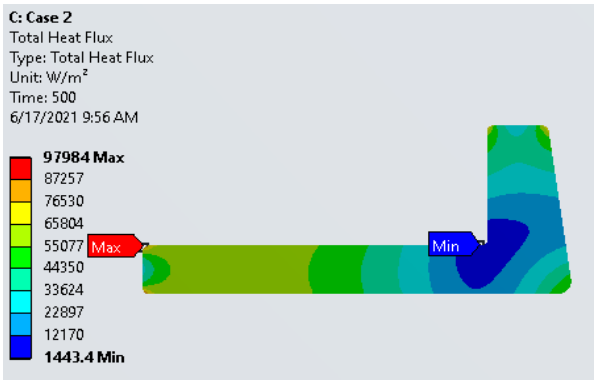

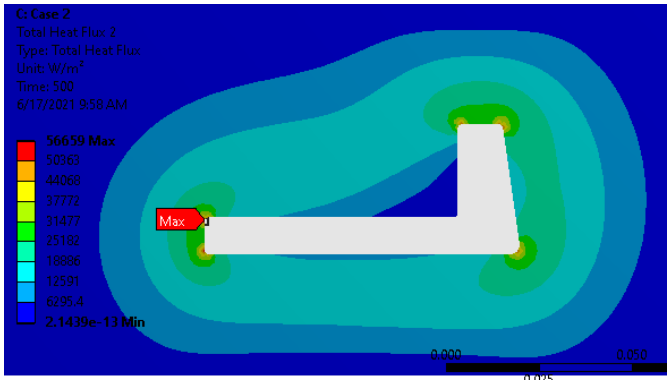

(a) *(b)*

Figure 4.21: Total heat flux contour in (a) cast and (b) mold for case 2

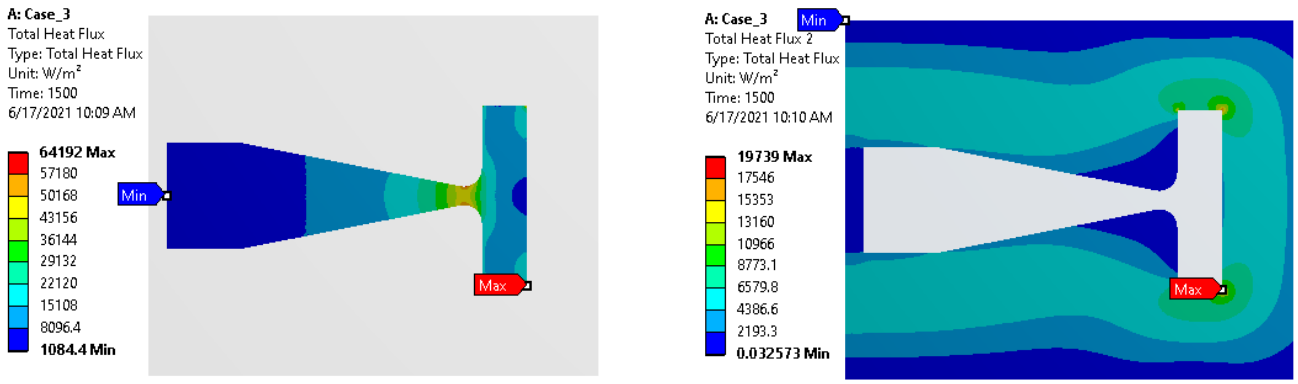

(a) *(b)*

Figure 4.22: Total heat flux contour in (a) cast and (b) mold for case 3

Per Figure 4.20 via Figure 4.22, the maximum and minimum total heat flux value at the last end time of simulation has been displayed on the cast and mold body for all cases. The maximum total heat flux is located on a high heat transfer region around the mold and cast contact wall. The location of maximum heat flux on cast and mold body is exact at a point of contact between two bodies. At the same time, the minimum heat flux value on the cast body is located in the outermost edge of the mold parts.

At the given instant time, the maximum and minimum nodal heat flux on the cast and mold is given in Table 4.2 below.

Table 4.2: Maximum and minimum nodal heat flux on the cast and mold

Parameter	**Case 1**		**Case 2**		**Case 3**	
Time	2700 sec		500 sec		1500 sec	
	Cast	Mold	Cast	Mold	Cast	Mold
Maximum heat flux $\left(kw/m^2\right)$	128.76	39.86	97.984	56.659	64.192	19.739
Minimum heat flux $\left(kw/m^2\right)$	0.146	$4.37*10^{-8}$	1.443	$2.14*10^{-16}$	1.084	$3.2*10^{-5}$

The table at the top shows the result of maximum and minimum nodal heat flux values. The heat transfer rate from the cast to the mold shows a maximum in all cases. Besides, the magnitude of heat flux on the mold side less than that of the cast part. The maximum heat flux values in the cast and mold parts show a high-temperature differential on the location, while the location with minimum heat flux has a maximum distance with the poured molten metal, and thus, there is a minimum temperature difference. Hence the maximum and minimum heat flux is presented on cast and mold parts at the location where the minimum and maximum nodal temperature results, respectively.

4.2 Parametric Study

A series of solidification modelling were conducted by varying parameters that affect the solidification process of casting. The parameters used in this study are Mold size, pouring temperature, and mold material property. The effects of each parameter on solidification time, the maximum and minimum nodal temperature on nodes at discrete time instant, and associated cooling curve evaluated for every three cases.

4.2.1 Mold Size Effect

The effect of mold size on the solidification during the sand-casting process demonstrated. The problems have been simulated for all cases with different mold sizes as tabulated below.

Table 4.3: Different mold sizes used in the simulation

Parameter		***Case 1***	***Case 2***	***Case 3***
Geometry 1	Hight (m)	0.400	0.100	0.200
	Length/width (m)	0.800	0.425	0.250
Geometry 2	Hight (m)	0.500	0.150	0.250
	Length/width (m)	0.800	0.425	0.275
Geometry 3	Hight (m)	0.600	0.150	0.250
	Length/width (m)	0.900	0.450	0.250
Geometry 4	Hight (m)	0.500	0.200	0.300
	Length/width (m)	0.900	0.450	0.275
Geometry 5	Hight (m)	0.600	0.200	0.300
	Length/width (m)	1.000	0.425	0.300

The maximum nodal temperature inside the cast under different mold sizes in Table 4.3 is shown in Figure 4.17 below. The solidification of molten metal inside the mold cavity extracts latent heat of fusion through the mold wall. The thickness of the mold wall affects the heat transfer from the melt to the mold since the heat flux is inversely related to the thickness of the mold. In this study, as given in the table above, the problems were simulated for five geometries each. Geometry 1 for all cases is the actual geometry of the mold used in the ABMI foundry shop. The rest four geometries used to investigate the effect of mold size on the solidification heat transfer. The result of the simulation shown in Figure 4.17 below.

As illustrated in Figure 4.23, the cooling curve for case 1 reveals that the cooling of the molten grey cast iron shows a decrease in temperature with time. For the actual geometry used in the foundry

(geometry 1), the solidification starts at around 505 seconds, and the molten metal is fully solidifying at 2246 seconds (37.4 minutes). The length of the mushy zone that incorporates both solid and liquid phases simultaneously is 1741 seconds (29 minutes). In general, the solidification of grey cast iron in actual mold takes 37.4 minutes.

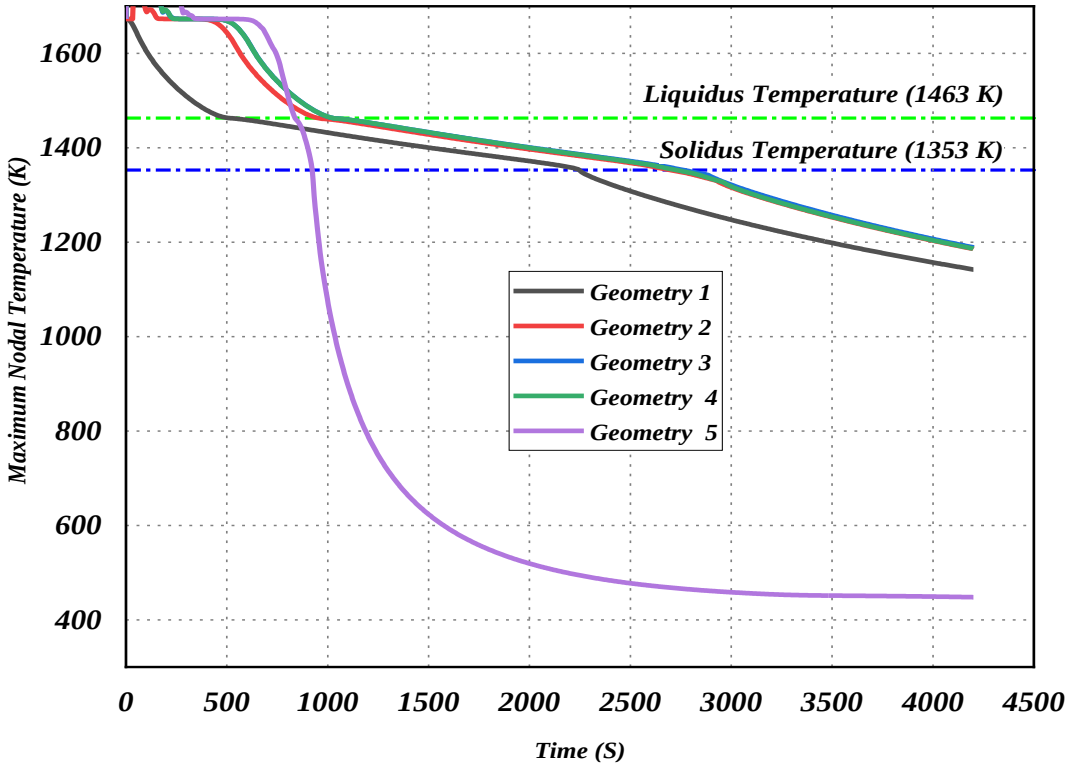

Figure 4.23: Cooling curve inside the cast body with different mold sizes for case 1

As shown in the same figure, the solidification of grey cast iron by using different geometries takes less time than the actual mold size used in the foundry. In the case of geometry 2, solidification starts at 494 seconds and ends at 2239 seconds. The solidification starts and end time results for geometry 3 are 492 seconds and 2227 seconds, respectively. The start and end of solidification time for geometry 4 are 491 seconds and 2193 seconds, respectively. Lastly, the solidification starts and end time for geometry 5 is 94 seconds and 170 seconds.

Following the cooling curve plot for case1, the cooling curve shows a relatively tight curve for all geometries except geometry 5. For geometry 5 the largest of all molds used in the simulation, the simulated cooling rate is high since the thickness of the mold increases vertically and horizontally. The result shows that increasing the mold size will minimize the solidification time of grey cast iron casting. Even though the solidification time decreases with increasing mold thickness, increasing the thickness may result in excess energy consumption.

The solidification pattern of case 2 can be seen in Figure 4.24; the result revealed that increasing the thickness of mold size results in less solidification time during the simulation. The cooling curve for five geometries shows almost the same cooling curve from the given figure except for geometry 4. Geometry 4 has the maximum thickness of the mold. The effect of mold thickness on the solidification shows close results for four different geometries; inconsequential thickness increment was the small actual geometry of the body. The solidification starts and end times for all other geometries and geometry 4 are 34 seconds and 176 seconds, 52 seconds, and 255 seconds. Thus geometry 4 has a maximum cooling rate and minimum solidification time.

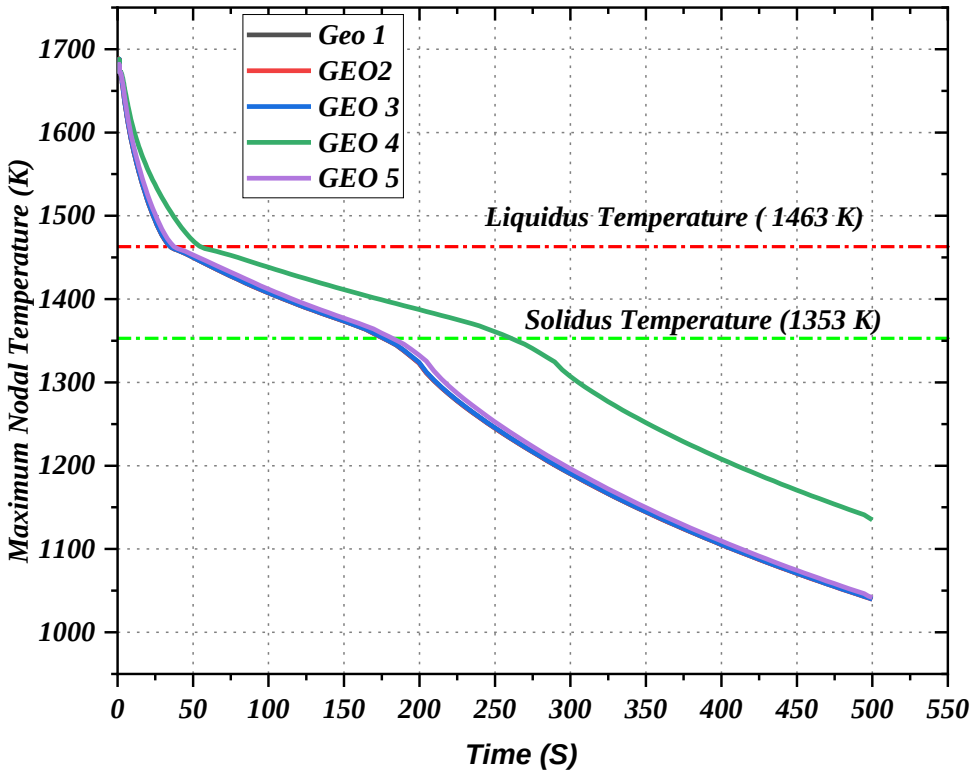

Figure 4.24: Cooling curve inside the cast body with different mold size for case 2

Besides the cooling curve under different mold geometry for case 3 shown in Figure 4.25, the result of the cooling curve under different mold sizes shows an overlapping graph. There is an insignificant difference in the maximum nodal temperature of the cast body under different mold thicknesses. The slight difference may be due to the range of solidification is small in pure aluminum casting.

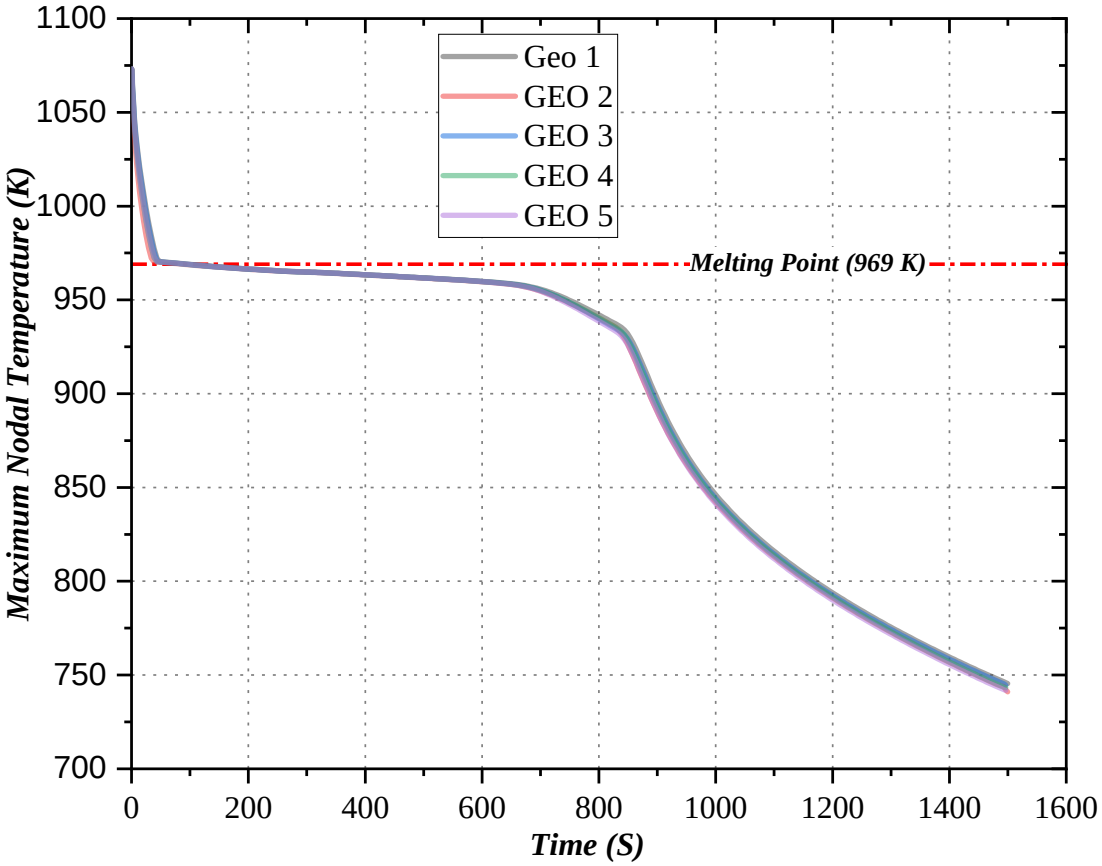

Figure 4.25: Cooling curve inside the cast body with different mold size for case 3

4.2.2 Mold Material Property Effect

Since the type and property of mold material used in foundry greatly influence the solidification of molten metal, this study simulates the different thermophysical properties of mold material. The solidification simulation under different mold properties presented in terms of cooling. For the simulation, there are five simulations, the first was simulated by using the actual measured density of sand with selected other properties, and the rest four scenarios used. The scenarios selected from actual material properties from previous experimental studies around the world. The scenarios used in the simulation listed in the previous chapter (section 3.3.2.1.2).

The variation of thermophysical property of mold material was examined by simulating each case of the problem and plotting their cooling curve on their maximum nodal temperature. The resulting cooling curve for each cases using different scenarios given in the previous chapter was given in Table 4.4 below. From the result of the cooling curve, the solidification starting and finishing time is tabulated below in Table 4.4.

Table 4.4: solidification time values under different mold property

	Solidification for Case 1		***Solidification for Case 2***		***Solidification for Case 3***	
	starts at (S)	*ends at (s)*	*starts at (S)*	*ends at (s)*	*starts at (S)*	*ends at (s)*
Actual	507	2243	34	174	59	129
Scenario 1	681	3236	47	260	102	207
Scenario 2	345	1398	21	105	92	137
Scenario 3	703	3245	48	248	67	175
Scenario 4	657	3118	46	254	71	201

The simulation of solidification of grey cast iron for ash cleaner door casting (case 1) illustrated in Figure 4.26. The evidence from the simulation implies that the cooling rate is high for scenario 2, which has the highest non-linear thermal conductivity relative to other scenarios. The simulation shows the completion of solidification with the shortest time that is 1398 seconds. The second-highest cooling rate was observed from the actual case, which has a maximum linear thermal conductivity. The solidification for the actual case ends at 2243 seconds. Even if the solidification completion time for the rest three scenarios has shown a small and insignificant difference, their cooling curve pattern shows close agreement, as illustrated in Figure 4.26(a). The end solidification time was 3236, 3245, and 3118 seconds for scenario1, scenario 3, and scenario 4.

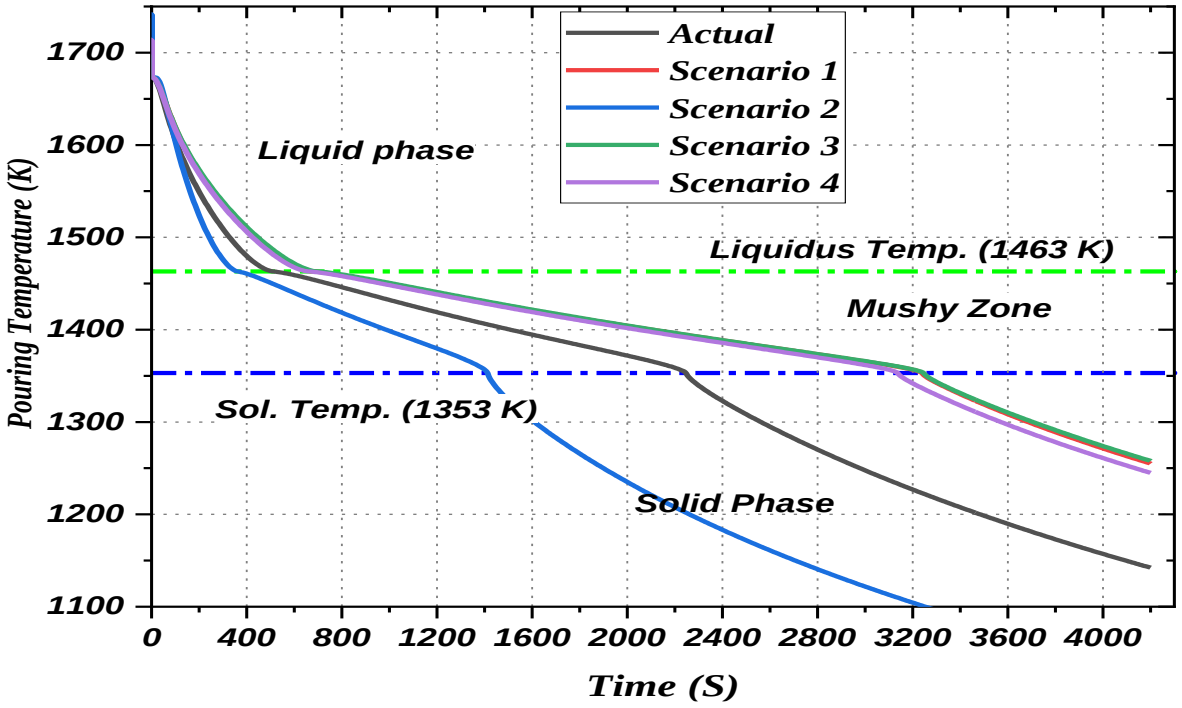

Figure 4.26: Cooling curve inside the cast body with varying mold material property for case 1

For case 2, the cooling curve as presented in Figure 4.27 below shows the solidification starting and end time in the table above. As presented in the cooling curve, a maximum cooling rate with minimum solidification time was exhibited in scenario 2 with a solidification end time of 105 seconds. The following minimum solidification time and maximum cooling rate were recorded during the actual case simulation with a solidification completion time of 174 seconds. As of case 1, other simulation shows close agreement. For scenario 1, scenario 3, and scenario 4, the molten grey cast iron is fully solidified at 260,248, 253 seconds.

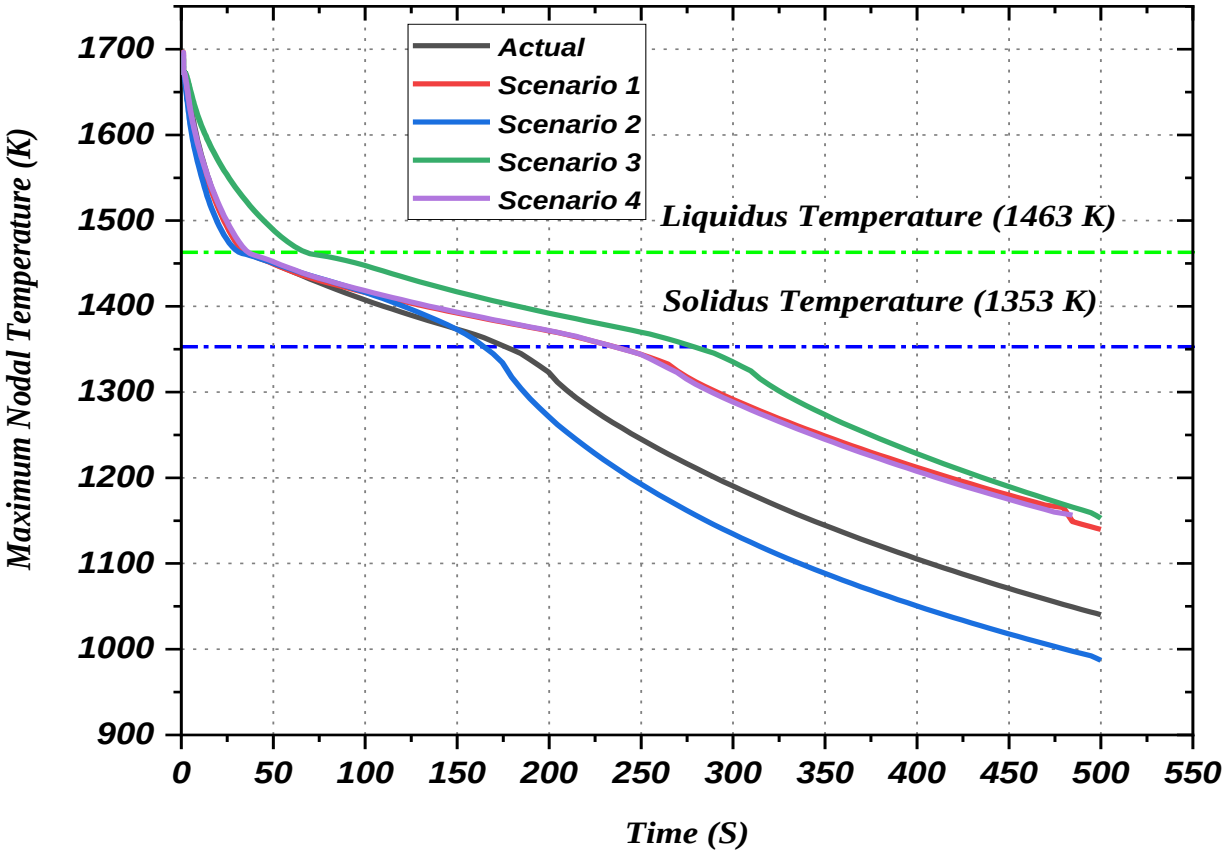

Figure 4.27: Cooling curve inside the cast body with varying mold material property for case 2

For casting a flywheel (case 3), the cooling curve results with different scenarios presented in Figure 4.28. As of the other two cases, scenario 2 exhibits the highest cooling rate with a short period of solidification. The Time taken to solidify the molten aluminum inside the mold material with the property of scenario 2 is only 137 seconds. the actual material property case of solidification takes 129 seconds. While the solidification of pure aluminum flywheel casting with the property of mold given under scenario 1, scenario 3, and scenario 4 takes 207, 175 and 201 seconds.

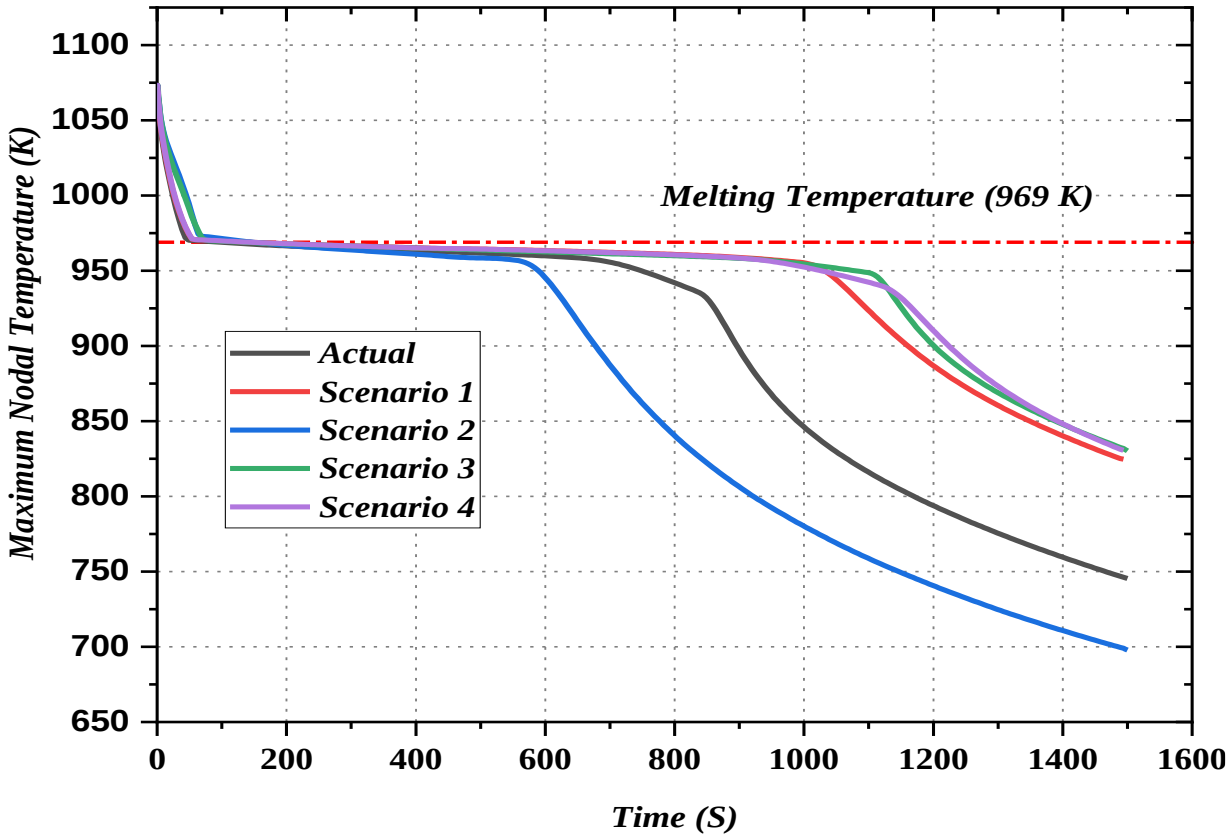

Figure 4.28: Cooling curve inside the cast body with varying mold material property for case 3

The simulation of solidification of sand-casting under different mold material properties shows that the change in the thermophysical property of mold material can significantly affect the solidification time a cooling rate of a sand-casting process. Solidification of metals inside the sand mold with high thermal conductivity would solidify with less time. Besides, the solidification is slow if thermal conductivity is low for sand. Thus, using appropriate mold material, consistent measurement of mold material property is vital in controlling the solidification of a sand-casting process.

4.2.3 Pouring Temperature Effect

The solidification simulation of three cases was demonstrated by varying the pouring temperature of the molten metal used for each case. All three cases set with the mesh size and mold wall thickness. The three cases having different pouring temperatures resulted in the difference in the cooling curves and solidification time, as shown in as can be seen from Figure 4.29, the resulting graph of the cooling curve for case 1 shows a decreasing trend of temperature with time. In figure presents the cooling curve for seven pouring temperature values. As the pouring temperature decreases from 1673 K to 1493 k, the solidification time decreases. The value of start and end time of solidification presented in Table 4.5. The maximum cooling rate and short solidification were achieved during the casting with

a pouring temperature of 1493k with 1193 seconds. Above and beyond, the longest solidification with the lowest cooling rate achieved with a pouring temperature of 1673 k at 2243 seconds.

The cooling curve for case 2 and case 3 also given in Figure 4.30and Figure 4.31. the result shows the same trend as in case 1. The solidification time at different pouring temperatures is given in Table 4.5 above. The cooling rate is exhibited high for the case with minimum pouring temperate with a short solidification period. At the same time, the solidification rate is slow for cases with maximum pouring temperature. Besides, the solidification takes the most prominent time to be completed in each case presented in the graph below.

Varying the pouring temperature of molten metal shows variation mostly on the solidification time of the process. This intern affects microstructure formation during solidification and consequently affects the final cast product property. (The pouring temperatures considered as the temperature inside the mold cavity). The solidification time values retrieved from the Simulation summarized in Table 4.5 below.

Table 4.5: solidification time values under different pouring temperature

	Solidification for Case 1		***Solidification for Case 2***		***Solidification for Case 3***	
Pouring temperature	*starts at (S)*	*ends at (s)*	*starts at (S)*	*ends at (s)*	*starts at (S)*	*ends at (s)*
1673	507	2243	34	177	-	-
1643	421	2053	28	161	-	-
1613	342	1866	23	143	-	-
1583	271	1687	19	128	-	-
1553	205	1514	13	114	-	-
1523	151	1348	10	98	-	-
1493	103	1193	6.5	86	-	-
1073	-	-	-	-	59	129
1053	-	-	-	-	43	103
1033	-	-	-	-	32	82
1013	-	-	-	-	50	95
993	-	-	-	-	37	77

As shown in Figure 4.16 (a), the resulting graph of the cooling curve for case 1 shows a decreasing temperature trend with time. In figure presents the cooling curve for seven pouring temperature values. As the pouring temperature decreases from 1673 K to 1493 k, the solidification time decreases. The value of start and end time of solidification presented in Table 4.5. the maximum cooling rate and short solidification were achieved during the casting with a pouring temperature of 1493k with 1193 seconds. Above and beyond, the longest solidification with the lowest cooling rate achieved with a pouring temperature of 1673 k with 2243 seconds.

Varying the pouring temperature of molten metal shows variation mostly on the solidification time of the process. This intern affects microstructure formation during solidification and consequently affects the final cast product property.

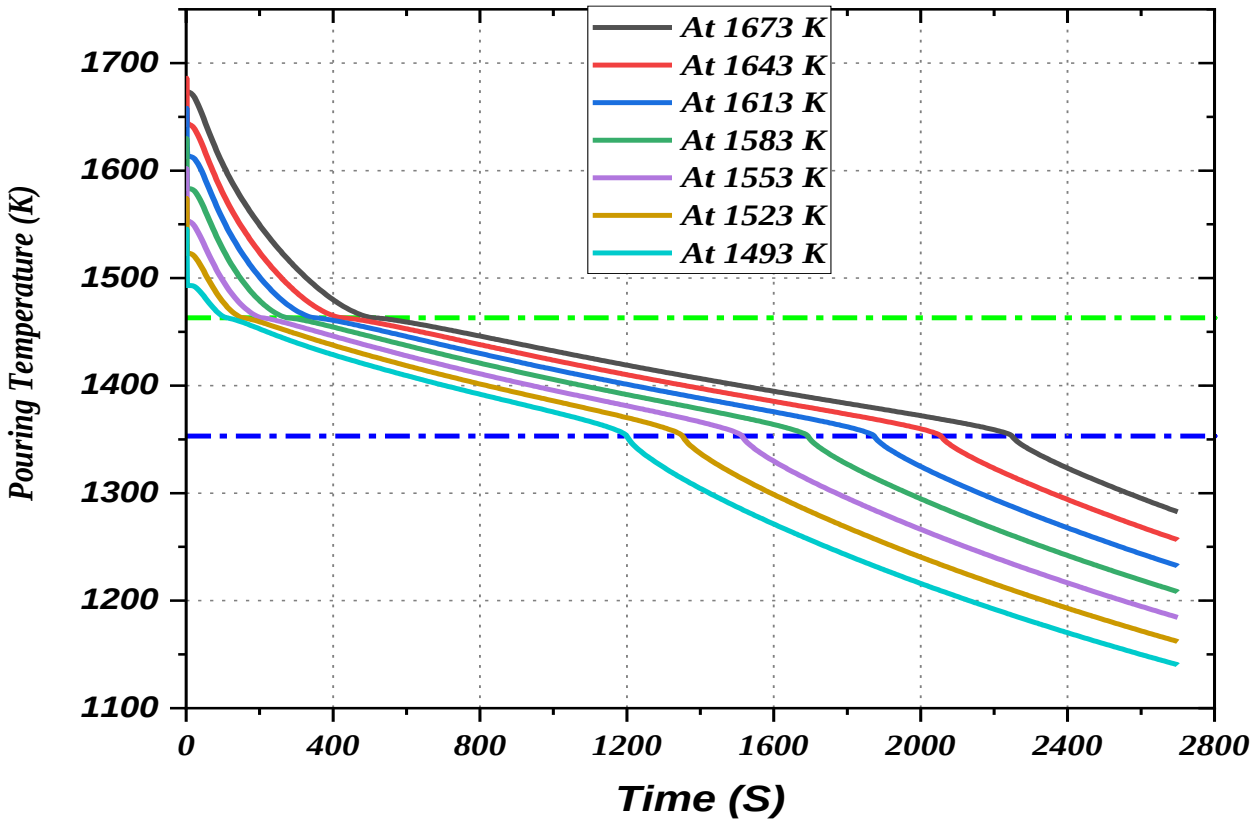

Figure 4.29 Cooling curve inside the cast body at different pouring temperatures for case 1

The cooling curve for case 2 also given in Figure 4.30. The result shows the same trend as in case 1. The solidification time at different pouring temperatures is given in Table 4.5 above. The cooling rate is exhibited high for the case with minimum pouring temperate with a short solidification period. At the same time, the solidification rate is slow for cases with maximum pouring temperature. Besides, the solidification takes the most significant time to complete in each case, as presented in the graph below.

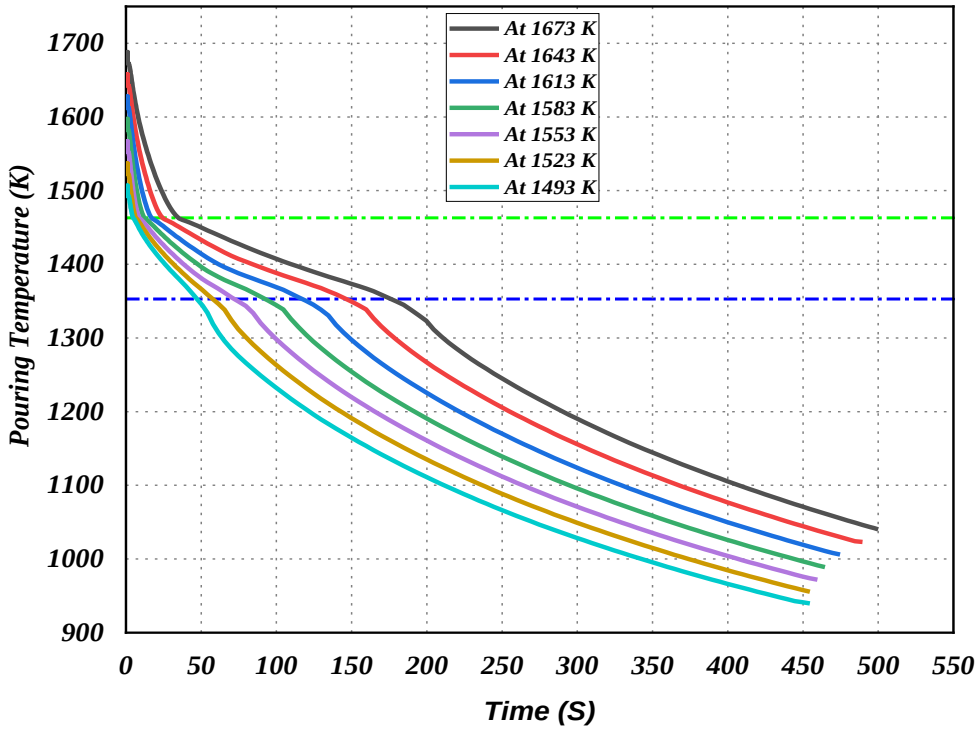

Figure 4.30: Cooling curve inside the cast body at different pouring temperatures for case 2

The cooling curve for case 3 also given in Figure 4.31; the result shows the same trend as in case 1. The solidification time at different pouring temperatures is given in Table 4.5 above. The cooling rate is exhibited high for the case with minimum pouring temperate with a short solidification period. At the same time, the solidification rate is slow for cases with maximum pouring temperature. Besides, solidification takes the most prominent time to complete in each case, as presented in the graph below.

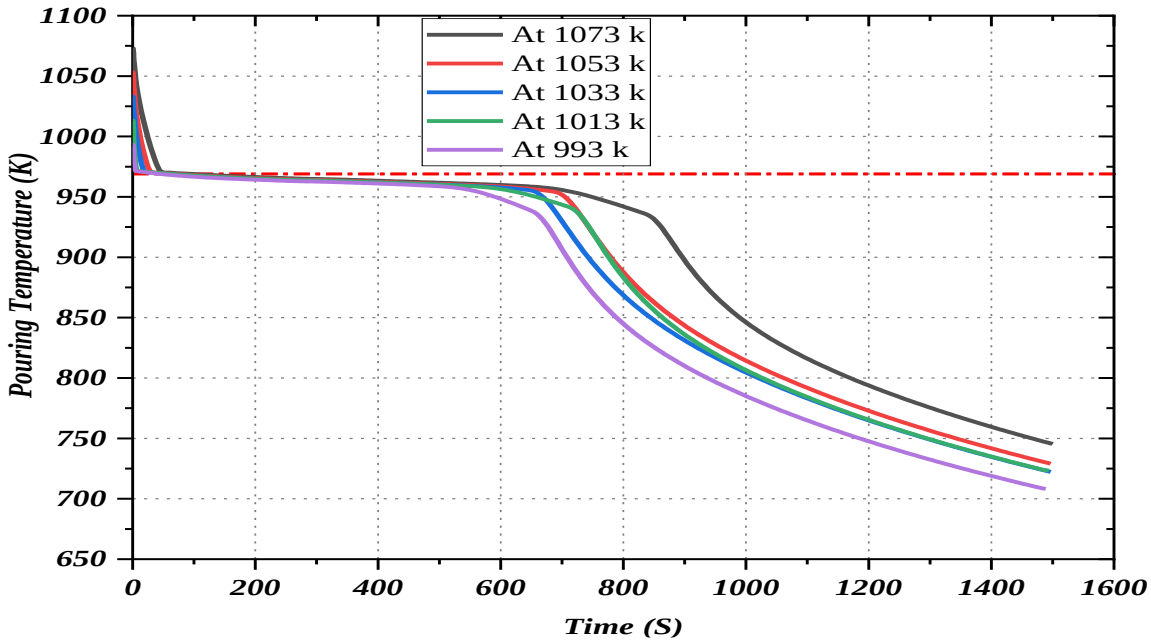

Figure 4.31: Cooling curve inside the cast body at different pouring temperatures for case 3

4.3 Validation of Results

Validation is the process of determining the degree to which a model is an accurate representation of the real world. The result validation is about validating the result of the computational method with an experimental data which is basic in a specific field of study.

This section of the study was concerned with determining whether the model accurately represents the process. The conceptual model is a formal definition of the system under consideration in logical or mathematical form, typically comprising the underlying theoretical equations. In this section, focus given to the validation of the models under this study. For this study, two experimentally demonstrated the result of solidification used.

4.3.1 Validation of Grey cast iron solidification

The validation of computational results for case 1 and case 2 is done based on an experimental study by Stefanescu and Kanetcar. The experimental study of grey cast iron solidification in the sand mold was referenced [101]. The cooling curve for the literature data given in Figure 4.32. Even if the material used in the experimental and computational (this study) were the same, the chemical composition of cast iron is different. Therefore, the range of solidification on the experimental study is small relative to the material used in this study. The liquidus and solidus temperatures for the experimental study is 1416 K and 1426 K. Even if the mushy zone range for the experimental study is short (10 k) and computational simulation (110 K), the cooling curve shows a good agreement. Thus, the computational model used for modelling the sand-casting process in ABMI is valid, considering the differences in the dimensions and the compositions of the cast iron between the present model and references

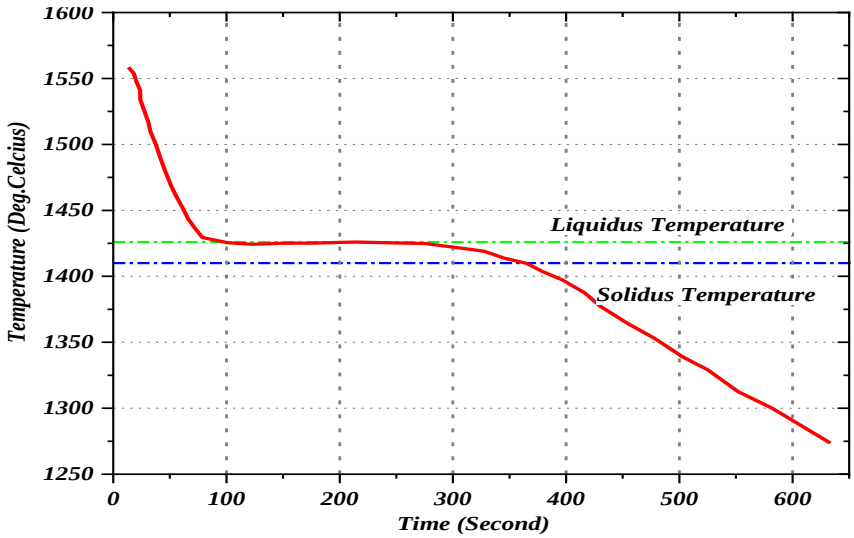

Figure 4.32: Experimental result for grey cast iron solidification

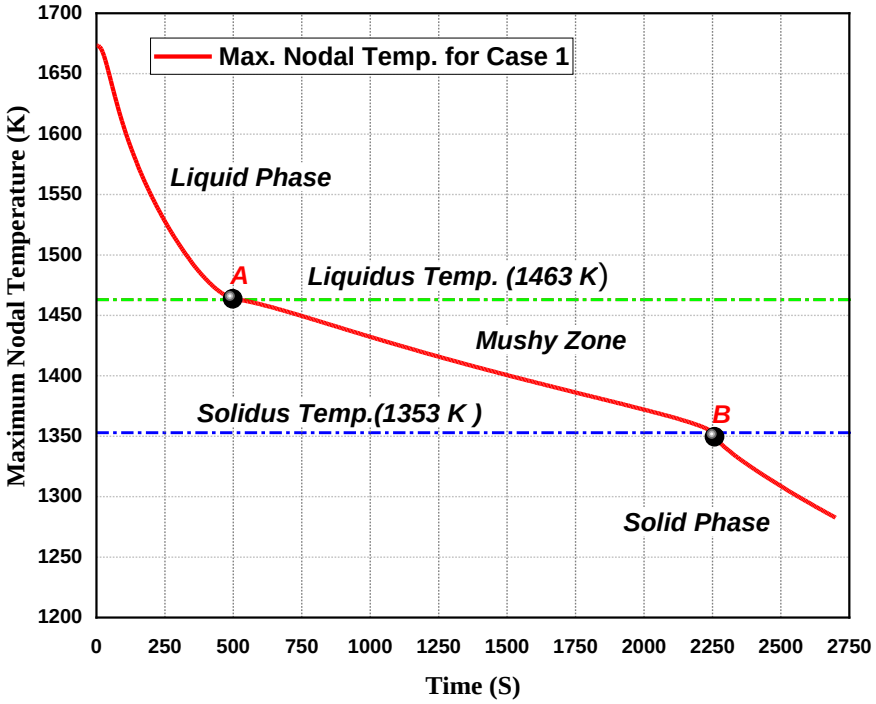

Figure 4.33: computational data result for grey cast iron solidification for case 1

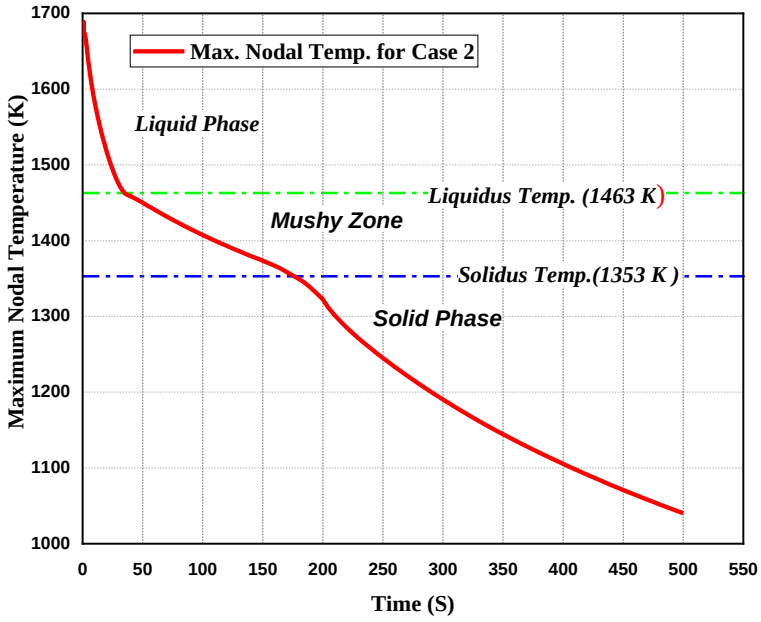

Figure 4.34: computational data result for grey cast iron solidification for case 2

4.3.2 Validation of Aluminum casting

The computational simulation result for aluminum casting (case 3) validated with an experimental solidification literature study for cylindrical aluminum casting inside a green sand mold. In the study performed by Sun and Chao, the details of the experimental study by Sun were given in reference

[102]. As shown in Figure 4.35(a) and (b), the cooling curve for computational simulation of the aluminum casting of a flywheel is compared with the experimental validation result.

From the computational investigation and experimental validation result compared, the cooling curve pattern for the simulation and experimental result shows a good agreement. Thus, the result of the computational model is reasonable, considering the differences in the dimensions and the pouring temperature of aluminum between the case 3 model and the reference.

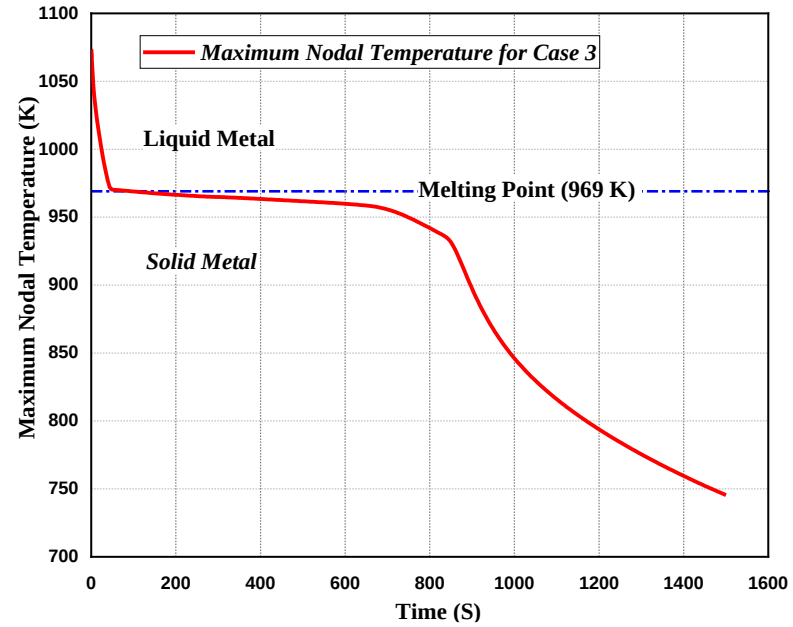

(a)

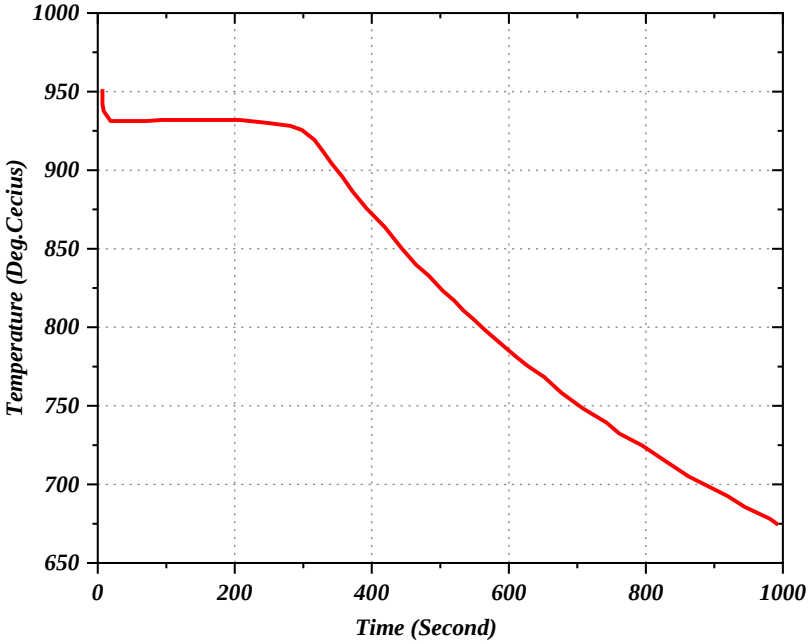

(b)

Figure 4.35: Comparison of computational data and experimental result for Aluminum solidification for (a) case 3 simulation, (b) experimental data

Chapter 5: Conclusion and Recommendation

5.1 Conclusion

This study deals with the computational simulation of solidification during sand casting process to predict the heat transfer phenomenon encountered during a specific casting process. Three cases were selected from the ABMI foundry purposely.

The study analysis shows that the molten metal temperature decreases drastically when it first contacts the mold wall. Since during the initial stage, pouring the liquid metal cast into the mold cavity, the whole metal fluid flows and occupies the mold cavity, the liquid metal mixes thoroughly and releases heat to the sand mold due to the high temperature difference between the cast and mold material. Complete thermal contact is observed between the cast and the mold which makes the heat transfer to pure conduction, where the resistance offered by this liquid metal is negligible since liquid phase is superheated metal. Once the cast metal reaches the liquidus point on cooling, the cast shrinks and releases latent heat and also a number of metal oxides are released which causes an air gap between the cast and the mold. Due to this air gap the heat transfer phenomenon now changes to a complex one where all modes of heat transfer can be observed simultaneously. Steep slope at the beginning of solidification indicates a rapid solidification (high cooling rate) where a great amount of heat is released while shallow slope indicates slow cooling (low cooling rate).

When the molten metal temperature decreases to liquidus temperature, latent heat of fusion of cast material releases and the liquid phase change to the solid phase via the transition phase called a mushy zone. The range of mushy zone for case 1 and case 2 was extensive since the cast material used is cast alloy; it changes phases with a specified temperature range (110k). Besides, the transition from liquidus range to solidus range in aluminum casting occurs almost at a constant temperature. The range for the mushy region used in this study was small (2k).

The result of solidification time, maximum and minimum nodal temperature at the end of solidification given in table below.

Table 5.1: Simulation result of different parameters.

Results	***Case 1***	***Case 2***	***Case 3***
Simulation time (seconds)	2700	500	1500

Solidification starting time (seconds)	515	35	57
Solidification end time (seconds)	2249	177	133
Initial molten metal temperature (K)	1673	1673	1000
Maximum nodal temperature at end of simulation (K)	1282.6	764.43	465.59
Minimum nodal temperature at end of simulation (K)	894.34	674.91	452.66

Solidification pattern shows the liquid and solid phases with transition period at discrete time. As expected, size of the solidified iron increases and size of the melted iron decreases as time progresses for all cases. The cooling curve presented to the maximum nodal temperatures inside the casting for all cases. The nodal temperature versus graph were plotted to show the cooling pattern at eight different locations for all cases. The result of nodal cooling curve shows, the cooling rate is high at nodes near the mold wall, and it takes a shorter time to reach the liquidus temperature. For nodes around the center of the cast, as presented in the figure, the cooling rate is small compared to nodes near to mold wall. Moreover, it takes much more time to reach a specific temperature.

A parametric study was performed to study the effect of mold size, pouring temperature and mold material property on the solidification of the sand-casting process. The results also reveal that the cooling rate is maximum for a casting with a smaller mold wall thickness, a maximum thermal conductivity value, and a smaller pouring temperature for all cases. Validation of computation result was performed with experimental study result from relevant literature; validation shows that results are reasonable despite poring temperature and geometry of models used in this study and literature validation study.

5.2 Recommendations

The output of the sand-casting process simulation could significantly enhance the productivity and competitiveness of ABMI. The technique used in modelling the sand-casting process gives an insight to the company to conduct large numbers of simulations within a short time and with significantly less cost than physical trials. Also, this study's result improves the industries' capacity in developing fundamental models to describe the physics and selected manufacturing process.

Result of sand-casting model used as a tool for process optimization in the foundry shop for both existing castings and those under development for the first time, by eliminating shop-floor. During modelling, several iterations carried out until the desired quality and yield achieved. Even with minor improvements on castings produced in large numbers can lead ABMI to a significant saving of material, energy, equipment and labor resources.

Since the convection effect is small on the cooling, and it takes much time to cool the casting the foundry could use forced convection like chilling process. Using different mold materials could provide an interesting insight of the casting process. Finally, measuring and recording the actual thermophysical and other casting related defect is vital in enhancing the production process flow, the company could take action to measure the property of sand and cast.

5.2.1 Future work

This study has demonstrated the heat transfer during the solidification of the sand-casting process. This work needs to be enhanced by incorporating filling stage and under the cooling stage for more general use. In this study, the effect of the gating system and riser is not studied; it would be helpful to extend this work by encompassing the overall process. In this study, only computational simulation of the solidification process was implemented. Therefore, an experimental study of solidification is more accurate and realistic to consider for future work. For more accurate computational simulation results, the following improvements recommended:

i. Use of accurate thermophysical properties of cast metal and sand mold.
ii. Simulation of the air-gap formation between cast and mold.
iii. Simulation of fluid-flow and convection in the liquid metal.

The other consideration for future work is the concept of microscopic modelling of the solidification process. In particular, significant future research and development have realized in the following five areas:

i. Prediction of casting defects (porosity, hot tear, etc.) by using computational method.
ii. Experimental study with numerical validation of sand-casting process.
iii. Combined thermal and mechanical study of solidification process.

References

[1] K. N. S. Lewis, Roland W., Perumal Nithiarasu, *Fundamentals of the Finite Element Method for Heat and Fluid Flow*. John Wiley & sons, Ltd, 2004.

[2] American Society of Metals(ASM), *ASM Handbook - Castings*, 15th ed. ASM International, 1998.

[3] B. Ravi, "Computer-aided casting design–past, present and future," *Indian Foundry J.*, vol. 45, no. 1, pp. 65–74, 1999.

[4] A. Prabhakar, M. Papanikolaou, K. Salonitis, and M. Jolly, "Sand casting of sheet lead: numerical simulation of metal flow and solidification," *Int. J. Adv. Manuf. Technol.*, vol. 8, 2019,

[5] S. Sulaiman and A. M. S. Hamouda, "Modeling of the thermal history of the sand casting process," *J. Mater. Process. Technol.*, vol. 113, no. 1–3, pp. 245–250, 2001,

[6] U. A. Dabade and R. C. Bhedasgaonkar, "Casting defect analysis using design of experiments (DoE) and computer aided casting simulation technique," *Procedia CIRP*, vol. 7, pp. 616–621, 2013,

[7] B. G. D. Gobin, "Physical modelling and numerical simulation of solid-liquid phase change in binary systems," *Trans. Model. Simul.*, vol. 6, pp. 11–21, 1993.

[8] M. T. Manzari, D. T. Gethin, and R. W. Lewis, "Optimisation of heat transfer between casting and mould," *Int. J. Cast Met. Res.*, vol. 13, no. 4, pp. 199–206, 2000,

[9] J. Hajkowski, P. Roquet, M. Khamashta, E. Codina, and Z. Ignaszak, "Validation Tests of Prediction Modules of Shrinkage Defects in Cast Iron Sample," *Arch. Foundry Eng.*, vol. 17, no. 1, pp. 57–66, 2017,

[10] T. Skrzypczak, E. Węgrzyn-Skrzypczak, and L. Sowa, "Numerical model of solidification process of Fe-C alloy taking into account the phenomenon of shrinkage cavity formation," *MATEC Web Conf.*, vol. 254, no. 02009, pp. 1–7, 2019,

[11] B. G. Thomas and M. Bellet, "Modeling of Stress, Distortion, and Hot Tearing," *Casting*, vol. 15, pp. 449–461, 2018,

[12] Y. Motoyama, S. Sekiguchi, T. Okane, and M. Yoshida, "Thermo-elasto-plastic fi nite element analysis of warping deformation during casting of gray cast iron," *J. Mater. Process. Tech.*, vol. 277, no. September 2019, p. 116454, 2020,

[13] H. Rathod, J. K. Dhulia, and N. P. Maniar, "Prediction of Shrinkage Porosity Defect in Sand Casting Process of LM25," *IOP Conf. Ser. Mater. Sci. Eng.*, vol. 225, no. 1, 2017,

[14] M. Salcudean and Z. Abdullah, “On the numerical modelling of heat transfer during solidification processes,” *Int. J. Numer. Methods Eng.*, vol. 25, no. 2, pp. 445–473, 1988,

[15] G. Petrone, G. Cammarata, and V. a Doria, “Simulation of PCM Melting Process in a Differentially Heated Enclosure,” 2012.

[16] H. Usmani, Asif , S. and Hong, *Finite element analysis for heat transfer*. London, 1994.

[17] T. L. Bergman and A. S. Lavine, *Fundamentals of Heat and Mass Transfer*, 8th ed. WILEY, 2017.

[18] American Society of Metals(ASM), *Metals process simulation*, vol. 22B. ASM International, 2010.

[19] D. M. Stefanescu, *Science and Engineering of Casting Solidification*, First. New York: Springer, 2015.

[20] C. M. Choudhari, B. N. Narkhede, and S. K. Mahajan, “Modeling and simulation with experimental validation of temperature distribution during solidification process in sand casting,” *Int. J. Comput. Appl.*, vol. 78, no. 16, pp. 23–29, 2013,

[21] J. F. and T. B, *A First Course in Finite Elements*. John Wiley and Son’s, 2007.

[22] R. W. Lewis, H. C. Huang, A. S. Usmani, and M. R. Tadayon, “Solidification in castings by finite element method,” *Mater. Sci. Technol. (United Kingdom)*, vol. 6, no. 5, pp. 482–490, 1990,

[23] S. M. Lee and W. J. Lee, “Finite-element analysis on thermomechanical behavior of a marine propeller casting in the sand-casting process,” *J. Mater. Eng. Perform.*, vol. 14, no. 3, pp. 388–394, 2005,

[24] E. L. Wilson and R. E. Nickell, “Application of the finite element method to heat conduction analysis,” *Nucl. Eng. Des.*, vol. 4, no. 3, pp. 276–286, 1966,

[25] G. A. Keramidas, “Finite Element of the Heat Conduction Equation with Temperature Dependent Coefficients,” *Math. Comput. Simul.*, vol. 22, pp. 248–255, 1980.

[26] S. N. Kulkarni and K. Radhakrishna, “Prediction of solidification time during solidification of aluminum base alloy castings cast in CO2-sand mold,” *Int. J. Adv. Manuf. Technol.*, vol. 34, no. 11–12, pp. 1098–1110, 2007,

[27] M. Samonds, K. Morgan, and R. W. Lewis, “Finite element modelling of solidification in sand castings employing an implicit-explicit algorithm,” *Appl. Math. Model.*, vol. 9, no. 3, pp. 170–174, 1985,

[28] “Multiscale simulation of Aluminium casting : Cooling rate and grain size,” Ruhr-Universit ¨at Bochum, 2017.

[29] A. W. Dametew, D. Kitaw, and F. Ebinger, "The Roles of TQM and JIT for Basic Metal Industries Global Competitiveness," *Ind. Eng. Manag.*, vol. 6, no. 2, pp. 1–12, 2017,

[30] D. Kitaw, S. T. Meselu, and E. Berhan, "Enhancing Competitiveness Through Innovative Lean Manufacturing (In Cases of Ethiopian Metal and Steel Industries)," in *Third International AfricaLics Conference*, 2017, pp. 1–17.

[31] "Ten Year Development Plan of Federal Democratic Republic of Ethiopia," Addis Ababa, 84AD.

[32] T. Hailemariam, "Design & Analysis of Casting Process of Mill Roller: A Case Study of Akaki Basic Metals Industry," Adama Science and Technology University, 2018.

[33] D. Netsanet, "Porosity Effect Analysis on The Dimension of Cast Pinion Gear, Drive Disc and Head Stock Components of Manganese Steel," Addis Ababa University, 2016.

[34] B. Tadele, "Minimization Of Sand Cast Defect Through Integration of Failure Mode Effect Analysis (FMEA) With Casting Simulation," Adama Scince and Technology University, 2017.

[35] L. Guta, T. Abdo, J. Aman, T. G/michael, N. Assefa, and M. Tufa, "The Development of Ethiopian Steel Industries : Challenges , Prospects , and Policy Options," Addis Ababa, 2016.

[36] Z. Yared, "Process capability analysis of sand casting of flange roller (A case study of Akaki basic metals industry)," Adama Science and Technology University, 2018. [Online]. Available: http://link.springer.com/10.1007/978-3-319-76887-8%0Ahttp://link.springer.com/10.1007/978-3-319-93594-2%0Ahttp://dx.doi.org/10.1016/B978-0-12-409517-5.00007-3%0Ahttp://dx.doi.org/10.1016/j.jff.2015.06.018%0Ahttp://dx.doi.org/10.1038/s41559-019-0877-3%0Aht

[37] A. A. Kassie, "Minimization of Casting Defects," *IOSR J. Eng.*, vol. 03, no. 05, pp. 31–38, 2013,

[38] A. Tegegne and N. Desalegn, "Analysis of Pores Size and Distribution Effects On the Total Dimensional Specification of Pinion Gear, Head Stock And Drive Disc of Manganese Steel (46MNSi4) Casts using Control Chart And Ishikawa Diagram (Case at Akaki-Basic Metals Industry –Ethiopia)," *Int. J. Eng. Trends Technol.*, vol. 67, no. 1, pp. 23–33, 2019,

[39] K. Salonitis, B. Zeng, H. A. Mehrabi, and M. Jolly, "The Challenges for Energy Efficient Casting Processes," *Procedia CIRP*, vol. 40, pp. 24–29, 2016,

[40] A. K. Tieu and I. S. Kim, "Simulation of the continuous casting process by a mathematical model," *Int. J. Mech. Sci.*, vol. 39, no. 2, pp. 185–192, 1997.

[41] P. Beeley, *Foundry Technology*. Butterworth-Heinemann, 2001.

[42] R. Singh, *Introductionto Basic Manufacturing Processes and Workshop Technology*, vol. 3. New Delhi: New Age International (P) Limited, 2013.

[43] S. G. Shabestari and M. Malekan, "Thermal Analysis Study of The Effect of the Cooling Rate of on The Microstructure And Solidification Parameters of 319 Aluminum Alloy," vol. 44, no. 3, pp. 305–312, 2005.

[44] K.-O. (Oscar) Yu, *Modeling for Casting and solidification processing*. New York: CRC Press LLC, 2002.

[45] M. M. Pariona and A. C. Mossi, "Numerical simulation of heat transfer during the solidification of pure iron in sand and mullite molds," *J. Brazilian Soc. Mech. Sci. Eng.*, vol. 27, no. 4, pp. 399–406, 2005,

[46] T. Suzuki, "Fundamentals of solidification," *Keikinzoku/Journal Japan Inst. Light Met.*, vol. 46, no. 3, pp. 156–161, 1996.

[47] W. U. H. Du, "Macro-Micro Modeling of Solidification," vol. 23, no. 5, pp. 622–629, 1999.

[48] M. M. Pariona, J. K. Rugenski, M. V. Cant, J. E. Spinelli, and A. Garcia, "Thermal stress analysis of a directionally solidified Al-1 wt%Ni alloy casting," *Finite Elem. Anal. Des.*, vol. 46, no. 10, pp. 889–895, 2010,

[49] J. A. and Dantzig and L. S.C, "Modeling of heat flow in sand castings: Part II. Applications of the boundary curvature method," *Metall. Trans. B*, vol. 16, no. 2, pp. 203–209, 1985,

[50] M. R. Barkhudarov, "Computer Modelling of Solidification of Pure Metals and Alloys," University of Sheffield, 1995.

[51] J. Miettinen and S. Louhenkilpi, "Calculation of thermophysical properties of carbon and low alloyed steels for modeling of solidification processes," *Metall. Mater. Trans. B*, vol. 25, no. 6, pp. 909–916, 1994,

[52] D. M. Stefanescu, G. Upadhya, and D. Bandyopadhyay, "Heat transfer-solidification kinetics modeling of solidification of castings," *Metall. Trans. A*, vol. 21, no. 3, pp. 997–1005, 1990,

[53] G. M. Poole, "Mathematical Modeling of Solidification Phenomena in Electromagnetically Stirred Melts," University of Alabama, 2014.

[54] A. Cosimo, V. Fachinotti, and A. Cardona, "An enrichment scheme for solidification problems," *Comput. Mech.*, vol. 52, no. 1, pp. 17–35, 2013,

[55] J. A. Pero-Sanz Elorz, M. J. Quintana Hernández, and L. F. Verdeja González, *Solidification and Solid-State Transformations of Metals and Alloys*. 2017.

[56] S. Sepideh, "Heat transfer during melting and solidification in heterogeneous material," Virginia Polytechnic Institute and State University, 1988.

[57] C. Hong, *Computer Modelling of Heat and Fluid Flow in Materials Processing*. London: IOP Publishing Ltd, 2004.

[58] B. Nedjar, "An enthalpy-based finite element method for nonlinear heat problems involving phase change," *Comput. Struct.*, vol. 80, no. 1, pp. 9–21, 2002,

[59] J. Guo and M. Samonds, "Modeling of alloy casting solidification," *Jom*, vol. 63, no. 7, pp. 19–28, 2011,

[60] M. A. A. Khan and A. K. Sheikh, "Simulation tools in enhancing metal casting productivity and quality: A review," *Proc. Inst. Mech. Eng. Part B J. Eng. Manuf.*, vol. 230, no. 10, pp. 1799–1817, 2016,

[61] N. Sultana, Y. Rahman, and A. Das, "Solidification and Filling Related Defects Analysis Using Casting Simulation Technique with Experimental Validation," *Int. J. Mech. Eng. Appl.*, vol. 6, no. 6, pp. 150–160, 2018,

[62] C. M. Choudhari, B. E. Narkhede, and S. K. Mahajan, "Methoding and simulation of LM 6 sand casting for defect minimization with its experimental validation," *Procedia Eng.*, vol. 97, pp. 1145–1154, 2014,

[63] A. F. Ferreira, W. B. Chrisóstimo, R. C. Sales, W. Jefferson, L. Garção, and N. D. P. Sousa, "Effect of pouring temperature on microstructure and microsegregation of as-cast aluminum alloy," 2019.

[64] S. Piseth and D. Masnur, "Solidification and Microstructures Characteristic in Unidirectional Solidification of Al-7 wt .% Si Alloy Solidification and Microstructures Characteristic in Unidirectional Solidification of Al-7 wt .% Si Alloy," no. March, 2020.

[65] E. Moumeni, "Solidification of cast iron - A study on the effect of microalloy elements on cast iron," Technical University of Denmark, 2013.

[66] T. Li, W. Tao, Z. Wang, X. Liu, and J. Hou, "Numerical simulation on the transient temperature field of anode rodding in aluminium reduction cells," *Metals (Basel).*, vol. 8, no. 12, 2018,

[67] C. Bailey, P. Chow, M. Cross, Y. Fryer, and K. Pericleous, "Multiphysics modelling of the metals casting process," *Proc. R. Soc. A Math. Phys. Eng. Sci.*, vol. 452, no. 1946, pp. 459–486, 1996,

[68] B. Skočilasová and J. Skočilas, "Effect of mold material on temperature distribution in alloy cast," in *AIP Conference Proceedings*, 2016, vol. 1768, no. 020017, pp. 1-.

[69] T. S. Prasanna Kumar, "Casting Simulation Methods," in *Comprehensive Materials Processing*, vol. 5, Elsevier, 2014, pp. 235–257.

[70] E. Pardo and D. C. Weckman, "A fixed grid finite element technique for modelling phase

change in steady-state conduction–advection problems," *Int. J. Numer. Methods Eng.*, vol. 29, no. 5, pp. 969–984, 1990,

[71] V. R. Voller and C. R. Swaminathan, "Fixed grid techniques for phase change problems: a review," *Int. J. Numer. Methods Eng.*, vol. 30, pp. 875–898, 1990.

[72] V. R. Voller, C. R. Swaminathan, and B. G. Thomas, "Fixed grid techniques for phase change problems: A review," *Int. J. Numer. Methods Eng.*, vol. 30, no. 4, pp. 875–898, 1990,

[73] Y. W. B. H. Kwon, *The Finite Element Method Usign MATLAB.pdf*. Florida: CRC Press LLC, 1997.

[74] J-N-Reddy, *An Introduction to the Finite Element Method*, Third Edit. New York: Mc Graw Hill, 2006.

[75] K. Ravindran and R. W. Lewis, "Finite element modelling of solidification effects in mould filling," *Finite Elem. Anal. Des.*, vol. 31, no. 2, pp. 99–116, 1998,

[76] O. C. Zienkiewicz and C. J. Parekh, "Transient field problems: Two-dimensional and three-dimensional analysis by isoparametric finite elements," *Int. J. Numer. Methods Eng.*, vol. 2, no. 1, pp. 61–71, 1970,

[77] G. Aguirre-Ramirez and J. T. Oden, "Finite element technique applied to heat conduction in solids with temperature dependent thermal conductivity," *Int. J. Numer. Methods Eng.*, vol. 7, no. 3, pp. 345–355, 1973,

[78] R. W. Lewis and P. M. Roberts, "Finite element simulation of solidification problems," *Appl. Sci. Res.*, vol. 44, no. 1–2, pp. 61–92, 1987,

[79] S. Sulaiman and A. M. S. Hamouda, "Modeling of the thermal history of the sand casting process," *J. Mater. Process. Technol. 113*, vol. 113, pp. 245–250, 2001.

[80] K. Krabbenhoft, L. Damkilde, and M. Nazem, "An implicit mixed enthalpy-temperature method for phase-change problems," *Heat Mass Transf. und Stoffuebertragung*, vol. 43, no. 3, pp. 233–241, 2006,

[81] D. J. Celentano, M. A. Cruchaga, and B. J. Schulz, "On the effect of natural convection on the thermal-microstructural evolution in gray cast-iron solidification," *Metall. Mater. Trans. B Process Metall. Mater. Process. Sci.*, vol. 37, no. 2, pp. 253–264, 2006,

[82] C. Li, G. B. Zhao, S. Y. Zhang, and X. Han, "Study on the Temperature Field of Casting Process in ANSYS," *Adv. Eng. Forum*, vol. 2–3, pp. 856–860, 2011,

[83] P. Kotas, C. C. Tutum, J. Thorborg, and J. H. Hattel, "Elimination of hot tears in steel castings by means of solidification pattern optimization," *Metall. Mater. Trans. B Process Metall. Mater. Process. Sci.*, vol. 43, no. 3, pp. 609–626, 2012,

[84] B. V. Patel and D. Diwedi, "Finite Element Analysis of Solidification of L-Shaped Casting Using Ansys Parametric Design," *Int. J. Adv. Res. Ideas Innov. Technol.*, no. 5, pp. 87–95, 2015.

[85] G. Kidu and T. Asmamaw, "Simulation based analysis of sand casting process parameters of 46MnSi 4 alloy steel trash plate castings applicable for sugar factory roller stand," *Int. J. Eng. Sci. Res. Technol.*, vol. 6, no. 2, pp. 454–466, 2017.

[86] T. H. Hirigo and B. Singh, "Design and analysis of sand casting process of mill roller Edge effect," *Int. J. Adv. Manuf. Technol.*, 2019, [Online]. Available: https://doi.org/10.1007/s00170-019-04270-4

[87] C. Y. I. U. Wing, "Finite Element Simulation of Solidification," *J. Mater. Process. Technol.*, vol. 23, pp. 83–95, 1990.

[88] J. V. Juan and N. Q. Peter, "Thermophysical Properties," in *ASM Handbook*, vol. 15, no. Ref 24, 2008, pp. 468–481.

[89] K. C. Mills, *Recommended values of thermophysical properties for selected commercial alloys*, 1st ed. Cambridge England: WOODHEAD PUBLISHING LIMITE D, 2002.

[90] American Society of Metals(ASM), *Properties and selection: Irons steels and high performance alloys*, 1st ed. 1990.

[91] R. Asthana, A. Kumar, and N. Dahotre, *Materials science in manufacturing*, vol. 22, no. 6. Elsevier Science & Technology Books •, 2005.

[92] ANSYS, "Advanced Heat Transfer Topics ANSYS Mechanical Heat Transfer," 2010.

[93] M. M. Pariona, G. A. Salem, F. Bertelli, and N. Cheung, "Numerical simulation for prediction of filling process in a sand mould," *Rev. Latinoam. Metal. y Mater.*, vol. 28, no. 2, pp. 99–110, 2009.

[94] M. M. Pariona, F. Bertelli, N. Cheung, and A. Garcia, "Mathematical Modeling of Mold-Filling and Solidification of Castings: Part II – Application to A Cu 5%Zn Alloy Casting in a Sand Mold," *Acta Metall. Slovaca*, vol. 3, pp. 187–198, 2009.

[95] H. R. Shahverdi, F. Farhadi, A. Karimitaheri, P. Davami, and K. Asgari, "A Mathematical Model for Air-gap Formation at the Metal—Mould Interface in the Computer Simulation of the Solidification of Al—12%Si in a Sand Mould," *Cast Met.*, vol. 6, no. 4, pp. 231–236, 1994,

[96] D. J. Celentano, M. A. Cruchaga, and B. J. Schulz, "On the Effect of Natural Convection on the Thermal-Microstructural Evolution in Gray Cast-Iron Solidification," *Metall. Mater. Trans. B*, vol. 37, no. B, pp. 253–264, 2006,

[97] J. P. Holman, *Heat Transfer*, Sixth Edit. New York: Mc Graw Hill, 1986.

[98] J. H. L. IV and J. H. L. V, *A Heat Transfer Text Book*, Fourth edi. Massachusetts: Phlogiston Press, 2017.

[99] Y. A. Çengel, *Heat Transfer a Practical Approach*, Second.

[100] T. L. BERGMAN, A. S. LAVINE, F. P. INCROPERA, and D. P. DEWITT, *Fundamental of Heat and Mass Transfer*, Seventh Ed. John Wiley & Sons Ltd, 2011.

[101] D. M. Stefanescu, "Modeling of Micro-structural Evolution of Eutectic Cast Iron and of the Gray / White Transition," no. November, 2015.

[102] H. C. Sun and L. S. Chao, "An investigation into the effective heat transfer coefficient in the casting of aluminum in a green-sand mold," *Mater. Trans.*, vol. 50, no. 6, pp. 1396–1403, 2009,

Appendices

Appendix A: Thermophysical property of cast metals

A1: Thermophysical property of grey cast iron. [89]

Temperature (K)	*K (W/m. K)*	*Density (kg/m^3)*	*Cp (J/kg.)*
298	49	7200	490
373	48	7180	510
473	46	7150	555
573	43	7121	600
673	42	7092	640
773	41	7063	700
873	38	7034	785
973	35	7006	1000
1013	35	6995	1170
1173	33	7020	660
1273	29	6992	610
1353	29	6964	660
1463	26	6764	950
1473	26	6759	950
1573	27	6709	950
1673	28	6659	950

A2: Thermophysical property of Aluminum [92]

Temperature (K)	*K (W/m. K)*	*Density (Kg/m^3)*	*Enthalpy (KJ/Kg)*
600	-		-
650	-		-
700	-		-
750	197.8		520
800			580
850			640
900			700

933.47	740
933.47	1109
950	1119
1000	1175
1050	1231
1100	1288

Appendix B: Geometry of Models

Case 1

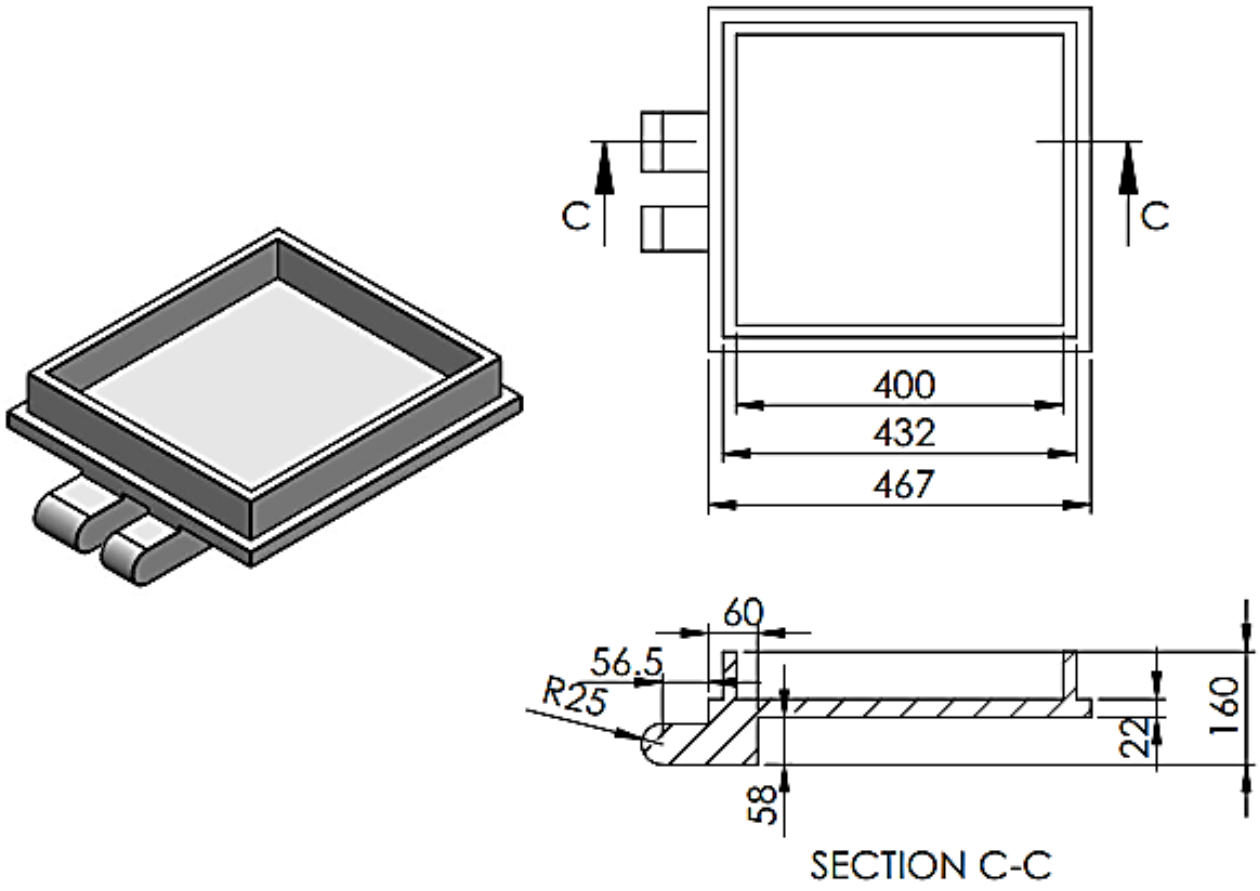

Figure B1: Geometry for case 1 (dimensions are in mm)

Case 2

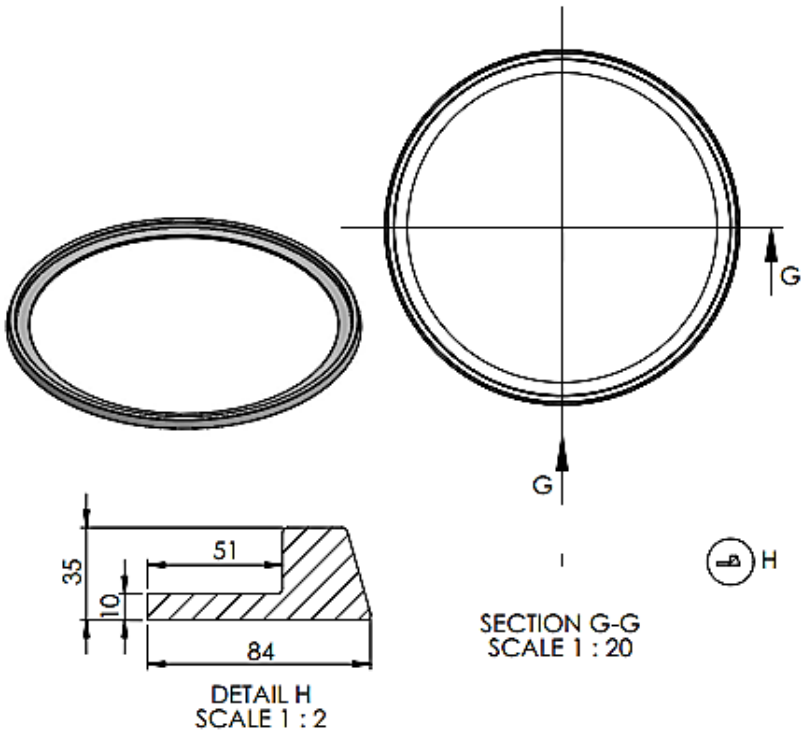

Figure B2: Geometry of case 2 (dimensions are in mm)

Case 3

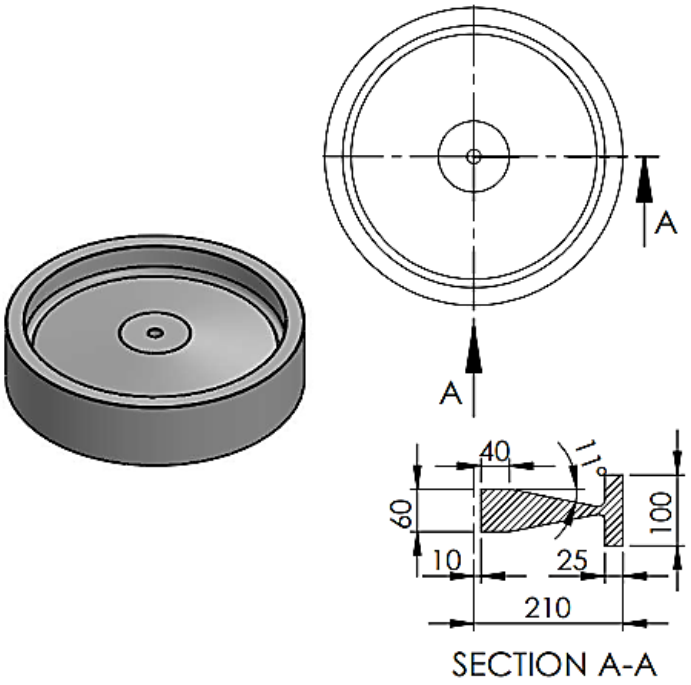

Figure B3: Geometry of case 3 (dimensions are in mm)